University of Nairobi
School of Physical Sciences
Department of Physics

A HYBRID OF FUZZY LOGIC AND SLIDING MODE TECHNIQUES FOR PHOTOVOLTAIC MAXIMUM POWER POINT TRACKING SYSTEMS UNDER PARTIAL SHADING

by

ROBINSON NDEGWA GATHONI
Bsc (Physics-University of Nairobi), MSc (Physics-University of Nairobi), MSc (Satellite and Orbital Platforms-University of La Sapienza, Rome Italy)
Registration No. I80/51887/2017

A thesis Submitted in Fulfillment of the Requirements for the award of the Degree of Doctor of Philosophy in Physics of the University of Nairobi

November, 2020

Declaration

I declare that this thesis is my original work, and has not presented elsewhere for research. Where other people's research has been used, this has been properly noted and cited in keeping with the University of Nairobi 's requirements.

Robinson Ndegwa
I80/51887/2017
Department of Physics
School of Physical Sciences
University of Nairobi

Signature ....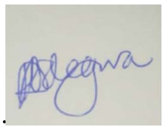......... Date...................20/11/2020

This thesis is submitted for examination with our approval as research supervisors:

Dr. Elijah Ayieta
University of Nairobi
Department of Physics
P.O. Box 30197 - 00100,
Nairobi, Kenya
ayietaeo@uonbi.ac.ke

Signature ....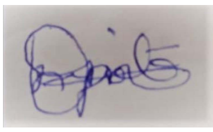......... Date...................20/11/2020

Prof. Justus Simiyu
Maasai Mara University
Department of Mathematics and Physical Sciences
P.O. Box 861 - 20500,
Narok, Kenya
justus@mmarau.ac.ke

Signature ............. Date...................20/11/2020

Dedication

This thesis is dedicated to the family of Gathoni (mum, my wife and children, my brother's family) and my best friends who have shown me that shared information is a knowledge acquired. I thank and admire them for their continued support, encouragement, inspiration and unconditional love.

Acknowledgments

I would like to express my special gratitude and appreciation to the people below who shared their wholehearted advice for my research and proved to be a milestone contributors towards my project's success:

To my supervisors Prof. Justus Simiyu and Dr. Elijah Ayieta for their continued critical support and encouragement. Thank you for your commitment and devotion in ensuring this project has turned out to be a good quality work. To our competent Principal of the College of Biological and Physical Sciences, Prof. Bernard Aduda, who, despite his tight schedules, spent his time updating, correcting and providing technical advice for all the research papers that were published from this study, despite not having been included as one of the authors. To my former student Esther Ngugi of Solinc Kenya Ltd, for her support during data collection process. To my Physics department colleagues, who have helped me reach this point of my education in various ways.

Thanks to my friends who have been with me through thick and thin, encouraging me and showing support even in times of failure, and making sure I did not give up. To my family for standing and praying with me, our prayers have been answered. Above all, I would like to thank the All-Powerful God, the creator of all things, the giver of power and knowledge for having given me the courage to face all adversities and emerge victorious.

Abstract

Solar energy harvesting using photovoltaic (PV) modules have been one of the most common sources of renewable energy for several decades. These modules have been used as a source of electricity for households, industries, in stand-alone, and grid-connected solar plants. The modules consist of semi-conductor solar cells combined in series and parallel. In order to make a solar system, the modules are usually linked in series. The performance of a solar system is affected by environmental factors like varying radiance and temperatures, shadowing caused by high-rise buildings, birds, fog, trees and dust. Such varying environmental conditions affect a solar cell's efficiency. Nevertheless, given all the effort made to mitigate the impact of all these environmental threats, some of the natural occurrences such as varying radiance, clouds, dust, wind-speed and change in temperature, can not be done away with. To improve the efficiency of the entire solar system, power extraction must be optimized under all weather conditions.

Fuzzy logic and sliding mode techniques are efficient, fast and reliable methods of tracking the maximum power point that have been used in this study. The application of these two approaches substantially increases system efficiency for all environmental conditions including partial shading instances. The sliding mode technique is a very fast, stable and robust algorithm that work effectively under very stable weather condition while the fuzzy logic has been exploited under partial shading conditions. Both methods rely heavily on a good understanding of the characteristics of PV modules, which are studied using I-V, P-V or P-I curves. In this work, three new algorithms have been used to simulate and model the characteristics of a PV module.

The algorithms are based on a single diode equivalent circuit, which has been chosen due to the simplicity of simulation and modeling and provides a fast convergence time. The algorithms are classified according to the method of obtaining the best values of the unknown five parameters of the diode model. Ideality factor (A), saturation current (I_o), photocurrent

(I_{ph}), series (R_s) and parallel (R_p) resistances are the five unknown parameters to be determined for characterization of a PV module using a diode model. These parameters have been extracted using the I-V curve's three critical points at short circuit point (SCP), open circuit point (OCP) and maximum power point (MPP). The first algorithm has been based on the choice of ideality factor below the optimal ideality factor (A_o), such that $0 \leq A \leq A_o$, whereas the other parameters depends heavily on the choice of A. The second algorithm has been based on the choice of ideality factor in the neighborhood of A_o and the third algorithm has been based on $A \geq A_o$. The three methods have been utilized to characterize the solar module using I-V and P-V curves and have output power errors of less than 0.5%.

For proof of concept of the three algorithms, PV module with IEC61215 specifications have carefully selected from Kyocera- KC130CGT. Additional experimental work has been carried out at Solinc Kenya Ltd using Solinc 60Wp and 250Wp PV modules, similar to those mounted on the rooftop of the building in Chiromo at School of Physical Sciences.

Table of Contents

Declaration **i**

Dedication **ii**

Acknowledgemnts **iii**

Abstract **iv**

Table of Contents **viii**

List of Abbreviations **ix**

List of Figures **xi**

List of Tables **xii**

1 Introduction **1**

1.1 Background 1

1.2 Statement of the Problem 3

1.3 Objectives of the Study 4

1.4 Justification and Significance of the Study 4

2 Literature Review **6**

2.1 Stand-alone, Grid and Hybrid Photovoltaic systems 6

2.2 Photovoltaic models 7

2.3 Conventional Techniques for MPPT of a PV System 8

2.4 Soft computing Techniques for MPPT of a PV System 9

3 Theory **12**

3.1 A single diode equivalent circuit model 12

3.1.1 Analysis of a PV model using the three crucial points from an I-V graph 13

3.1.2 Analysis of the five-unknown parameters 14

3.1.3 Improved analysis of I-V relationship using Newton-Raphson technique . 21

3.1.4 I-V and P-V characterization using NOCT and actual irradiance 22

3.1.5 PV MPPT based on boost converter model 24

3.1.6 Sliding mode technique (SMT) for PV MPPT 27

3.1.7 Fuzzy logic technique 31

4 Research Design and Methodology **35**

4.1 Introduction 35

4.2 Photovoltaic model algorithms 36

4.2.1 Algorithm for A, R_s and R_{sh} analyses 36

4.2.2 Algorithm of five-model parameters for $A < A_o$ 37

4.2.3 Algorithm of five-model parameters for $A \geq A_o$ 37

4.2.4 Algorithm of five-model parameters for $1 \leq \mathrm{A} \leq A_o$ 37

4.2.5 Photovoltaic PV model using Matlab 40

4.3 Boost converter using MATLAB 40

4.4 Sliding mode based MPPT controller 43

4.5 Fuzzy logic based MPPT controller 43

4.5.1 Fuzzy logic designer 43

4.5.2 Fuzzy membership functions (MFs) and rules 46

4.6 Partial shading of a P-V system using MATLAB 46

5 Result Analysis and Discussion **48**

5.1 Extraction of five-model parameter for $A \leq A_o$ 50

5.2 Analysis of I-V and P-V curves for $A \leq A_o$ 53

5.3 Extraction of five-model parameter for $A \geq A_o$ 53

5.4 Analysis of I-V and P-V curves for $A \geq A_o$ 59

5.5 Analysis of five-parameters using $0 \leq A \leq A_o$ 59

5.6 Comparison of extracted parameters with other approaches in literature for KC130GT 65
5.7 I-V and P-V curves for Solinc 60Wp, KC130GT and Solinc 250Wp modules using the four approaches 65
5.8 I-V and P-V characterization at ambient temperature, NOCT and actual irradiance 69
5.9 I-V and P-V Curves under Partial Shading 72

6 Conclusion and Recommendations 74

References 90

Appendices 91

List of Abbreviations

A	Diode ideality factor
A_o	Optimal ideality factor
D	Diode diffusion factor independent of temperature
E_g	Band gap energy (eV)
err	Error
I	Module output current (A)
I_o	Saturation current (A)
I_{mpp}	Maximum power point current (A)
I_{ph}	Light-generated current (A)
I_{sc}	Short-circuit current (A)
J_o	Dark saturation current density
k	Boltzmann constant (JK^{-1})
mpp	Maximum power point
N_s	Number of photovoltaic cells
$NOCT$	Nominal operating cell temperature
opt	Optimal
P_{max}	Maximum power (W)
q	Electron charge(C)
R_s	Series resistance (Ω)
R_{sh}	Shunt resistance (Ω)
s_a	Actual irradiance (W/m^2)
s_{STC}	Irradiance at standard test condition
STC	Standard test conditions
T_a	Cell temperature (K)
T_{STC}	STC temperature (K)
V	Module output voltage (V)
V_{mpp}	Maximum power point voltage (V)
V_{oc}	Open-circuit voltage (V)
IEC	International Electrotechnical Commission

List of Figures

3.1 A PV cell equivalent circuit using a single diode model 12

3.2 A PV system model connected to a DC-DC boost converter and MPPT controller 24

3.3 Duty cycle and sliding surface responses away from MPP 30

3.4 Fuzzy MPPT input and output variables 31

3.5 Duty cycle and sliding surface responses away from MPP 32

3.6 Fuzzy degree of membership versus input variable error e 33

3.7 Fuzzy degree of membership versus input variable change in error Δe 33

3.8 Fuzzy degree of membership versus input variable change in error Δe 34

4.1 A block diagram of the Photovoltaic solar system 35

4.2 An algorithm for evaluating the A, R_s and R_{sh} using I_{sc}, I_{mpp}, V_{mpp} and V_{oc} . . 36

4.3 An algorithm for evaluating A_o, $A < A_o$, I_{ph}, I_o, R_{sh} and R_s 38

4.4 An algorithm for evaluating A_o, $A \geq A_o$, I_{ph}, I_o, R_{sh} and R_s 39

4.5 An algorithm for calculating current (I) using Newton-Raphson technique and plotting IV and PV curves 41

4.6 Photovoltaic PV Model Using Matlab-Simulink 42

4.7 A DC-DC boost converter circuit using Matlab-Simulink 42

4.8 A Hall-effect current sensor and voltage drop circuit using Proteus Software . . . 43

4.9 Sliding Mode Based MPPT Controller for Solar systems using Matlab 44

4.10 A Fuzzy Logic Based MPPT Controller using Matlab 44

4.11 A Fuzzy Logic Based MPPT Controller using Matlab 45

4.12 Fuzzy Logic Designer 45

4.13 Fuzzy Membership Functions (MFs) and Rules 46

4.14 Partial shading of a PV module using Matlab 47

4.15 A hybrid Fuzzy Logic sliding mode Based MPPT Controller using Matlab 47

5.1 I-V and P-V curves for Solinc 60W using Gsola XJCM-10A solar simulator . . . 49

5.2 I-V and P-V curves for Solinc 250W using Gsola XJCM-10A solar simulator . . 49

5.3 A graph of ideality factor against saturation current (A) 50

5.4 A graph of R_{sh} versus R_s for Solinc 60Wp 51

5.5 A graph of R_{sh} versus R_s for KC130GT 52

5.6 A graph of R_{sh} versus R_s for Solinc 250Wp 52

5.7 A graph of (a) current vs voltage (b) power vs voltage for Solinc 60Wp, $A \leq A_o$ 54

5.8 A graph of (a) current vs voltage (b) power vs voltage for KC130GT, $A \leq A_o$. 55

5.9 A graph of (a) current vs voltage (b) power vs voltage for Solinc 250Wp, $A \leq A_o$ 56

5.10 A graph of R_{sh} versus R_s for Solinc 60Wp 57

5.11 A graph of R_{sh} versus R_s for KC130GT 58

5.12 A graph of R_{sh} versus R_s for Solinc 250Wp 58

5.13 A graph of (a) current vs voltage (b) power vs voltage for Solinc 60Wp for $A \geq A_o$ 60

5.14 A graph of (a) current vs voltage (b) power vs voltage for KC130GT for $A \geq A_o$ 61

5.15 A graph of (a) current vs voltage (b) power vs voltage for Solinc 250Wp for $A \geq A_o$ 62

5.16 A graph of (a) current vs voltage (b) power vs voltage for Solinc 60Wp, $0 \leq A \leq A_o$ 66

5.17 A graph of (a) current vs voltage (b) power vs voltage for KC130GT, $0 \leq A \leq A_o$ 67

5.18 A graph of (a) current vs voltage (b) power vs voltage for Solinc 250Wp, $0 \leq A \leq A_o$ 68

5.19 A graph of current versus voltage for KC130GT at different irradiance levels . . 70

5.20 A graph of power versus voltage for KC130GT at different irradiance levels . . 70

5.21 A graph of current versus voltage for KC130GT showing various temperatures curves at $1000W/m^2$ 71

5.22 A graph of power versus voltage for KC130GT showing various temperatures curves at $1000W/m^2$ 71

5.23 Graphs of current and power versus voltage for KC130GT showing local and global MPPs 73

List of Tables

3.1 Fuzzy rules 34

5.1 Solinc 60Wp, Kyocera KC130GT and Solinc 250Wp photovoltaic modules data at STC 48

5.2 Extracted parameters for Solinc 60Wp, Kyocera KC130GT and Solinc 250Wp PV modules 50

5.3 Extracted parameters for Solinc 60Wp, Kyocera KC130GT and Solinc 250Wp photovoltaic modules for $A \geq A_o$ 57

5.4 Extracted parameters and simulated Data for Solinc 60Wp 64

5.5 Extracted parameters and simulated data for KC130GT 64

5.6 Extracted parameters and simulated data for Solinc 250Wp 64

5.7 Extracted parameters and simulated data for KC130GT 65

5.8 Simulated data and extracted parameters values for KC130GT at air temperature of 20^oC and NOCT of 47^oC and different irradiance levels 69

5.9 Simulated data and extracted model parameters values for KC130GT photovoltaic module at various air and NOCT temperatures for $1000W/m^2$ irradiance level 72

Chapter 1

Introduction

1.1 Background

Solar photovoltaic (PV) modules have been used as a source of electricity for decades in areas without grid-connected power supplies. Using solar photovoltaic system as a source of energy is beneficial over fossil fuels since it has no environmental issues like atmospheric greenhouse gas emissions that result to acidic rain, depletion of ozone layers and global climate change (Dincer, 2000; Gunerhan *et al.*, 2008; Barreto, 2018; Ozturk and Dincer, 2019). Solar power is inexhaustible, and remains a major source of renewable energy (Twidell and Weir, 2015). Non-renewable energy sources such as oil , natural gas, coal and bituminous rocks emit air pollutants such as methane, carbon dioxide and nitrogen dioxide, and are the leading environmental threat to pediatric health and equity worldwide (Perera, 2018). PV solar system therefore remains a major source of clean energy which greatly supplements non-renewable sources (Bielecki *et al.*, 2020; Dixit, 2020; Liu *et al.*, 2020; Taghizadeh-Hesary *et al.*, 2019).

PV modules are composed of solar cells which convert solar energy to electricity (Sze and Ng, 2006; Mertens, 2018). Solar cells are connected in series and parallel to form a solar module that harvest useful energy (Würfel and Würfel, 2016). The solar cells are clustered together in series during the assembly process, and bypass diodes are added to solve one of the most common problems faced by solar systems where solar cells receive non-uniform irradiance and are partially shaded (Vemuru *et al.*, 2012; Robles-Campos *et al.*, 2019; Vieira *et al.*, 2020; Kruglykhin *et al.*, 2020). The major challenges solar modules face when partially shaded are that the cells under shadowing act as reverse biased diodes generating reverse voltages

(Hanitsch *et al.*, 2001). The reverse biased cells absorb power instead of producing it, that could contribute to heat dissipation. The heating causes thermal stress leading to hot spots in nearby cells (Silvestre and Chouder, 2008). Applying the by-pass diode to minimize the effect of partial shading, results in multiple maximum power points (MPPs) (Hu *et al.*, 2012; Mäki and Valkealahti, 2014; Ramyar *et al.*, 2016). The distinction of local and global maximum power points in partially shaded solar systems remains a research topic that has been explored in this research. This has been achieved by investigating the capabilities of the fuzzy logic and sliding mode techniques for maximum power point tracking (MPPT). The method of Fuzzy Logic can distinguish the local MPP from the global MPP and has been developed to trace the global MPP (Eydi *et al.*, 2020). However, the sliding mode technique fails to track the global MPP. These approaches depend on the characterization of solar system using current, voltage and power relationships.

Maximum power point (P_{mpp}), short circuit current (I_{sc}) and open circuit voltage (V_{oc}) are main operating points that characterize the solar system graphically in I-V, P-V or P-I curve (Walker, 2001; Salam *et al.*, 2013). A clear understanding of the I-V and P-V characteristics is important before implementing an MPPT controller (Eltamaly and Abdelaziz, 2019; Ahmad *et al.*, 2019; Mikkili *et al.*, 2020). This helps to design the topology of a DC-DC converter whose duty cycle is powered by the MPPT controller's output (Raghavendra *et al.*, 2020). For stand-alone, grid and hybrid PV systems, the DC-DC converter interfaces the solar modules with a load that can be either a battery bank or a DC-AC inverter. An MPPT controller can be implemented using an embedded system based on either microcontrollers, field-programmable gate array (FPGA) or digital signal processor (DSP) (Fares *et al.*, 2013).

Solar system modeling and computer-aided simulations are important for understanding its characteristics, efficiency and performance, and for assessing the effects of solar irradiance and temperatures (Nguyen and Lehman, 2006; Dey *et al.*, 2016). Modeling and simulation are also critical for evaluating the efficiency of a PV system before its implementation. For PV solar installers who want to assess the performance and efficiency of different PV system before implementation, the first prerequisite is to have a reliable and efficient model that mimic the actual system (Seyedmahmoudian *et al.*, 2013).

A single diode equivalent circuit has been widely use to model the PV cells due to availability of powerful analytical software such as open source GNU octave (Chin *et al.*, 2015). Several algorithms have been developed to determine the five-model parameters of a single diode (Jordehi, 2016). These methods can be classified as analytical methods (Chan and Phang, 1987), numerical methods (Ghani *et al.*, 2014) and metaheuristic methods using evolutionary algorithms and soft computing (Saha *et al.*, 2018). A fast and accurate analytical method for determining photovoltaic module parameters using a single diode mode has been applied in this work to characterize the PV modules before applying them in a standalone or grid- connected solar power plant.

In this research, a novel hybrid method that incorporates fuzzy logic (FL) and sliding mode algorithm to track the maximum power under partial shading is explored, which is a departure from conventional hybrid approaches based on modified hill climbing FL controller (HC-FLC) and adaptive perturb and observation (P&O-FLC) (Boukenoui and Mellit, 2019; Zou *et al.*, 2019).

1.2 Statement of the Problem

PV modules have become a common source of electric power, and have been used to produce grid-connected and stand-alone electricity to complement traditional power generation methods. Nevertheless, despite the abundance of solar energy worldwide, these have hardly been utilized especially in developing nations. The solar modules available on the market are in separate pieces and require skilled personnel to professionally install them. The standalone PV system consists of several modules, a battery pack, a wire harness and DC-AC inverter which is most commonly used for domestic use. The most suitable 1KW Solar Power System for domestic use would require four modules of 250 Watts, wire harness, deep cycle battery bank and powerful inverter. This is not affordable to most domestic users needing such a system. However, PV systems with sturdy MPPT boost efficiency in extracting output power by more than 70 percent. This is beneficial because there is less demand for more solar modules which leads to lower installation costs. Additionally, a PV system may be the best alternative to supplement traditional methods of generating power.

Partial shading of a PV device significantly reduces the output power from the PV system. The use of by- pass diodes to mitigate the partial shading effects generate multiple MPPs.

These multiple MPPs are composed of several local MPPs and a single global MPP requiring MPPT controllers that can identify their various positions and pin the global one out. Conventional MPPT controllers can not differentiate the multiple MPPs and their operation in such a situation is impaired, resulting in a reduction of their performance to less than 70%. The hybrid Fuzzy-logic and sliding-mode controller presented in this work has been designed to separate the global MPP from the local MPPs in order to significantly improve the power efficiency up to 75 percent.

1.3 Objectives of the Study

The overall objective of this research has been to develop a hybrid Fuzzy-logic and sliding-mode based MPPT for a PV system that is robust, efficient and stable compared with the conventional controllers under partial shading

The specific objectives of this study have been

(i) To study and analyze the PV module's I-V and P-V characterization using mathematical models of diode equivalent circuit

(ii) To apply the model in objective (i) above, to a hybrid Fuzzy-logic and sliding-mode based MPPT

(iii) To simulate and design a boost converter for the above MPPT

(iv) To assess the performance of the MPPT under partial shading

1.4 Justification and Significance of the Study

PV solar systems have been an efficient renewable electric power generator. The use of solar modules to transform solar radiation into electric power has been used to generate electricity in many situations where electricity is not available. Despite the availability of solar irradiation over a limited span of a day and varying irradiation levels, solar energy remains the main source of renewable power for grid-connected distribution and domestic applications.

The electric power produced by the solar modules is proportional to the solar irradiance levels. However, other factors such as atmospheric temperature and solar cell efficiency affect the production of power from solar system. Increased temperature in the atmosphere raises the surface temperature of the module and affects power output. The characteristic curves of current against voltage and power against voltage may be used to assess the performance of the PV system. The most important parameters from the curves are current and voltage at MPP, which have a specific point of operation. The direct transfer of solar energy is based on commercially off-the-shelf solar modules and solar rechargeable batteries connected directly to DC-AC inverters. In partially shaded conditions, these systems are less efficient, and very unstable. However, solar systems with an embedded MPPT improve efficiency in power harvesting.

Traditionally perturb-observe and hill-climbing MPPT algorithms have been the most utilized techniques due to their practicality in analogue and digital circuitry. The sliding mode technique has better and very high efficiency, and quick convergence time in an un-shaded environment. However, the technique fails to distinguish the local and global MPP under shaded environment. Soft computing algorithms are also emerging which have increased MPPT performance even under partial shading. Fuzzy logic is one of the most popular and powerful soft computing algorithms that track the global MPP efficiently when applied in partially shaded situations . A hybrid system incorporating Fuzzy logic and sliding mode techniques offers a fast, reliable and very stable MPPT controller in all weather conditions.

Chapter 2

Literature Review

2.1 Stand-alone, Grid and Hybrid Photovoltaic systems

Electric power consumption has greatly increased throughout the world due to population growth which has led to an expansion in the number of real estate and rapid industrial development Lu *et al.* (2019). This has given rise to alternative electric power sources other than the conventional centralized sources such as hydroelectric, geothermal , fossil fuels and nuclear power plants (Ebhota and Jen, 2020). Renewable energy sources such as solar, tidal energy, biomass, and wind have emerged as an alternative to supplement the rapid rise in demand for energy (García Vera *et al.*, 2019). The declines in costs of production and improvements in efficiency for photovoltaic solar cells have resulted in an increase in their production, resulting in the availability of affordable and efficient solar modules (Raugei *et al.*, 2012; Kittner *et al.*, 2016; Brockway *et al.*, 2019). Demand for stand-alone, grid-connected and hybrid photovoltaic solar systems is therefore rising exponentially (Yang *et al.*, 2010; Goel and Sharma, 2017; Lasnier and Juen, 2017). The standalone system is an independent decentralized power source that is optimized to supply electricity for a local demand (Kaundinya *et al.*, 2009). The hybrid system consists of two or more unrelated different sources of electric power, while in grid-connected systems, the excess electricity generated from standalone sources is pumped into national electricity supply lines (Meinhardt and Cramer, 2000).

Some of the factors affecting the use of PV systems include the availability of solar irradiation, effects of ambient condition, low power conversion efficiency and power versus current non-linearity (Meral and Dincer, 2011). Additionally, standalone systems use power storage batteries that raise installation costs and suffer from rapid power discharge (Bensaha *et al.*, 2020; Khatib and Muhsen, 2020). These drawbacks have attracted many research studies for modeling , simulating and analyzing solar photovoltaic (PV) modules before being mounted in a PV system facility, which helps to understand their behavior and characteristics in real environment (Jordehi, 2016; Abbassi *et al.*, 2018).

2.2 Photovoltaic models

A photovoltaic (PV) cell / module can be modeled using single diode, double diode and triple diode equivalent circuit in an effort to understand its non-linear current-voltage (I-V) and power-voltage (P-V) characteristics (Rauschenbach, 2012; Ogliari and Leva, 2019). The single-diode model (SDM) is less complex with five unknown parameters whereas the double-diode model is more complex, with seven unknown parameters (Khatibi *et al.*, 2019). The triple diode model (TDM) is a complex model with nine unknown parameters (Segev *et al.*, 2012; Qais *et al.*, 2020). The extraction of these unknown parameters has been a longstanding and common subject of research to this day.

For simplicity, mathematical characterization and modeling of a solar cell has been based on a single-diode equivalent circuit (Phang *et al.*, 1984b; Chan and Phang, 1987). The main purpose of modeling a solar module using a single diode equivalent circuit is to obtain optimum parameters so that the diode model matches the experimental data (Batzelis, 2019). In a single-diode model the main parameters to be determined are the photocurrent (I_{ph}), diode ideality factors (A), saturation current (I_0), series (R_s) and shunt (R_{sh}) resistances (De Soto *et al.*, 2006). There are several single-diode techniques that are based on five-, four- or three-parameter models Humada *et al.* (2016). These models have varying levels of accuracy and different mathematical derivations. In the four-parameter model, the shunt resistance is considered inherently high, and its contribution is ignored, whereas in the three-parameter model both series and shunt resistances are disregarded (Chenni *et al.*, 2007; Khezzar *et al.*, 2014). Neglecting the shunt resistance effects in the four-parameter model is a major drawback since the model fails to fit the experimental I–V curve when exposed to high temperature variations (Dongue *et al.*, 2012; Ma *et al.*, 2014). The five-parameter model is an all-inclusive approach which is superior than four and three parameter models in consideration of the fact that it take into account the parasitic effects of series and shunt resistances (Celik and Acikgoz, 2007).

Several methods for estimating the five-model parameters have been suggested, which can be classified according to analytical approaches, numerical approaches and metaheuristic approaches using soft-computing and evolution algorithms or their hybrids (Khan *et al.*, 2019). In this report, analytical and numerical approaches have been applied to arrive at fast, accurate and practical results for five-model parameters that are easily applicable for maximum power tracking analyses .

2.3 Conventional Techniques for MPPT of a PV System

Perturb and observe algorithm (P&O) is one of the conventional methods widely used in research and industrial solar PV MPPT due to its simplicity and ease of implementation, using both digital and analog technology (Liu and Lopes, 2004; Femia *et al.*, 2005; Abdel-Salam *et al.*, 2020). Despite its popularity, the technique fails to track MPP when solar irradiance fluctuates and it often oscillates near MPP even in steady state conditions leading to power losses. Modified P&O MPPT methods have been reported that tries to overcome these drawbacks and improve its efficiency (Belkaid *et al.*, 2017; Alik and Jusoh, 2017; Bhan *et al.*, 2019). Likewise, the P&O efficiency has been enhanced using variable step size approaches (Al-Diab and Sourkounis, 2010; Duan *et al.*, 2015; Dadfar *et al.*, 2020). Systems based on microcontrollers, FPGA and DSP that affected by the PV module's intrinsic capacitance have been used to instigate reliable P&O (Huynh and Cho, 1996; Hua *et al.*, 1998; Jiang *et al.*, 2005; Dadfar *et al.*, 2020).

Hill climbing (HC) algorithm is similarly common MPPT method which relies on DC-DC converter's duty-cycle perturbation (Xiao and Dunford, 2004; Bahari *et al.*, 2016; Ulinuha and Zulfikri, 2020). A hybrid of fuzzy logic and HC MPPT methods shows imperative performance in varying weather conditions (Alajmi *et al.*, 2010). An improved MPPT control strategy has been studied based on incremental conductance algorithms to increase the performance and economy of PV systems (Nafeh *et al.*, 1998; Shang *et al.*, 2020; Shengqing *et al.*, 2020). Other popular conventional MPPT techniques includes ripple correlation control (RCC) (Midya *et al.*, 1996; Krein, 1999; Esram *et al.*, 2006), extremum Seeking Control (ESC) (Bratcu *et al.*, 2008; Leyva *et al.*, 2006; Yau and Wu, 2011; Li *et al.*, 2011; Brunton *et al.*, 2010; Lei *et al.*, 2010; Leyva *et al.*, 2011), ESC based on sliding Mode (Yau *et al.*, 2013), ESC based on Newton-Like

(Zazo *et al.*, 2012; Li *et al.*, 2014), fractional open circuit voltage (FVOC) (Ahmad, 2010; Huang and Hsu, 2016; Noguchi *et al.*, 2002), fractional short circuit current (FSCC) (Noguchi *et al.*, 2002; Sher *et al.*, 2015; Sandali *et al.*, 2014; Owusu-Nyarko *et al.*, 2019) and sliding mode control (SMC) (De Soto *et al.*, 2006; Levron and Shmilovitz, 2013; Chaibi *et al.*, 2019; Bouchriha *et al.*, 2019; Zheng *et al.*, 2020). These methods have low convergence time,slow MPP tracking and speed high oscillations in the vicinity of MPP even in the static state (Walker *et al.*, 2011). The implementation of these conventional methods works well in a hybrid combination of soft computing techniques for monitoring MPP under partial shading (Ram *et al.*, 2017; Belhachat and Larbes, 2019).

2.4 Soft computing Techniques for MPPT of a PV System

Soft computing techniques for PV MPPT have been used to increase speed and efficiency and reduce computation requirement (De Brito *et al.*, 2012; Basha and Rani, 2020). Several comprehensive studies have been carried out to compare and contrast various soft computing methods showing their merits and demerits (Dileep and Singh, 2017; Eltamaly *et al.*, 2018; Hashim and Salam, 2019; Motahhir *et al.*, 2020b). These soft computing techniques have been grouped in to four categories (Bingöl and Özkaya, 2019). The first category has the methodology of artificial intelligence consisting of adaptive neural-fuzzy inference systems (ANFIS)(Otieno *et al.*, 2009; Li *et al.*, 2009; Al-Majidi *et al.*, 2019; Farah *et al.*, 2020), artificial neural network (ANN) (Elobaid *et al.*, 2015; Allahabadi *et al.*, 2019; Chouay and Ouassaid, 2019; Divyasharon *et al.*, 2019) and fuzzy logic (Takun *et al.*, 2010; Bendib *et al.*, 2014; Abd Alhussain and Yasin, 2020).

These various techniques have been rated according to the number of sensors, complexity, accuracy of tracking, economy, transient tracking speed and efficiency, and have been found to be superior to conventional methods (Dileep and Singh, 2017; Kolluru *et al.*, 2019; Basha and Rani, 2020; Ali *et al.*, 2020). The second group has evolutionary computation techniques with two distinct methodologies, the evolutionary algorithm and swarm intelligence. The evolutionary algorithm can be classified as genetic algorithm (Daraban *et al.*, 2014; Ibrahim *et al.*, 2019) and differential evolution (Tajuddin *et al.*, 2013; Zhang and Sui, 2020). The swarm intelligence techniques have several algorithms such as artificial bee colony algorithm (soufyane Benyoucef *et al.*, 2015; Hassan *et al.*, 2017; Motahhir *et al.*, 2020a), ant colony optimization (Jiang *et al.*, 2013; Titri *et al.*, 2017; Priyadarshi *et al.*, 2019; Kinattingal *et al.*, 2020), bat algorithm (Titri *et al.*, 2019; da Rocha *et al.*, 2020; Amalo *et al.*, 2020), cat swarm optimization (Nie *et al.*, 2017; Guo *et al.*, 2018; da Rocha *et al.*, 2020), chicken swarm optimization Wu *et al.* (2018); Sharma *et al.* (2019) , cuckoo search algorithm (Nugraha *et al.*, 2019; Mosaad *et al.*, 2019; Abo-Elyousr *et al.*, 2020; Basha *et al.*, 2020), firefly algorithm (Mohanty *et al.*, 2019; Huang *et al.*, 2020), Grey wolf optimization (Atici *et al.*, 2019; Debnath *et al.*, 2020; Tjahjono *et al.*, 2020) and particle swarm optimization (Beltran *et al.*, 2019; Dharshan *et al.*, 2020; Eltamaly *et al.*, 2020). Category three has been identified as flower pollination algorithm (Yousri *et al.*, 2019a,b) while the fourth category has been classified as Jaya algorithm (Huang *et al.*, 2017, 2019).

The Solar PV system with by-pass diodes display multiple MPPs and one global MPP when subjected to partial shading conditions (Chin *et al.*, 2011). In partial shading conditions, MPP tracking using traditional techniques track local MPP rather than global MPP (Psarros *et al.*, 2014). Hence, the hybrid conventional MPPT techniques have been used to track global MPP under partial shading conditions (Saravanan and Babu, 2016). Some of the most common hybrid techniques include artificial neural network with P&O (ANN-P&O) (El-Helw *et al.*, 2017), bat search algorithm with P&O (Bat-P&O) (Karagoz and Demirel, 2017), firefly algorithm with Incremental Conductance (INC-FFA) (Yetayew *et al.*, 2016), Fireworks with P&O (FWA-P&O) (Manickam *et al.*, 2016), fuzzy logic with modified hill climbing (Alajmi *et al.*, 2010), fuzzy logic with P&O (Macaulay and Zhou, 2018; Mahdi *et al.*, 2020), grey wolf with P&O (GWO-P&O) (Mohanty *et al.*, 2016), particle swarm optimization with P&O (PSO-P&O)(Avila *et al.*, 2017). Several authors have also reported hybrids of two soft computing techniques such as fish swarm with PSO (Duan *et al.*, 2017; Mao *et al.*, 2018), jaya algorithm with differential evolution (Jaya-DE) (Kumar *et al.*, 2017b), PSO with shuffled frog leaping algorithm (PSO –SFLA) (Mao *et al.*, 2017) and whale optimization with differential evolution (WODE) (Kumar *et al.*, 2017a). Such algorithms have different speed of tracking and can be classified according to simplicity of implementation (Belhachat and Larbes, 2018).

Fuzzy sliding mode controller (FSMC) for Photovoltaic system has been studied using Mamdani and Takagi-Sugeno optimization processes (Yau and Chen, 2012; Derri *et al.*, 2016; Miqoi *et al.*, 2017; Zeb *et al.*, 2019). In these FSMC methods, the fuzzy logic approach has been applied to reduce the oscillation around the operating point to eliminate the chattering phenomena present in the sliding mode technique. The phenomenon of chattering leads to decreased photovoltaic system efficiency (Xu *et al.*, 2019). A sliding mode control method has also been exploited to develop an adaptive nonlinear controller that regulate the output voltage of DC-DC boost converter in Photovoltaic system (Subroto *et al.*, 2017; Bag *et al.*, 2018). The FSMC and adaptive SMC approaches require additional circuits compared to conventional SMCs that rely on equivalent control approaches to reduce chattering phenomena. The traditional first order SMC method for PV systems guarantee stability and robustness to load variations and change in weather (Chu and Chen, 2009; Garraoui *et al.*, 2015). The other advanced SMC types, such as terminal sliding mode control (TSMC), super twisting theorem (STT), and artificial intelligent (AI) algorithm-based SMC, are complex and need more computational power (Ahmad *et al.*, 2020).

In this study, a novel approach has been explored using a hybrid of fuzzy logic and conventional sliding mode control techniques. The fuzzy logic tracks global MPP under partially shaded conditions while the sliding mode control has fast convergence, reliability, robustness, high efficiency and stable performance under static conditions. Using a single diode model of a PV system, the current, voltage and power fluctuations at the MPP are first simulated. The error in power and change in the error become inputs to the fuzzy inference system. Based on the simulation results, the hybrid approach has fast convergence speed and high precision efficiency.

Chapter 3

Theory

3.1 A single diode equivalent circuit model

Figure 3.1 shows a single diode equivalent circuit with a current source connected to R_s and load in series, and parallel to both the diode and the shunt resistor R_{sh}.

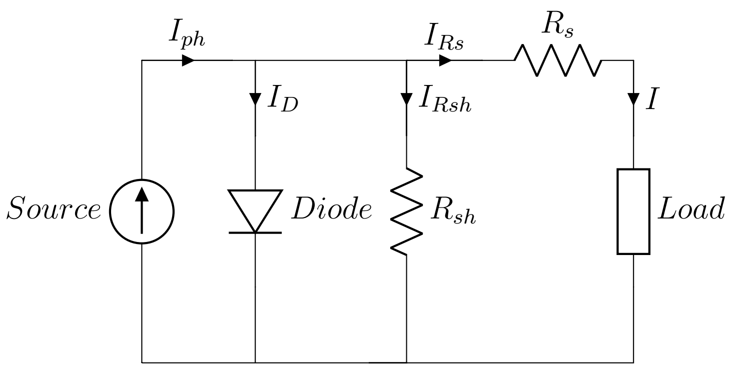

Figure 3.1: A PV cell equivalent circuit using a single diode model

Using Kirchhoff's current law (KCL), the currents in the circuit can be related as

$$I_{ph} - I_D = I_{R_{sh}} + I_{R_s} \tag{3.1}$$

and using Kirchhoff's voltage law (KVL), the output voltage (V) can be expressed as

$$V = V_{ph} - V_{R_s} = V_{R_{sh}} - V_{R_s} = V_D - V_{R_s} \tag{3.2}$$

The Shockley's diode (Shockley, 1949) has an exponential current-voltage relation given as

$$I_D = I_o exp\frac{qV_D}{AkT} - I_o \tag{3.3}$$

Where, I_o is the diode saturation currents in micro-amperes.

Figure 3.1 can be mathematically defined through the combination of the three equations (3.1-3.3) to obtain

$$I = I_{ph} - I_o\left(exp\frac{q(V+IR_s)}{AkT} - 1\right) - \frac{V+IR_s}{R_{sh}} \tag{3.4}$$

Where; k is the Boltzmann's Constant $= 1.380649 \times 10^{-23} m^2 s^{-2} kg K^{-1}$, q is the charge of an electron $= 1.602177 \times 10^{-19} C$ and T is the module surface temperature $= 298.15K$ at STC.

3.1.1 Analysis of a PV model using the three crucial points from an I-V graph

The key points in an I-V curve on a PV model graph are the short circuit point (SCP), the maximum power point (MPP), and the open circuit point (OCP). The characteristic and operation of the photovoltaic cell/module can easily and generally be studied through these points. These cardinal points can be applied in equation (3.4). Therefore, the I-V analyzes can be performed as follows at each point:

(i) At short circuit, $I = I_{sc}, V = 0$; Thus equation (3.4) can be evaluated as

$$I_{sc} = I_{ph} - I_o\left(exp\frac{I_{sc}R_s}{AN_sV_t} - 1\right) - \frac{I_{sc}R_s}{R_{sh}} \tag{3.5}$$

or

$$I_{ph} = I_{sc} + I_o\left(exp\frac{I_{sc}R_s}{AN_sV_t} - 1\right) + \frac{I_{sc}R_s}{R_{sh}} \tag{3.6}$$

Where $V_t = \frac{kT}{q} = 0.0256926$ is the thermal voltage and N_s is the number of cells in series for a solar module.

(ii) At Open Circuit, $I = 0, V = V_{oc}$;

Similarly, equation (3.4) can be rewritten as

$$I_{ph} = I_o \left(exp \frac{V_{oc}}{AN_sV_t} - 1 \right) + \frac{V_{oc}}{R_{sh}} \tag{3.7}$$

(iii) At Maximum Power Point, $I = I_{mpp}, V = V_{mpp}$;

Again, substituting $I = I_{mpp}$ and $V = V_{mpp}$ in equation (3.4) gives

$$I_{mpp} = I_{ph} - I_o \left(exp \frac{V_{mpp} + I_{mpp}R_s}{AN_sV_t} - 1 \right) - \frac{V_{mpp} + I_{mpp}R_s}{R_{sh}} \tag{3.8}$$

The five unknown parameters can be evaluated and calculated using the experimental data in equations 3.6 -3.8.

3.1.2 Analysis of the five-unknown parameters

There are five unknown parameters in the transcendental equation (3.4) which must be determined. These parameters are ideality factor (A), saturation current (I_o), photocurrent (I_{ph}), series (R_s) and shunt (R_{sh}) resistances. The following sections 3.3.1 to 3.3.3 discuss a detailed analysis of I_{ph}, I_o and A. Section 3.3.4 discusses analysis of R_s and R_{sh}.

(I) **Analysis of photocurrent (I_{ph})**

The photocurrent (I_{ph}) can be calculated using equations (3.5), (3.6) or by rewriting equation (3.8) as

$$I_{ph} = I_{mpp} + I_o \left(exp \frac{V_{mpp} + I_{mpp}R_s}{AN_sV_t} - 1 \right) + \frac{V_{mpp} + I_{mpp}R_s}{R_{sh}} \tag{3.9}$$

(II) **Analysis of saturation current (I_o)**

The saturation current can be analyzed using three distinct approaches. First, by reevaluating equation (3.4) at short circuit point (SCP), open circuit point (OCP) and maximum power point (MPP). Second, by combining two equations that have derived at the three points. Third, by using the concept of an ideal diode, where the saturation current depend on diffusion of minority carriers from the neutral regions to the depletion region in the absence of irradiation (Rauschenbach, 1971; Castaner and Silvestre, 2002). Furthermore, the saturation current also depends on the parameters of the semiconductor cross-sectional area, the temperature and the intrinsic carrier concentration (Neville, 1995; Sze and Ng, 2006; Castaner and Silvestre, 2002). In addition, the intrinsic carrier concentration number depends on the semiconductor energy bandgap, the state conduction and valence band densities. These three approaches are discussed in the following sections.

(a) **Analysis of saturation current (I_o) at short circuit point (SCP), maximum power point (MPP) and open circuit point (OCP)**

(i) At the short circuit point, equation (3.5) can be rearranged to give

$$I_o = \frac{I_{ph}R_{sh} - I_{sc}R_{sh} - I_{sc}R_s}{R_{sh}\left(exp\left(\frac{I_{sc}R_s}{AN_sV_t}\right) - 1\right)} \tag{3.10}$$

(ii) At maximum power point, equation (3.8) can be reorganized to obtain

$$I_o = \frac{I_{ph}R_{sh} - I_{mpp}R_{sh} - V_{mpp} - I_{mpp}R_s}{R_{sh}\left(exp\frac{V_{mpp}+I_{mpp}R_s}{AN_sV_t} - 1\right)} \tag{3.11}$$

Assuming $R_s \approx 0$, $R_{sh} \approx \infty$ and $I_{ph} \approx I_{sc}$, then applying them in equation (3.11), gives

$$I_o = \frac{I_{sc} - I_{mpp}}{\left(exp\frac{V_{mpp}}{AN_sV_t} - 1\right)} \tag{3.12}$$

(iii) At the open circuit point, equation (3.7) can be rearranged to give

$$I_o = \frac{I_{ph}R_{sh} - V_{oc}}{R_{sh}\left(exp\left(\frac{V_{oc}}{AN_sV_t}\right) - 1\right)} \tag{3.13}$$

Again, assuming $R_{sh} \approx \infty$ and $I_{ph} \approx I_{sc}$, equation (3.13) yields

$$I_o = \frac{I_{sc}}{exp\left(\frac{V_{oc}}{AN_sV_t}\right) - 1} \tag{3.14}$$

(b) **Analysis of saturation current (I_o) calculation by combining two equations**

The saturation current can also be calculated by combining two of either equations (3.6), (3.7) or (3.9).

Substituting equations (3.6) and (3.7) cancels I_{ph} as discussed by Sera *et al.* (2007), Hejri *et al.* (2013) and Atay and Eminoğlu (2019). Therefore, the saturation current can be derived as

$$[I_o]_{I_{sc},V_{oc}} = \frac{I_{sc}R_{sh} + I_{sc}R_s - V_{oc}}{R_{sh}\left[exp\left(\frac{V_{oc}}{AN_sV_t}\right) - exp\left(\frac{I_{sc}R_s}{AN_sV_t}\right)\right]} \tag{3.15}$$

Once more, taking $R_s \approx 0$ and $R_{sh} \approx \infty$, and applying in (3.15) gives

$$\left[I_{o_{opt}}\right]_{I_{sc},V_{oc}} = \frac{I_{sc}}{exp\left(\frac{V_{oc}}{AN_sV_t}\right)} \tag{3.16}$$

Similarly, equation (3.6) can be substituted with equation (3.9) at SCP and MPP to obtain

$$[I_o]_{I_{sc},P_{mpp}} = \frac{V_{mpp} + I_{mpp}R_{sh} + I_{mpp}R_s - I_{sc}R_s - I_{sc}R_{sh}}{R_{sh}\left[exp\left(\frac{I_{sc}R_s}{AN_sV_t}\right) - exp\left(\frac{V_{mpp}+I_{mpp}R_s}{AN_sV_t}\right)\right]} \tag{3.17}$$

Returning to $R_s \approx 0$ and $R_{sh} \approx \infty$, equation (3.17) reduces to

$$\left[I_{o_{opt}}\right]_{I_{sc},P_{mpp}} = \frac{I_{sc} - I_{mpp}}{exp\left(\frac{V_{mpp}}{AN_sV_t}\right)} \tag{3.18}$$

Finally, combining equations (3.7) and (3.9) at OCP and MPP, the saturation current formula can be derived as

$$[I_o]_{V_{oc},P_{mpp}} = \frac{V_{mpp} - V_{oc} + I_{mpp}R_{sh} + I_{mpp}R_s}{R_{sh}\left(exp\frac{V_{oc}}{AN_sV_t} - exp\frac{V_{mpp}+I_{mpp}R_s}{AN_sV_t}\right)} \tag{3.19}$$

Again, assuming $R_s \approx 0$ and $R_{sh} \approx \infty$, equation (3.19) can be rewritten as

$$\left[I_{o_{opt}}\right]_{V_{oc},P_{mpp}} = \frac{I_{mpp}}{exp\frac{V_{oc}}{AN_sV_t} - exp\frac{V_{mpp}}{AN_sV_t}} \tag{3.20}$$

(c) **Analysis of saturation current as a function of bandgap energy**

The saturation current densities for solar cells depend on the type of junction and for a

Schottky junction, the derivation reported by Ataboev *et al.* (2019) gives

$$J_o = qBN_VN_C\left[\frac{1}{N_A}\sqrt{\frac{D_n}{\tau_n}}+\frac{1}{N_D}\sqrt{\frac{D_p}{\tau_P}}\right]exp\left(\frac{-E_g}{kT}\right) \tag{3.21}$$

where, q is elementary charge, B is cross sectional area of solar cell, N_V, is the effective density of states in the valence band, N_C is the effective density of states in the conduction band, N_A is acceptor impurities concentration, D_n is electron diffusion coefficient, τ_n is electron (minority carrier) lifetime, N_D is donor impurities concentration, D_p is hole diffusion coefficient, τ_p is hole (minority carrier) lifetime, E_g is the energy bandgap, k is Boltzmann's constant and T is the cell surface temperature.

Equation (3.21) can be exploited for analysis of solar module's saturation current as explained by Chenni *et al.* (2007). Therefore,

$$I_o = I_{0_{STC}}\left[\frac{T}{T_{STC}}\right]^3 exp\frac{-qE_g}{AN_sk}\left[\frac{1}{T_{STC}}-\frac{1}{T}\right] \tag{3.22}$$

The $I_{0_{STC}}$ can be determined using equations (3.10) to (3.20) at a standard temperature of 25^oC.

(III) **Analysis of ideality factor (A)** The ideality factor is one of the main parameters to be carefully calculated, since other unknown parameters depend heavily on it and vice versa. Starting with the optimal ideality factor, other ideality factor can be arbitrarily selected such that $0 \le A \le A_o$.

Assuming that the exponential term ($exp\left(\frac{I_{sc}R_s}{AN_sV_t}\right)$) in equations (3.15) and (3.17) has insignificant value compared to other exponential terms. Therefore,

$$I_o = \frac{I_{sc}R_{sh}+I_{sc}R_s-V_{oc}}{R_{sh}exp\left(\frac{V_{oc}}{AN_sV_t}\right)} \tag{3.23}$$

and

$$I_o = \frac{I_{sc}R_s+I_{sc}R_{sh}-V_{mpp}-I_{mpp}R_{sh}-I_{mpp}R_s}{R_{sh}exp\left(\frac{V_{mpp}+I_{mpp}R_s}{AN_sV_t}\right)} \tag{3.24}$$

Equations (3.23) and (3.24) can be equated to obtain ideality factor A as

$$A = \frac{V_{oc} - V_{mpp} - I_{mpp}R_s}{N_s V_t \left[ln \left(\frac{I_{sc}R_{sh}+I_{sc}R_s-V_{oc}}{I_{sc}R_{sh}+I_{sc}R_s-I_{mpp}R_{sh}-I_{mpp}R_s-V_{mpp}} \right) \right]} \tag{3.25}$$

Again, the ideality factor can be determined using logarithms of equations (3.7) and (3.8) and after rearrangement to get

$$A = \frac{V_{oc} - V_{mpp} - I_{mpp}R_s}{N_s V_t \left[ln \left(\frac{I_{ph}+I_o-\frac{V_{oc}}{R_{sh}}}{I_{ph}+I_o-I_{mpp}-\frac{V_{mpp}+I_{mpp}R_s}{R_{sh}}} \right) \right]} \tag{3.26}$$

Assuming $R_s \approx 0$ and $R_{sh} \approx \infty$ and substituting them in equations (3.25) and (3.26) yields

$$A = \frac{V_{oc} - V_{mpp}}{N_s V_t [ln(\frac{I_{sc}+I_o}{I_{sc}+I_o-I_{mpp}})]} \tag{3.27}$$

But in the denominator of (3.27), $I_{sc} \gg I_o$. Hence,

$$A_o = \frac{V_{oc} - V_{mpp}}{N_s V_t [ln(\frac{I_{sc}}{I_{sc}-I_{mpp}})]} \tag{3.28}$$

Where, A_o is the optimal ideality factor.

(IV) **Shunt resistance (R_{sh}) and series resistance (R_s)**

The series and shunt resistance can be analyzed at maximum power point as follows

$$R_{sh} = \frac{V_{mpp} + I_{mpp}R_s}{I_{ph} - I_{mpp} - I_o \left(exp(\frac{V_{mpp}+I_{mpp}R_s}{AN_sV_t}) - 1 \right)} \tag{3.29}$$

In addition, the series and shunt resistance can also be analyzed by combination of equations (3.6) at SCP and (3.7) at OCP to obtain

$$R_{sh} = \frac{V_{oc} - I_{sc}R_s}{I_{sc} + I_o exp(\frac{I_{sc}R_s}{AN_sV_t}) - I_o exp(\frac{V_{oc}}{AN_sV_t})} \tag{3.30}$$

Likewise, the combination of equations (3.6) at SCP and (3.8) at MPP gives

$$R_{sh} = \frac{V_{mpp} + I_{mpp}R_s - I_{sc}R_s}{I_{sc} - I_{mpp} - I_o exp(\frac{V_{mpp}+I_{mpp}R_s}{AN_sV_t}) + I_o exp(\frac{I_{sc}R_s}{AN_sV_t})} \tag{3.31}$$

Further, combining equations (3.7) and (3.8) yields

$$R_{sh} = \frac{V_{oc} - V_{mpp} - I_{mpp}R_s}{I_{mpp} + I_o exp(\frac{V_{mpp}+I_{mpp}R_s}{AN_sV_t}) - I_o exp(\frac{V_{oc}}{AN_sV_t})} \tag{3.32}$$

The vanishing slopes at MPP, SCP and OCP can also be used to calculate R_s and R_{sh} resistances (Kennerud (1969); Phang *et al.* (1984a); Sera *et al.* (2007); Cubas *et al.* (2013); El Achouby *et al.* (2018)). The partial derivative of I with respect to V in I-V relationship has been applied in P-V relationship, since P depends on both I and V. Therefore, differentiating equation (3.4) with respect to V gives

$$\frac{\partial I}{\partial V} = -\frac{I_o}{AN_sV_t}\left\{\left(1 + \frac{\partial I}{\partial V}R_s\right) exp\left(\frac{V + IR_s}{AN_sV_t}\right)\right\} - \frac{1}{R_{sh}}\left(1 + \frac{\partial I}{\partial V}R_s\right) \tag{3.33}$$

The slope at SCP gives

$$\left[\frac{\partial I}{\partial V}\right]_{I=I_{sc}} = -\frac{1}{R_{sh}} \tag{3.34}$$

and at OCP

$$\left[\frac{\partial I}{\partial V}\right]_{V=V_{oc}} = -\frac{1}{R_s} \tag{3.35}$$

At MPP, the slope with respect to voltage gives

$$\frac{\partial P}{\partial V} = \left(\frac{\partial I}{\partial V}\right) V + I = 0 \tag{3.36}$$

At MPP, $I = I_{mpp}$ and $V = V_{mpp}$. Replacing them in equation (3.33) and applying it in equation (3.36) yields

$$-\frac{I_{mpp}}{V_{mpp}} = -\frac{I_o}{AN_sV_t}\left\{\left(1 - \frac{I_{mpp}}{V_{mpp}}R_s\right) exp\left(\frac{V_{mpp} + I_{mpp}R_s}{AN_sV_t}\right)\right\} - \frac{1}{R_{sh}}\left(1 - \frac{I_{mpp}}{V_{mpp}}R_s\right) \tag{3.37}$$

Equation(3.37) can be rearranged as follows

$$R_{sh} = \frac{V_{mpp} - I_{mpp}R_s}{I_{mpp} - \frac{I_o}{AN_sV_t}\left(V_{mpp} - I_{mpp}R_s\right) exp\left(\frac{V_{mpp}+I_{mpp}R_s}{AN_sV_t}\right)} \tag{3.38}$$

(V) **Evaluation and analysis of R_{sh} and R_s pairs**

The R_{sh} and R_s pairs can be analytically calculated using MPP, SCP and OCP using either equations (3.29-3.32) or (3.38). These equations have unknown R_s, I_o and A on the R.H.S. The simplest approach of analyzing R_{sh} and R_s pairs is by applying equation (3.16) in to equation (3.32). This replaces I_o of equation (3.32) to get

$$R_{sh} = \frac{V_{oc} - V_{mpp} - I_{mpp}R_s}{I_{mpp} - I_{sc} + I_{sc}exp\left(\frac{V_{mpp}-V_{oc}+I_{mpp}R_s}{AN_sV_t}\right)} \tag{3.39}$$

The values of ideality factor can be arbitrarily selected in the proximity of A_o and applied in equation (3.39). There are three ways of choosing the ideality factor, either $A \approx A_o$, or $A \geq A_o$ or $0 \leq A \leq A_o$, provided R_s and R_{sh} are within the limits introduced by Villalva *et al.* (2009). These limits can be obtained using

$$R_{s_{max}} = \frac{V_{oc} - V_{mpp}}{I_{mpp}} \tag{3.40}$$

and

$$R_{sh_{min}} = \frac{V_{mpp}}{I_{sc} - I_{mpp}} - R_{s_{max}} \tag{3.41}$$

The ideality factor is selected to ensure that the simulated maximum power ($P_{mpp}(sim)$) corresponds to the maximum power obtained experimentally, $P_{mpp}(expt)=I_{mpp}V_{mpp}$.

Where,

$$P_{mpp}(sim) = V_{mpp}(I_{ph} - I_o(exp\frac{V_{mpp} + I_{mpp}R_s}{AN_sV_t} - 1) - \frac{V_{mpp} + I_{mpp}R_s}{R_{sh}}) = P_{mpp}(expt) \tag{3.42}$$

It is possible to replace the value of I_{ph} in equation (3.42) with equation (3.6) by letting the term $I_o exp\left(\frac{I_{sc}R_s}{AN_sV_t}\right) \approx 0$ since it has negligible value. Also, assuming $I_{sc} \ggg I_o$ yields,

$$I_{ph} = I_{sc} + \frac{I_{sc}R_s}{R_{sh}} \tag{3.43}$$

Finally, I_o of equation (3.18) can be applied in equation (3.42) to give

$$P_{mpp}(sim) = V_{mpp}(I_{sc} + \frac{I_{sc}R_s}{R_{sh}} - (\frac{I_{sc} - I_{mpp}}{exp\frac{V_{mpp}}{AN_sV_t}})(exp\frac{V_{mpp} + I_{mpp}R_s}{AN_sV_t} - 1) - \frac{V_{mpp} + I_{mpp}R_s}{R_{sh}}) = P_{mpp}(expt) \tag{3.44}$$

Equations (3.39) and (3.44) has been be solved simultaneous using a open source GNU Octave software (see Appendix VIII). The values of A are selected sequentially until $(P_{mpp}(sim))$ matches $P_{mpp}(expt)$ or has an error margin of less than 0.5% (Carrero *et al.*, 2010).

Where,

$$P_{mpp}Error = \Delta P_{mpp}\% = \frac{P_{mpp} - I_{mpp}V_{mpp}}{I_{mpp}V_{mpp}} \times 100\% \tag{3.45}$$

3.1.3 Improved analysis of I-V relationship using Newton-Raphson technique

The derivations of the five-model parameters described in the previous section depend on SCP, MPP and OCP. However, the Newton-Raphson method has been applied to iteratively solve equation (3.4) in order to find all the points of an I-V plot. The technique is based on approximation of a given function f(I)=0 (Reis *et al.*, 2017).

Starting with a single-variable function f(I), equation (3.4) can be rearranged as

$$\mathrm{f}\,(\mathrm{I}) = \mathrm{I_{ph}} - \mathrm{I_o}\left[\exp\left(\frac{\mathrm{V} + \mathrm{IR_s}}{\mathrm{AN_sV_t}}\right) - 1\right] - \frac{\mathrm{V} + \mathrm{IR_s}}{\mathrm{R_{sh}}} - \mathrm{I} = 0 \tag{3.46}$$

The partial derivative of equation (3.46) w.r.t I gives

$$\frac{\partial\,(\mathrm{f}\,(\mathrm{I}))}{\partial \mathrm{I}} = \frac{-\mathrm{I_oR_s}}{\mathrm{AN_sV_t}}\exp\left(\frac{\mathrm{V} + \mathrm{IR_s}}{\mathrm{AN_sV_t}}\right) - \frac{\mathrm{R_s}}{\mathrm{R_{sh}}} - 1 \tag{3.47}$$

Therefore, applying a linear approximation based on Newton-Raphson method, equations (3.46) and (3.47) can be combined to give

$$I_{j+1} = I_j - \frac{f\left(I_j\right)}{\frac{\partial(f(I_j))}{\partial I}} = I_j - \frac{I_{ph} - I_o\left[exp\left(\frac{V+I_jR_s}{AN_sV_t}\right) - 1\right] - \frac{V+I_jR_s}{R_{sh}} - I_j}{\frac{-I_oR_s}{AN_sV_t}exp\left(\frac{V+I_jR_s}{AN_sV_t}\right) - \frac{R_s}{R_{sh}} - 1} \tag{3.48}$$

Where j represents the number of iterative process.

Equations (3.46-3.48) have been used to iteratively determine all current and voltage values. The I and V values are consequently applied in the following power equation given as

$$P = I_{ph}V - I_oV\left[exp\frac{V + IR_s}{AN_sV_t} - 1\right] - \frac{V^2}{R_{sh}} - VI\frac{R_s}{R_{sh}} \tag{3.49}$$

Finally, equations (3.46) and (3.49) are used for plotting IV and PV curves, respectively.

3.1.4 I-V and P-V characterization using NOCT and actual irradiance

The five-model parameters dependence on actual solar irradiation (s_a) and module's surface temperature T should be evaluated to reproduce a nominal operating condition (El Achouby *et al.*, 2018; Zaimi *et al.*, 2019).

At SCP,

$$I_{sc}(s_a, T) = \frac{s_a}{s_{STC}}\left[I_{sc_{STC}} + K_{I_{sc}}\left(T - T_{STC}\right)\right] \tag{3.50}$$

Where, $K_{I_{sc}}$ is the temperature coefficient of I_{sc} in $A/^oC$.

At MPP,

$$I_{mpp}(s_a, T) = \frac{s_a}{s_{STC}}\left[I_{mpp_{STC}} + K_{I_{mpp}}\left(T - T_{STC}\right)\right] \tag{3.51}$$

Where, $K_{I_{mpp}}$ is the temperature coefficient of I_{mpp} in $A/^oC$. $K_{I_{mpp}}$ is not included on the manufacturer's data sheet. This can be determined putting the data at STC and NOCT in to equation (3.51).

Solar modules with ISO/IEC standards has data profiles for STC at $1000W/m^2$ and nominal operation cell temperature (NOCT) values at $800W/m^2$ at 20^oC (McEvoy *et al.*, 2003; Schwingshackl *et al.*, 2013). The nominal operation cell temperature has been used to obtain the module temperature (T) using

$$T = T_a + \frac{[T_{NOCT} - 20]s_a}{800} \tag{3.52}$$

Where T_a is the ambient temperature.

Again at MPP,

$$V_{mpp}(s_a, T) = V_{mpp_{STC}} + K_{\nu,mpp}\left(T - T_{STC}\right) + \alpha_{\nu,mpp}\left(s_a - s_{STC}\right) + \beta_{\nu,mpp}\left(s_a - s_{STC}\right)^2 \tag{3.53}$$

Where, $\alpha_{V_{mpp}}$ and $\beta_{V_{mpp}}$ are coefficients of solar irradiance at MPP.

At OCP,

$$V_{oc}(s_a, T) = V_{oc_{STC}} + K_{\nu,oc}\left(T - T_{STC}\right) + \alpha_{\nu,oc}\left(s_a - s_{STC}\right) + \beta_{\nu,oc}\left(s_a - s_{STC}\right)^2 \tag{3.54}$$

Where $\alpha_{V_{oc}}$, $\beta_{V_{oc}}$ are coefficients of solar irradiance at OCP.

Equations (3.53) and (3.54) are quadratic polynomials, which require careful determination of the polynomial coefficients of the second degree. In order to overcome this drawback, a simplified approach have been adopted in this work for determining $V_{oc}\left(s_a, T\right)$ and $V_{mpp}\left(s_a, T\right)$, where

$$V_{oc}\left(s_a, T\right) = A\left(s_a, T\right) N_s V_t\left(T\right) \left[ln\left(I_{sc}\left(s_a, T\right)\right) - ln\left(I_o\left(s_a, T\right)\right)\right] \tag{3.55}$$

and,

$$V_{mpp}\left(s_a, T\right) = V_{oc}\left(s_a, T\right) - A_o N_s V_t(T) \times \left[ln\left(\frac{I_{sc}\left(s_a, T\right)}{I_{sc}\left(s_a, T\right) - I_{mpp}\left(s_a, T\right)}\right)\right] \tag{3.56}$$

These cardinal points can be used to extract the five-model parameters at different irradiance and temperature using the approaches presented in sections 3.1.1 to 3.1.3.

First, the saturation current dependence on module temperature can be achieved by rewriting equation (3.22) as

$$I_o\left(s_a, T\right) = I_{0_{STC}} \left[\frac{T}{T_{STC}}\right]^3 exp\left(-\frac{qE_g}{A\left(s_a, T\right) N_s k}\left[\frac{1}{T_{STC}} - \frac{1}{T}\right]\right) \tag{3.57}$$

Also equation (3.16) can be rewritten as

$$I_o = \frac{I_{sc}(s_a, T)}{exp\left(\frac{V_{oc}(s_a,T)}{A(s_a,T)N_sV_t(T)}\right)} \tag{3.58}$$

The I_o values of equation (3.57) have been compared with I_o of equation (3.58) for conformity. Second, I_{ph} depends on the surface temperature of the solar module and the solar irradiance (Sera *et al.*, 2007; Zaimi *et al.*, 2019), which can be deduced using

$$I_{ph}\left(s_a, T\right) = \frac{s_a}{s_{STC}}[I_{ph_{STC}} + K_I(T - T_{STC})] \tag{3.59}$$

Finally, $I_{mpp}(s_a, T)$, $V_{mpp}(s_a, T)$, $I_o(s_a, T)$ and $I_{ph}(s_a, T)$, of equations (3.51), (3.56), (3.58) and (3.59), respectively have been applied in equation (3.29) to get

$$R_{sh}(s_a, T) = \frac{V_{mpp}(s_a, T) + I_{mpp}(s_a, T)R_s(s_a, T)}{I_{ph}(s_a, T) - I_{mpp}(s_a, T) - I_o(s_a, T)\left(exp(\frac{V_{mpp}(s_a,T)+I_{mpp}(s_a,T)R_s(s_a,T)}{A(s_a,T)N_sV_t}) - 1\right)} \tag{3.60}$$

Th values of A, $R_s(s_a, T)$ and $R_{sh}(s_a, T)$ can be extracted through an iterative process presented in section 3.1.2 using equation 3.60.

3.1.5 PV MPPT based on boost converter model

Figure 3.2 shows a single diode equivalent circuit connected to a DC-DC boost converter and MPPT.

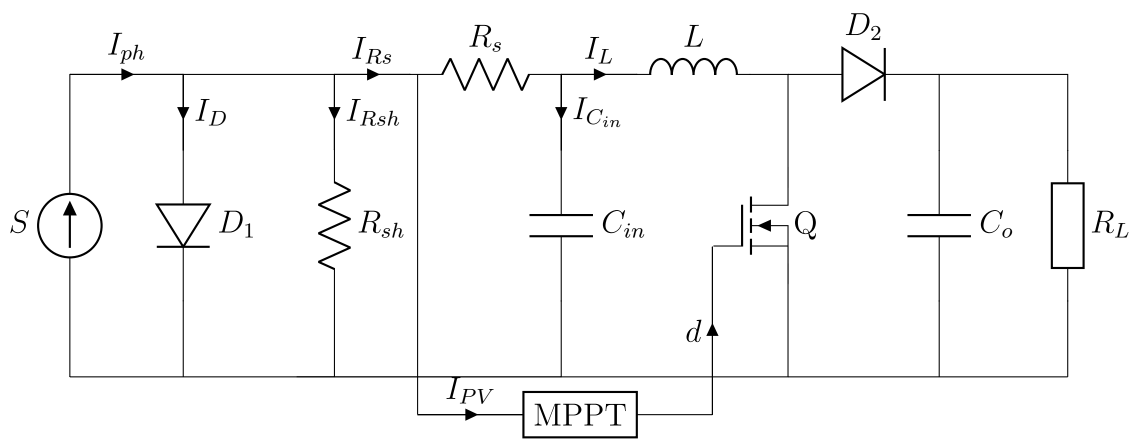

Figure 3.2: A PV system model connected to a DC-DC boost converter and MPPT controller

The DC-DC boost converter circuit consists of two capacitors C_{in} and C_{out}, an inductor (L), a diode D_2, load resistance R_L and a MOSFET switch Q. The converter can be modeled using state space derivation. The dynamic model of a boost converter can be represented in two states, when the switch (Q) is on or off (Charaabi *et al.*, 2020). The current passes through the inductor and the switch when Q is ON, and can be evaluated as

MOSFET ON

$$\frac{\partial i_L}{\partial t} = \frac{V_{pv}}{L} \tag{3.61}$$

and

$$\frac{\partial V_{C_o}}{\partial t} = \frac{V_{C_o}}{C_o R} \tag{3.62}$$

Similarly using the state space representation,

$$\dot{X}_1 = A_1 x + B_1 u \tag{3.63}$$

Applying equations (3.61) and (3.62) in equation (3.63) gives

$$\begin{bmatrix} \dot{i}_L \\ \dot{V}_{C_o} \end{bmatrix} = \begin{bmatrix} 0 & 0 \\ 0 & \frac{-1}{R_L C_o} \end{bmatrix} \begin{bmatrix} i_L \\ V_{C_o} \end{bmatrix} + \begin{bmatrix} \frac{1}{L} \\ 0 \end{bmatrix} \begin{bmatrix} V_{pv} \end{bmatrix} \tag{3.64}$$

MOSFET OFF

The current passes through the inductor, D_2 C_{out} and the load when Q is OFF, and can be evaluated as

$$\frac{\partial i_L}{\partial t} = \frac{V_{pv} - V_L}{L} \tag{3.65}$$

and

$$\frac{\partial V_{C_o}}{\partial t} = \frac{i_L}{C_o} - \frac{V_o}{C R_L} \tag{3.66}$$

Where, Vo is the output voltage and iL is the inductor current. In state space representation,

$$\dot{X}_2 = A_2 x + B_2 u \tag{3.67}$$

Again, applying equations 3.65 and 3.66 in equation 3.67 yields,

$$\begin{bmatrix} \dot{i}_L \\ \dot{V}_{C_o} \end{bmatrix} = \begin{bmatrix} 0 & \frac{-1}{L} \\ \frac{1}{C_o} & \frac{-1}{R_L C_o} \end{bmatrix} \begin{bmatrix} i_L \\ V_{C_o} \end{bmatrix} + \begin{bmatrix} \frac{1}{L} \\ 0 \end{bmatrix} \begin{bmatrix} V_{pv} \end{bmatrix} \tag{3.68}$$

Introducing the state space averaging method, the dynamic system state variables can be derived as

$$\begin{aligned} A &= A_1 d + A_2(1-d) \\ B &= B_1 d + B_2(1-d) \\ C &= C_1 d + C_2(1-d) \\ D &= D_1 d + D_2(1-d) \end{aligned} \tag{3.69}$$

Therefore, equations 3.64 and 3.68 can be combined into one set of state equation to represent the entire dynamic of the system as

$$\begin{bmatrix} \dot{i}_L \\ \dot{V}_{C_o} \end{bmatrix} = \begin{bmatrix} 0 & \frac{-(1-d)}{L} \\ \frac{1-d}{C_o} & \frac{-1}{R_L C_o} \end{bmatrix} \begin{bmatrix} i_L \\ V_{C_o} \end{bmatrix} + \begin{bmatrix} \frac{1}{L} \\ 0 \end{bmatrix} \begin{bmatrix} V_{pv} \end{bmatrix} \tag{3.70}$$

The model can be written in compact form as

$$\dot{X} = (1-d)\dot{X}_1 + d\dot{X}_2 \tag{3.71}$$

Where

$$\dot{X} = \begin{bmatrix} \dot{i}_L & \dot{V} \end{bmatrix}^T \tag{3.72}$$

and

$$\dot{X}_1 = \begin{bmatrix} \left(\frac{V_{pv}}{L} - \frac{V_{C_o}}{L}\right) & \left(\frac{i_L}{C_o} - \frac{V_{C_o}}{R_L C_o}\right) \end{bmatrix}^T \tag{3.73}$$

and

$$\dot{X}_2 = \begin{bmatrix} \left(\frac{V_{pv}}{L}\right) & \left(-\frac{V_{C_o}}{R_L C_o}\right) \end{bmatrix}^T \tag{3.74}$$

3.1.6 Sliding mode technique (SMT) for PV MPPT

Sliding mode technique guarantee robustness against various uncertainties caused by measurement error and external disturbances when obtaining duty cycle. The technique has two modes of operation, the approaching mode and the sliding mode. In approaching mode the sliding surface $S = 0$ is selected in such a way that the state of the system reaches the surface and persistently produces maximum power output. In sliding mode the system state is confined to the sliding surface and guided to a point of operation (Chu and Chen, 2009; Garraoui *et al.*, 2015). The sliding surface for PV system can be defined as

$$S(t,x) = \frac{\partial P_{pv}}{\partial I_{pv}} = \frac{(I_{pv}V_{pv})}{\partial_{pv}} = I_{pv}\left(\frac{\partial V_{pv}}{\partial I_{pv}} - \frac{V_{pv}}{I_{pv}}\right) = 0 \tag{3.75}$$

From equation (3.75), the switching surface can be derived as

$$\left(\frac{\partial V_{pv}}{\partial I_{pv}} - \frac{V_{pv}}{I_{pv}}\right) = 0 \tag{3.76}$$

A simple sliding mode control design can be written as

$$d = d_{eq} + \xi sgn(S) \tag{3.77}$$

Where, d_{eq} is called equivalent control and ξ is a positive scaling constant.

The equivalent control ensures that every trajectory starting from the manifold S(x) = 0 remains on it, and ξsgn(S) can be considered as the MPP tracking effort. In equations (3.71) and (3.75), the equivalent control can be calculated by obtaining the s-derivative as follows

$$\dot{s} = \left[\frac{\partial S}{\partial X}\right]^T \dot{X} = \left[\frac{\partial S}{\partial X}\right]^T \left(f(x) + g(x)\, d_{eq}\right) = 0 \tag{3.78}$$

Therefore

$$d_{eq} = \frac{\left[\frac{\partial S}{\partial X}\right] f(x)}{\left[\frac{\partial S}{\partial X}\right] g(x)} = 1 - \frac{V_{pv}}{V_{C_o}} \tag{3.79}$$

But duty cycle $d \in 0, 1$, thus

$$d = \begin{cases} 1, & \text{if}, d_{eq} + \xi s \geq 0 \\ d_{eq} + \xi s, & \text{if}, 0 < d_{eq} + \xi s < 1 \\ 0, & \text{if}, d_{eq} + \xi s \leq 0 \end{cases} \tag{3.80}$$

Using Lyapunov stability criterion

$$V = \frac{1}{2} S^2 \tag{3.81}$$

Its derivative gives

$$\dot{V} = S\dot{S} < 0 \tag{3.82}$$

This guarantee an asymptotic convergence to the sliding surface

From equations (3.75) and (3.78), the $\dot{S}$ can written as

$$\dot{s} = \left[\frac{\partial S}{\partial X}\right]^T \dot{X} = \left(3 \times \frac{\partial R_{pv}}{\partial I_{pv}} + I_{pv} \times \frac{\partial^2 R_{pv}}{\partial I_{pv}^2}\right) \times \left(-\frac{V_C}{L}(1-d) + \frac{V_{pv}}{L}\right) \tag{3.83}$$

Where $R_{pv} = \frac{V_{pv}}{I_{pv}}$, so,

$$\frac{\partial R_{pv}}{\partial I_{pv}} = \frac{\partial}{\partial I_{pv}} \left[\frac{V_{pv}}{I_{pv}}\right] = \frac{1}{I_{pv}} \frac{\partial V_{pv}}{\partial I_{pv}} - \frac{V_{pv}}{I_{pv}^2} \tag{3.84}$$

and

$$\frac{\partial^2 R_{pv}}{\partial I_{pv}} = \frac{1}{I_{pv}} \frac{\partial^2 V_{pv}}{\partial I_{pv}^2} - \frac{1}{I_{pv}^2} \frac{\partial V_{pv}}{\partial I_{pv}} + \frac{2V_{pv}}{I_{pv}^3} \tag{3.85}$$

Assuming $R_s \approx 0$ and $R_{sh} \approx \infty$ and substituting them in equations (3.4), the PV characteristic equation can be defined as

$$V_{pv} = AN_s V_t ln\left(\frac{I_{ph} + I_o - I_{pv}}{I_o}\right) \tag{3.86}$$

Thus

$$\frac{\partial V_{pv}}{\partial I_{pv}} = -AN_s V_t \left(\frac{I_o}{I_{ph} + I_o - I_{pv}}\right) < 0 \tag{3.87}$$

Differentiating equation (3.87) gives

$$\frac{\partial^2 V_{pv}}{\partial I_{pv}^2} = -AN_s V_t \left(\frac{I_o}{\left(I_{ph} + I_o - I_{pv}\right)^2}\right) < 0 \tag{3.88}$$

Both equations (3.87) and (3.88) are negative definite since they both have negative sign on the R.H.S and satisfy the Lyapunov stability criterion. Relating equations (3.83)-(3.85), (3.87) and (3.88), and applying them in equation (3.78) gives

$$\left[\frac{\partial S}{\partial X}\right]^T = \left(3 \times \frac{\partial R_{pv}}{\partial I_{pv}} + I_{pv} \times \frac{\partial^2 R_{pv}}{\partial I_{pv}^2}\right) = 3\times\left(\frac{1}{I_{pv}}\frac{\partial V_{pv}}{\partial I_{pv}} - \frac{V_{pv}}{I_{pv}^2}\right)+I_{pv}\times\left(\frac{1}{I_{pv}}\frac{\partial^2 V_{pv}}{\partial I_{pv}^2} - \frac{1}{I_{pv}^2}\frac{\partial V_{pv}}{\partial I_{pv}} + \frac{2V_{pv}}{I_{pv}^3}\right)$$
$$= \frac{1}{I_{pv}}\frac{\partial V_{pv}}{\partial I_{pv}} - \frac{V_{pv}}{I_{pv}^2} + \frac{\partial^2 V_{pv}}{\partial I_{pv}^2} < 0 \quad (3.89)$$

Because equations (3.87) and (3.88) are definite negative, if $\frac{V_{pv}}{I_{pv}^2}$ is definite positive, then equation (3.89) is definite negative. The attainability of s=0 can be obtained through $\dot{V} = S\dot{S} < 0$. Three cases of equation (3.80) must be tested to test stability.

Case 1: $0 < d < 1$,

$$\dot{x}_1 = \dot{i}_L = -\frac{V_{CO}}{L}(1-d) + \frac{V_{pv}}{L} \quad (3.90)$$

or

$$\dot{i}_L = -\frac{V_{CO}}{L}(1 - d_{eq} - \xi s) + \frac{V_{pv}}{L} \quad (3.91)$$

or

$$\dot{i}_L = -\frac{V_{CO}}{L}\left(1 - \left(1 - \frac{V_{pv}}{V_{C_o}}\right) - \xi s\right) + \frac{V_{pv}}{L} \quad (3.92)$$

Therefore,

$$\dot{i}_L = \frac{V_{CO}}{L}\xi s \quad (3.93)$$

Also,

$$\dot{x}_2 = \dot{V}_{C_o} = \frac{(1-d)}{C_o}i_L - \frac{V_{C_o}}{R_L C_o} = \frac{(1-d_{eq}-\xi s)}{C_o}i_L - \frac{V_{C_o}}{R_L C_o} \quad (3.94)$$

From equations (3.89) and (3.93), the following conditions hold,

$$\begin{cases} s > 0, \quad \text{if, } \dot{s} = \left[\frac{\partial S}{\partial X}\right]^T \dot{X} < o \\ s < 0, \quad \text{if, } \dot{s} = \left[\frac{\partial S}{\partial X}\right]^T \dot{X} > o \end{cases} \quad (3.95)$$

It then follows from equation (3.95) that equation (3.82) is satisfied for $0 < d < 1$.

Case 2: d =1,

$$\dot{x}_1 = \dot{i}_L = -\frac{V_{CO}}{L}(1-d) + \frac{V_{pv}}{L} = \frac{V_{pv}}{L} > 0 \quad (3.96)$$

Two situations arise for $d = d_{eq} + \xi s = 1$,

(i) $d_{eq} = 1$:

If $d_{eq} = 1$, then from equation (3.79), $V_{pv} = 0$. Hence, looking at the operation of sliding surface and duty cycle in Figure 3.3, the system is operating on the L.H.S of MPP. The diagram demonstrates the operating schemes for both situations in equation (3.95). The sketch also demonstrates the operation schemes for both duty cycle and the sliding surface s.

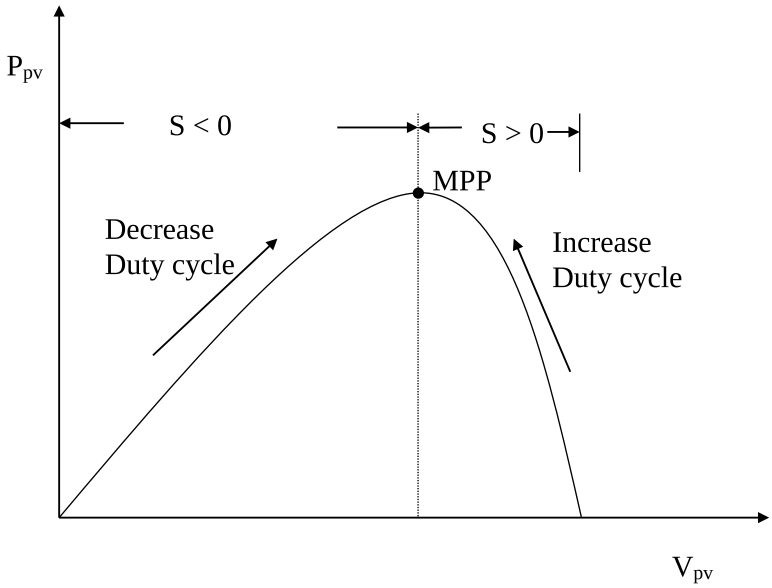

Figure 3.3: Duty cycle and sliding surface responses away from MPP

(ii) $d_{eq} < 1$:

If $d_{eq} < 1$, then $s > 0$ implies that Lyapunov criterion equation (3.79) is satisfied. Therefore if d=1 the system is stable if only and only if $d_{eq} < 1$.

Case 3: $d = 0$,

If $d = 0$, then equation (3.77) implies

$$\dot{x}_1 = \dot{i}_L = -\frac{V_{C_O}}{L}(1-d) + \frac{V_{pv}}{L} = -\frac{V_{pv}}{L} + \frac{V_{pv}}{L} \tag{3.97}$$

If duty cycle is zero the boost converter voltage output $V_o = V_C$ exceeds the solar (V_{pv}) voltage. This makes equation (3.97) negative definite, which results a positive definite $\dot{s}$. Again it is necessary to examine the two situation for d_{eq} when d=0 and $d_{eq} > 0$

i) $d_{eq} = 0$,

If $d_{eq} = 0$, then $V_{pv} = V_o$ implying that PV module is directly connected to the load.

Accordingly, the system is operating on the R.H.S of MPP where $s > 0$ duty should be increased thus contradicting the assumption that $d = 0$.

ii) $d_{eq} > 0$

If $d_{eq} > 0$ and $d = 0$ then $d_{eq} = -\xi s$. This leads to $s < 0$ situation when d_{eq} is positive definite. In order to ensure that the controller does not saturate on the states $d = 0$ and $d = 1$, the positive scaling constant should be small. Considering the maximum absolute value $|s|_{max}$,

Therefore, $\xi \leq \frac{1}{|s|_{max}}$ Where,

$$|s|_{max} = \frac{\partial V_{pv}}{\partial I_{pv}} = -AN_sV_t\left(\frac{I_o}{I_{ph} + I_o - I_{pv}}\right) \approx R_L \tag{3.98}$$

3.1.7 Fuzzy logic technique

Fuzzy logic technique has been applied on the basis of Fuzzy set theory in PV MPPT controller under Partial Shading Condition (Won *et al.*, 1994; Verma *et al.*, 2020). A variable (e) has a certain degree of membership in the fuzzy set theory, and may be a member of one or more sets within a continuous range of 0 to 1. The Fuzzy logic has four interfaces demonstrated in Figure 3.4. These include the fuzzification interface, inference, rules (knowledge base) and defuzzification interface.

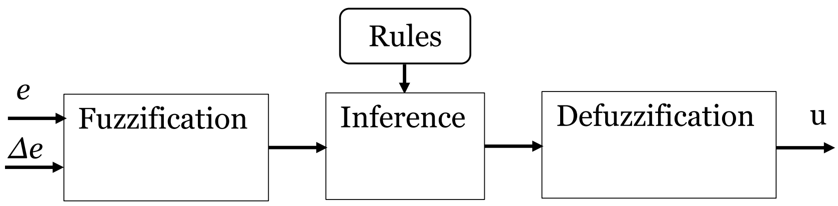

Figure 3.4: Fuzzy MPPT input and output variables

The inputs are translated into respective linguistic values within the fuzzification interface. These linguistic values form the membership functions which decide a variable 's range at a specific level. The steps involved in mapping a given input towards an output are formulated in fuzzy inference. This interface promotes identification of trends and provides a framework for decision making. Further, if-then rules and logical operations are implemented in the inference stage. The final part of the fuzzy logic consists of the defuzzifier, which transforms the fuzzy variables into output crisp sets.

Fuzzy logic controller for PV system MPPT presented in this work has error ($e(t)$) and change of error ($\Delta e(t)$) inputs that constitutes fuzzy membership functions. The power derivative $\frac{\partial P}{\partial V}$ gives the error e at any instant n. Where,

$$e(t) = \frac{P_n(t) - P_{n-1}(t)}{V_n(t) - V_{n-1}(t)} \tag{3.99}$$

and

$$\Delta e(t) = e_n(t) - e_{n-1}(t) \tag{3.100}$$

The positive error ($+e(t)$) indicate that the controller is operating on R.H.S of MPP and negative error ($-e(t)$) reflects an increasing power on the L.H.S of MPP as illustrated in Figure 3.5. However, at MPP, $\frac{\partial P}{\partial V} = 0$, implying that the error $e(t) = 0$. If the controller is running on R.H.S, a negative value of Δe is needed to turn the operating point to the right to reach MPP and vice versa.

Figures 3.6 and 3.7 display the standardized MPPT membership function of error (e) and change in error (Δe), the input variables in triangular form respectively.

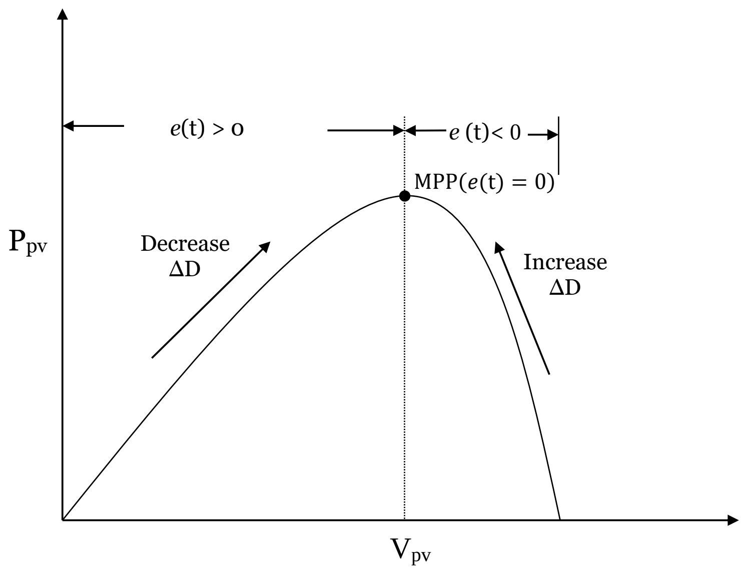

Figure 3.5: Duty cycle and sliding surface responses away from MPP

Figure 3.8 represents the output membership function that gives the change in duty cycle. he change in duty cycle (ΔD) is used as the output which is used to switch the DC-DC converter on and off. As shown in figures 3.6-3.8, the fuzzy's input and output variables are translated to the linguistic variables such as NB (negative big), NS (negative small), ZE (zero),

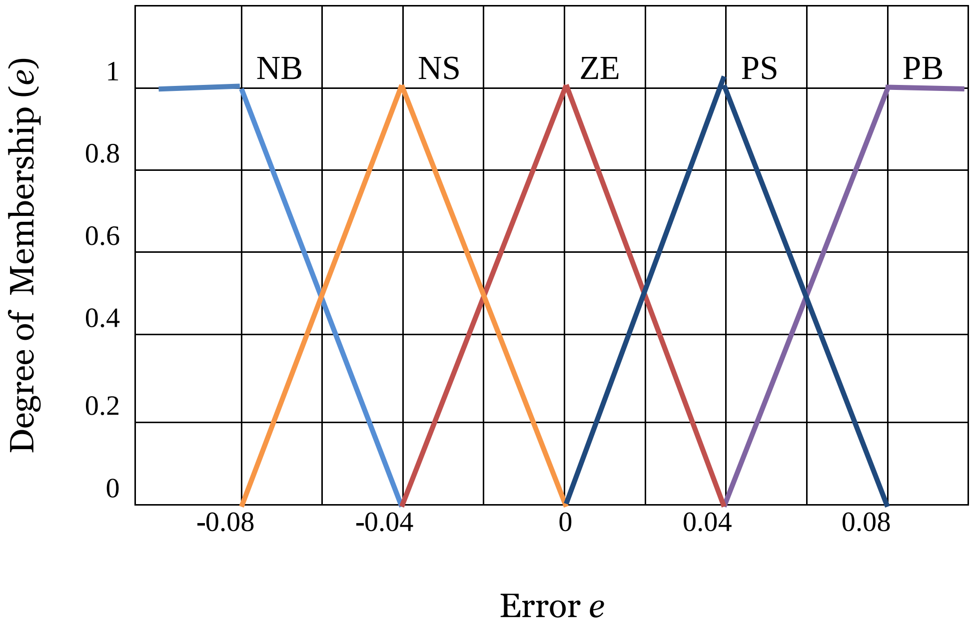

Figure 3.6: Fuzzy degree of membership versus input variable error e

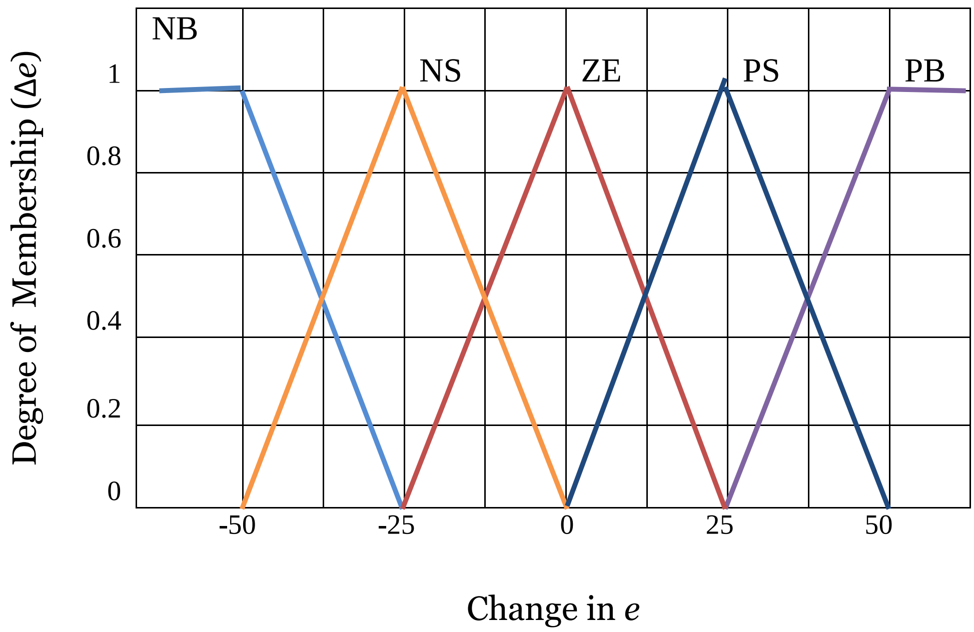

Figure 3.7: Fuzzy degree of membership versus input variable change in error Δe

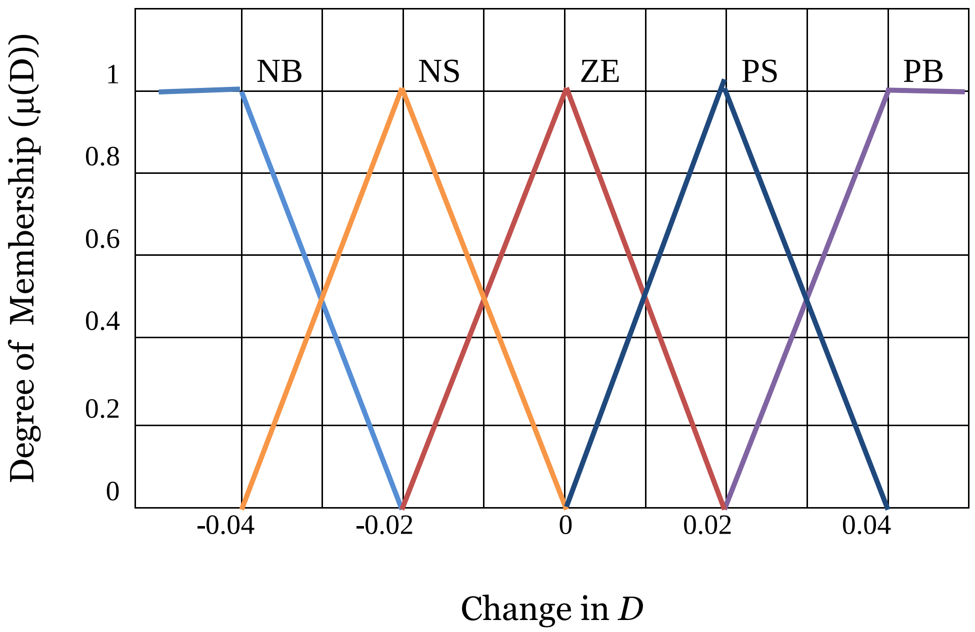

Figure 3.8: Fuzzy degree of membership versus input variable change in error Δe

PS (positive small) and PB (positive big) using simple fuzzy subsets.There are 25 fuzzy if-then rules summarized in Table 3.1. In order to maintain the PV system at global MPP, these rules are used to monitor the duty cycle of the DC-DC converter.

Table 3.1: Fuzzy rules

e \ Δe	NB	NS	ZE	PS	PB
NB	ZE	ZE	NB	NB	NB
NS	ZE	ZE	NS	NS	NS
ZE	NS	ZE	ZE	ZE	PS
PS	PS	PS	PS	ZE	ZE
PB	PB	PB	PB	ZE	ZE

Chapter 4

Research Design and Methodology

4.1 Introduction

Figure 4.1 displays a block diagram of the PV system, which has been explored in this study. A DC-DC boost converter and a hybrid MPPT unit of Fuzzy logic and sliding controllers are interfaced with the solar system. The MPPT unit generate a control signal for pulse width modulation (PWM) that switch the converter ON and OFF. The boost converter amplifies the PV current and voltage which is supplied to a standalone system or grid-connected system with a DC-AC inverter. Modeling and simulations of PV MPPT systems have been implemented using both the datasheet and experimental data. The following section discusses the proposed use of Matlab Simulink and GNU Octave software to model a PV module.

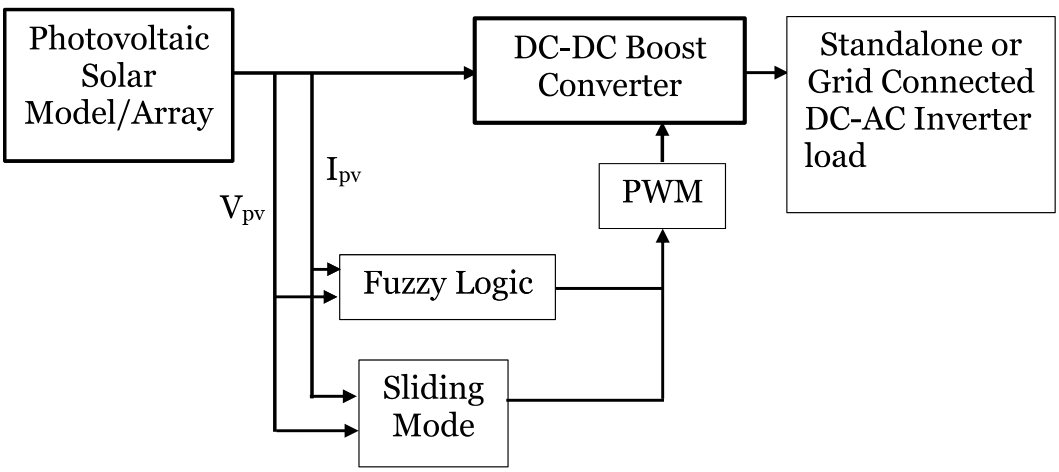

Figure 4.1: A block diagram of the Photovoltaic solar system

4.2 Photovoltaic model algorithms

The novel single-diode-based algorithms presented in this work have a simple and quick procedure for extracting the five $A, I_o, I_{ph}, R_s, R_{sh}$ unknown parameters. Beginning with the algorithm for analyzing R_{sh} vs R_s relationship, three additional algorithms for $A < A_o$, $1 \leq A \leq A_o$ and $A \geq A_o$ are also provided.

4.2.1 Algorithm for A, R_s and R_{sh} analyses

The algorithm demonstrated in Figure (4.2) explains a simple novel procedure to test the relationship between A, R_s and R_{sh} of equation (3.39). The procedure was carried out using an efficient numerical analysis program based on an open source GNU-octave (Hansen, 2011).

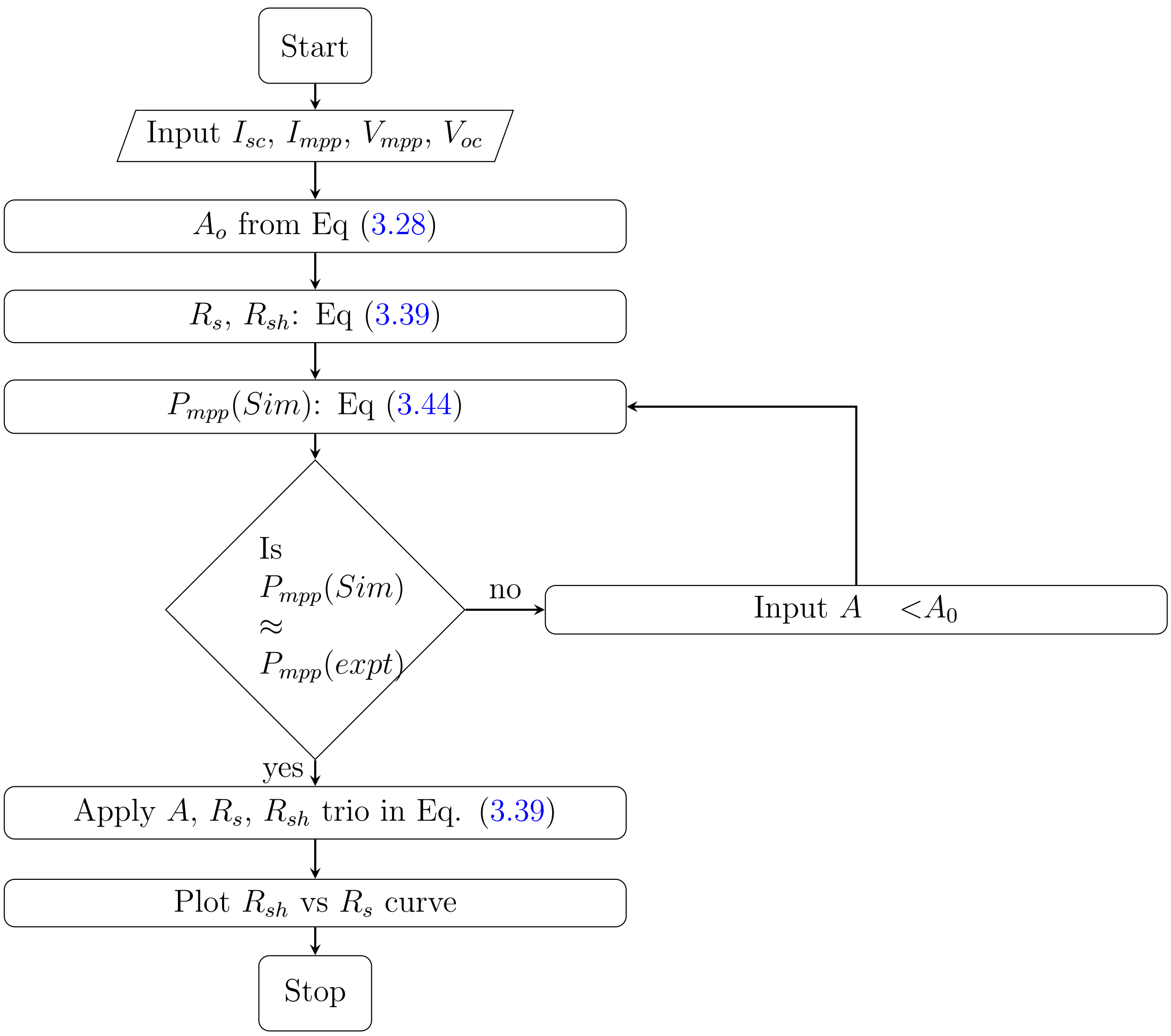

Figure 4.2: An algorithm for evaluating the A, R_s and R_{sh} using I_{sc}, I_{mpp}, V_{mpp} and V_{oc}

4.2.2 Algorithm of five-model parameters for $A < A_o$

Figure 4.3 shows a simplified analytical procedure for extracting the unknown parameters of a five-parameter single diode model. The workflow starts with the initialization of the values of I_{sc}, I_{mpp}, V_{mpp} and V_{oc} from the datasheet profile or experimental data. Followed by calculations of A_o using equation (3.28), I_0 using equation (3.16), R_{sh} & R_s using equation (3.39) and I_{ph} using equation (3.43). Then P_{mpp} is calculated using equation (3.44), while error in P_{mpp} is equation calculated using (3.45). The algorithm evaluates if $\Delta P_{mpp} \leq 0.5\%$ & $\Delta\ V_{oc} \leq 0.1\%$, where A is adjusted in proximity of A_o for $A < A_o$ to maintain an acceptable error-margin. Finally the process end with I-V and P-V plots.

4.2.3 Algorithm of five-model parameters for $A \geq A_o$

The third new algorithm is based on $A \geq A_o$ for extraction of five unknown parameters for a single diode PV model. It only works with the values $A \geq A_o$, $R_s > 0$ of equation 3.29, which gives reliable positive values of R_sh. Figure 4.4 shows the flowchart for the second algorithm that has been used to extract A_o, A, I_o, I_{ph}, R_{sh} and R_s.

4.2.4 Algorithm of five-model parameters for $1 \leq$ A $\leq A_o$

There are four most suitable data extraction approaches in this algorithm, where 1≤ A ≤ A_o is used for evaluating I and V using Newton-Raphson process. Such approaches are based on the choice of equations for calculating saturation current. Approach 1 is based on I_o currents that depend on A, I_{sc},, V_{oc}, R_s and R_{sh} using equations (3.13), (3.15) and (3.23). Approach 2 is based on the current of I_o which depends on A, I_{sc}, and V_{oc} and is determined using either equation (3.14) or (3.16). Approach 3 is based on I_o current of equation (3.19) at both V_{oc} and V_{mpp} and is dependent on R_s and R_{sh} resistances. Finally, approach 4 is based on I_o current given by equation (3.20) at both V_{oc} and V_{mpp} that is independent on R_s and R_{sh} resistances. However, with Io defined by equations (3.11 -3.12), (3.17-3.18) and (3.24) the data for both I and V are unsatisfactory.

These approaches can be implemented using the algorithm shown in Figure 4.5, which outlines all the steps needed to get the data to plot the I-V and P-V curves as follows.

- The process starts with initialization of I_{sc}, I_{mpp}, V_{mpp}, V_{oc}, N_s and V_t.

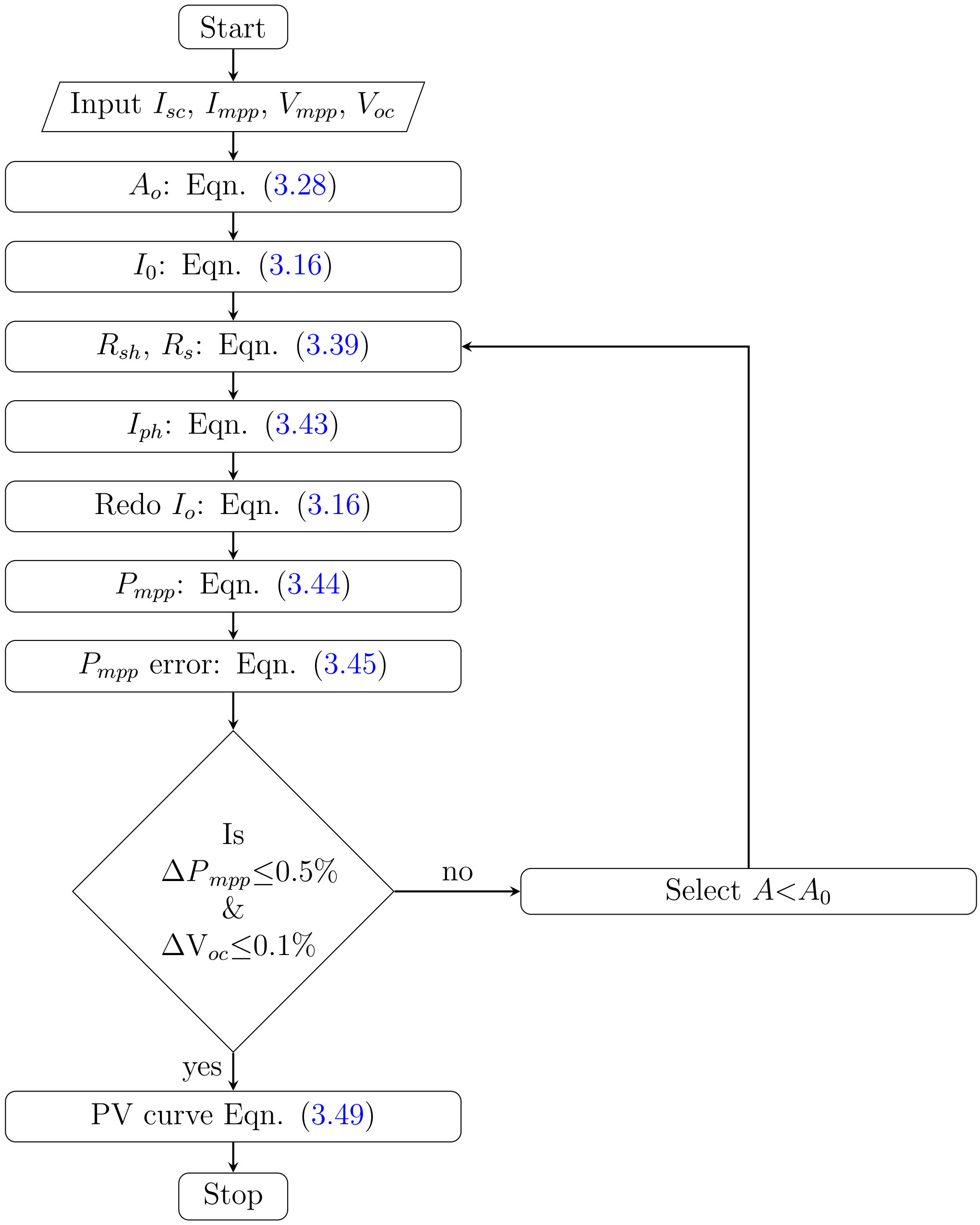

Figure 4.3: An algorithm for evaluating A_o, $A < A_o$, I_{ph}, I_o, R_{sh} and R_s

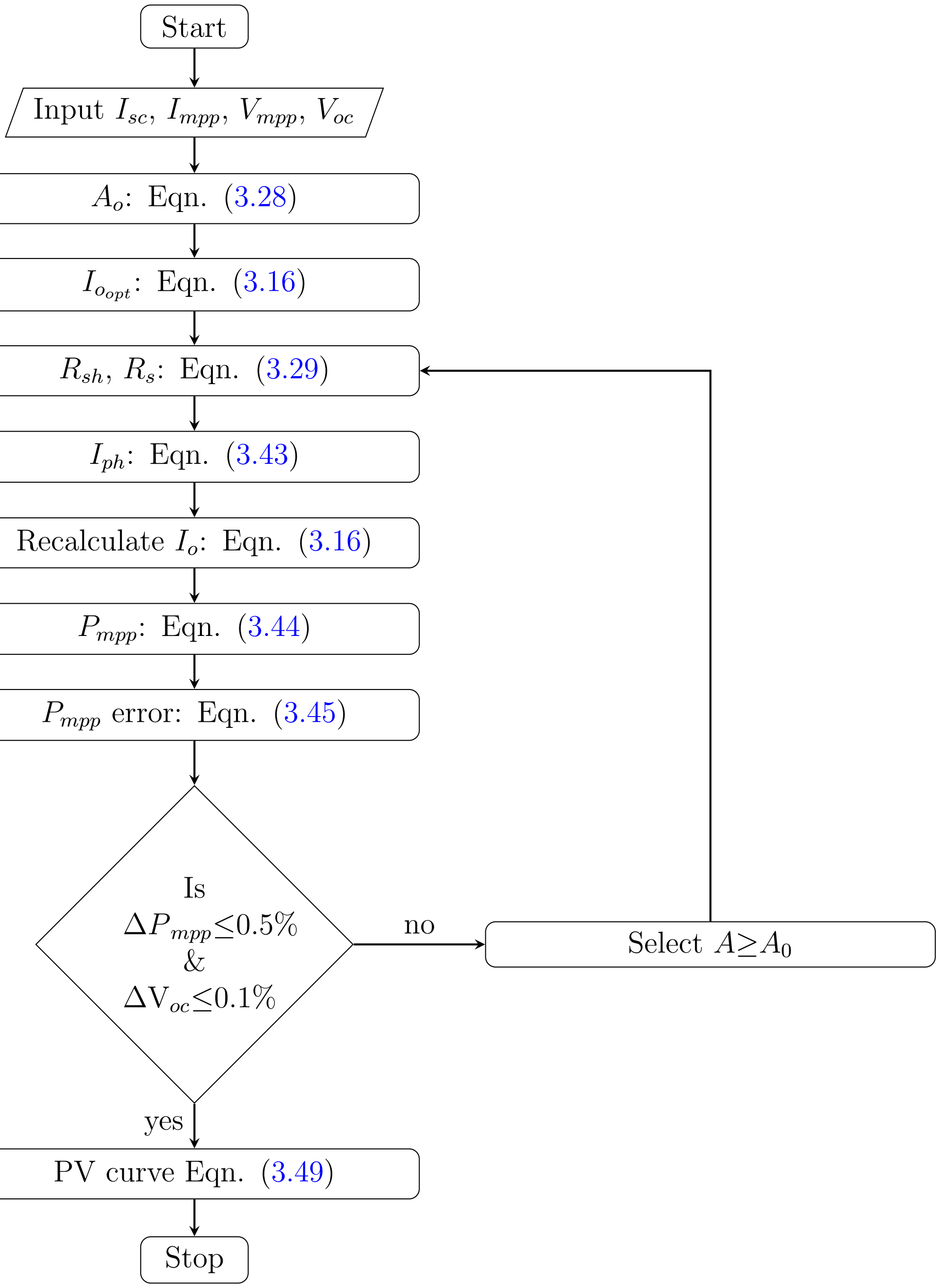

Figure 4.4: An algorithm for evaluating A_o, $A \geq A_o$, I_{ph}, I_o, R_{sh} and R_s

- Followed by setting the number of iterations, NiMax for current approximation and NvMax for voltage resolution plus precision description for R_s increment defined by $Rsinc$
- Then A, R_s and R_{sh} are estimated.
- Followed by calculation of I_o and I_{ph} for the first iteration
- The process is repeated severally for each iteration with an increment of R_s (R_s=R_s+Rsinc) until NiMax and NvMax are reached by solving equations (3.46-3.48)
- Then error in P_{mpp} is calculated followed by extraction of most acceptable values for A, R_s, R_{sh}, I_o and I_{ph}
- When the power error exceeds 0.5%, the cycle is repeated by entering a new ideality factor value.
- Eventually, the cycle finishes with plotting of I-V and P-V curves and I_{sc}, V_{oc} and V_{mpp} markers, if the power error is less than or equal to 0.5%

4.2.5 Photovoltaic PV model using Matlab

Figure 4.6 (a) displays a basic Model PV system using MATLAB Simulink. The model was used at constant irradiance and temperature at 1000W/m^2 and 25^{o}C respectively to produce the I-V and P-V curves. Figure 4.6 (b) shows a simplified circuit with comprehensive relation of all PV system outputs. These were multiplexed into different outputs which are connected to the CRO shown in Figure 4.6 (c).

4.3 Boost converter using MATLAB

A boost converted is easily simulated using an inductor, a diode, a capacitor, a resistor and an IGBT transistor switch as shown in Figure 4.7. A controlled voltage source mimic a PV current and voltage source.

Figure 4.8 displays a hall effect current sensor calibration circuit using Proteus software and voltage sensor circuit with microcontroller based display unit. A hall-effect-based current sensor

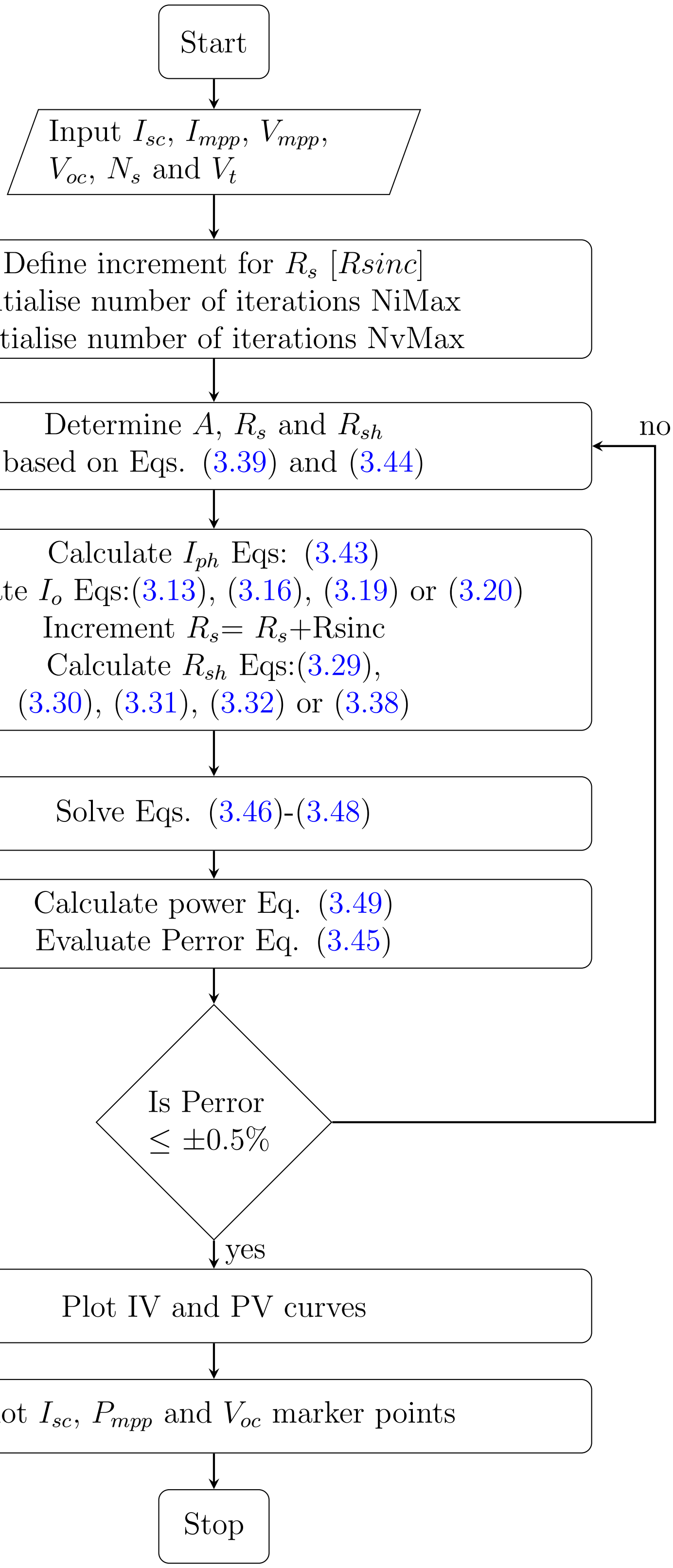

Figure 4.5: An algorithm for calculating current (I) using Newton-Raphson technique and plotting IV and PV curves

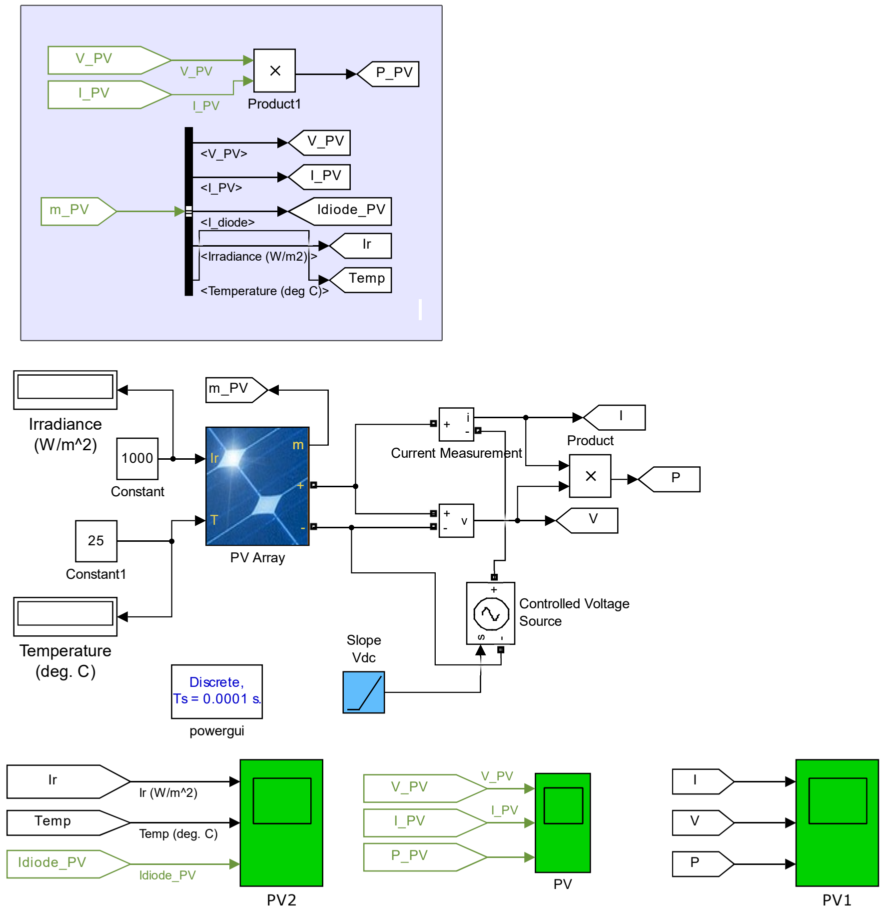

Figure 4.6: Photovoltaic PV Model Using Matlab-Simulink

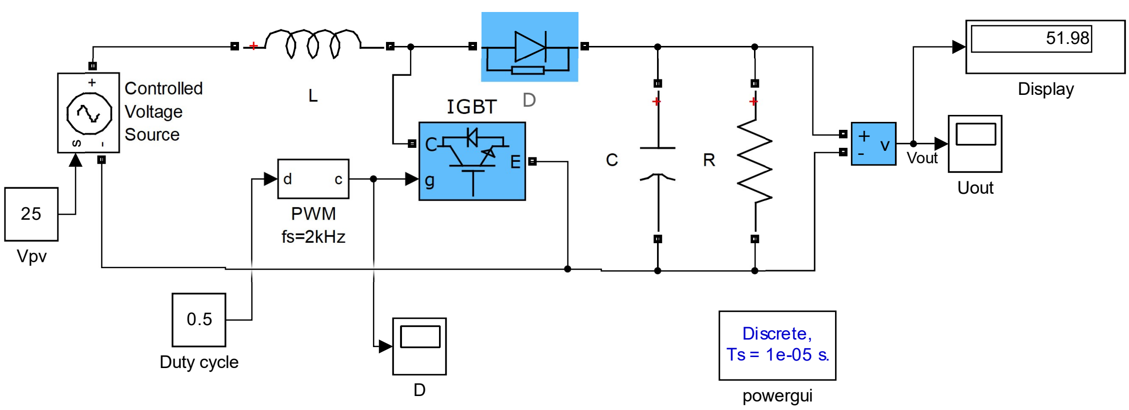

Figure 4.7: A DC-DC boost converter circuit using Matlab-Simulink

and voltage divide circuits between the PV system and the boost converter were implemented in the MPPT system.

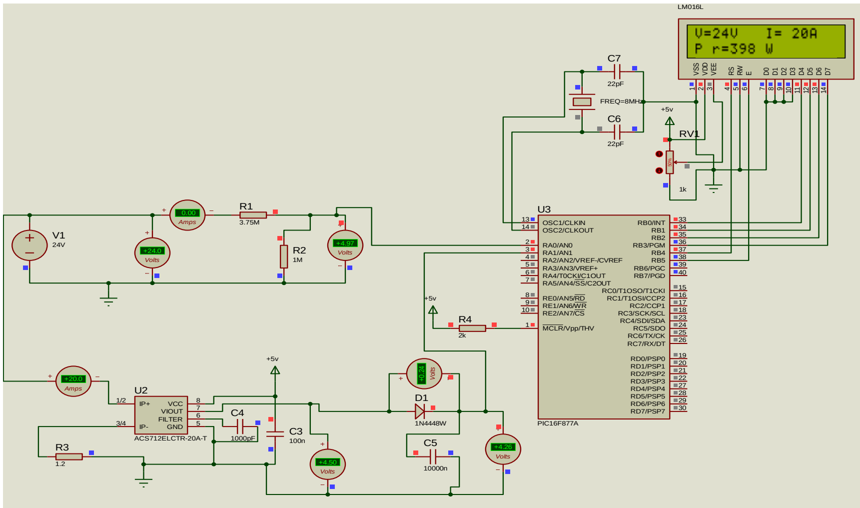

Figure 4.8: A Hall-effect current sensor and voltage drop circuit using Proteus Software

4.4 Sliding mode based MPPT controller

Figure 4.9 shows an MPPT Controller based on sliding mode technique that has been implemented using Matlab-Simulink. The circuit has a PV system, current and voltage sensors, a single stage boost converter that step up the DC voltage and SMC implementation blocks.

4.5 Fuzzy logic based MPPT controller

Figure 4.10 represents simulation blocks in a Matlab Simulink for a Fuzzy logic controller that implements the Fuzzy Inference Method.

4.5.1 Fuzzy logic designer

In Matlab, the Fuzzy logic designer shown in Figure 4.12 allows the input and output membership functions to be easily modified. The error $\left(\frac{\partial P}{\partial V}\right)$ and error change in error (∂E) are the inputs and the fuzzy logic designer output gives the change in duty cycle.

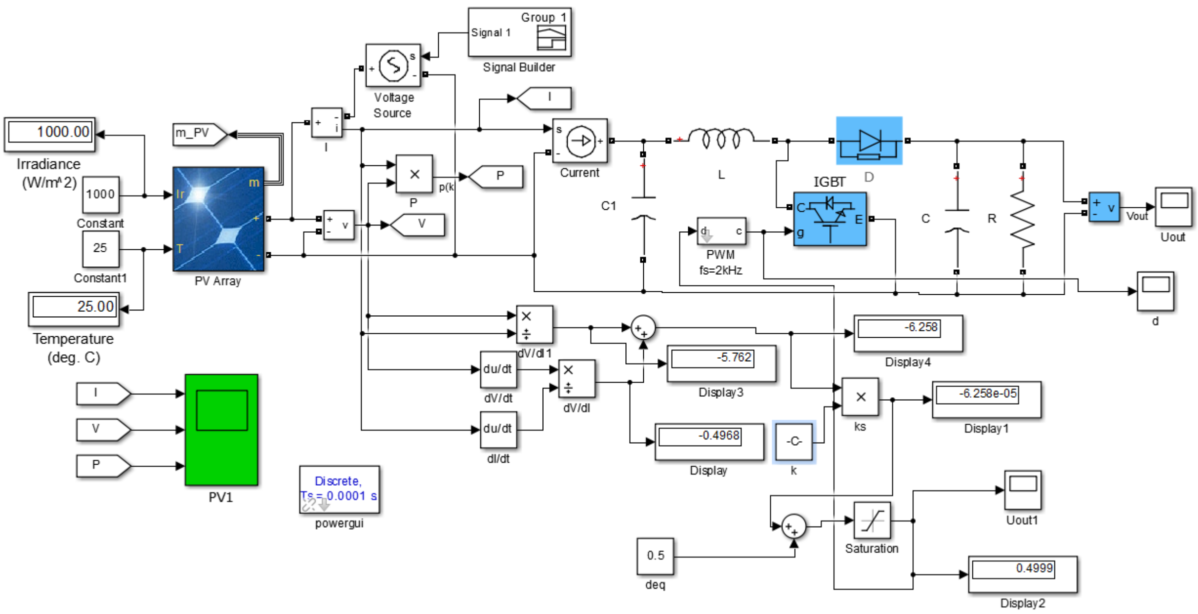

Figure 4.9: Sliding Mode Based MPPT Controller for Solar systems using Matlab

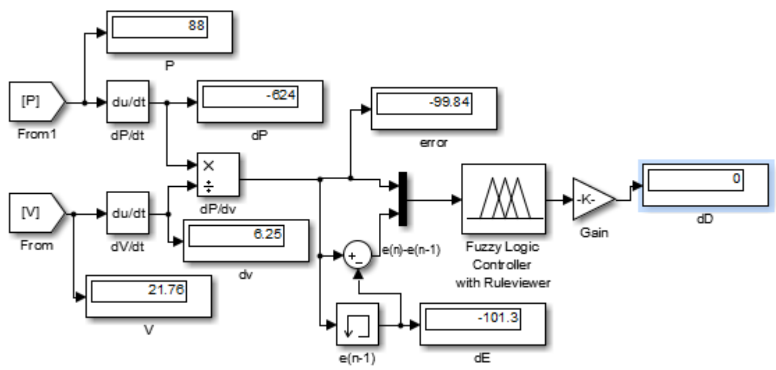

Figure 4.10: A Fuzzy Logic Based MPPT Controller using Matlab

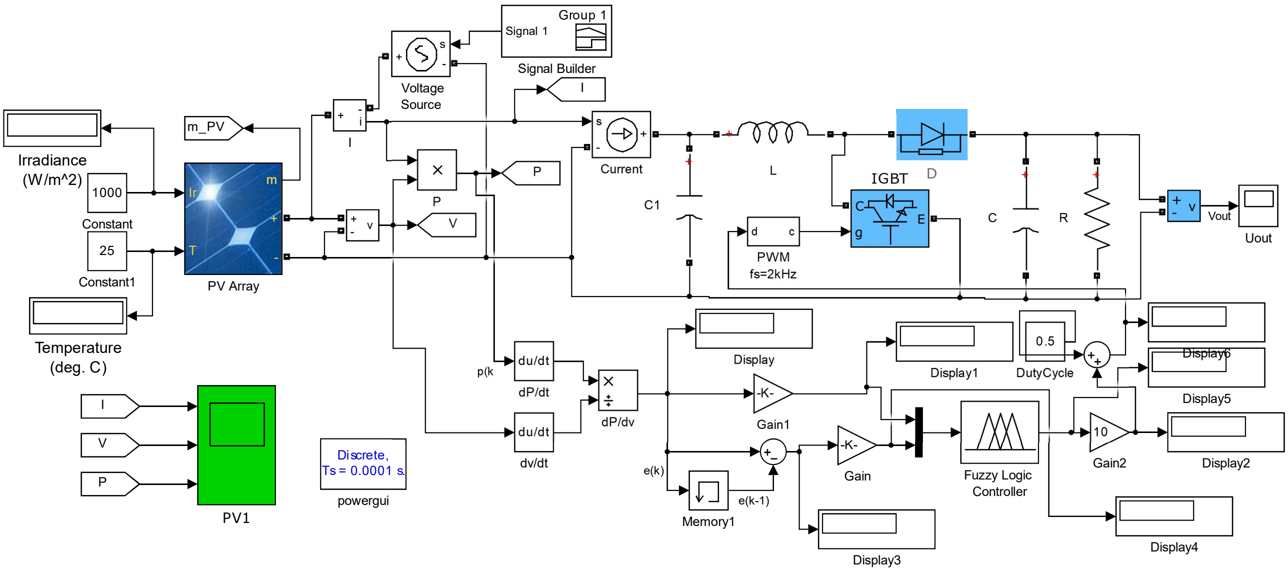

Figure 4.11: A Fuzzy Logic Based MPPT Controller using Matlab

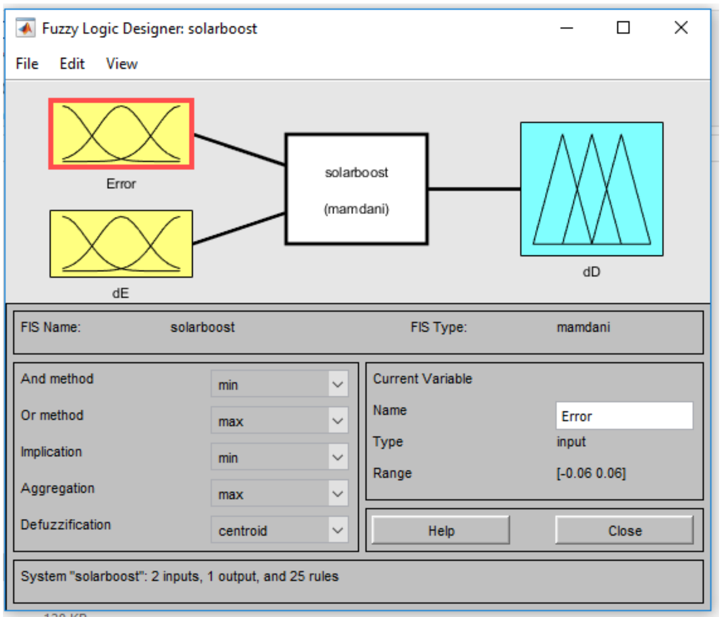

Figure 4.12: Fuzzy Logic Designer

4.5.2 Fuzzy membership functions (MFs) and rules

Fuzzy memberships are based on a multiple input single output (MISO) scheme with two e and de inputs, and one dD output. These appear as variables of the FIS in the membership editor shown in Figure 3.21.

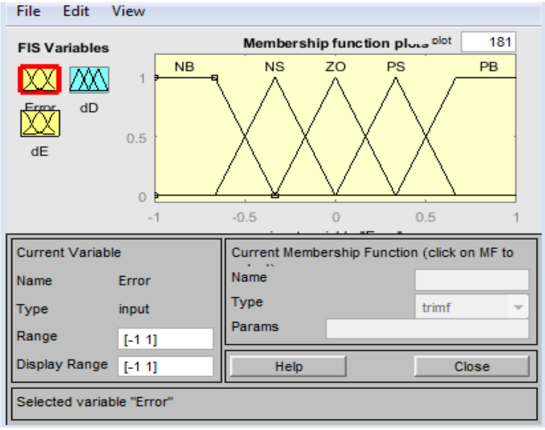

(a) Error

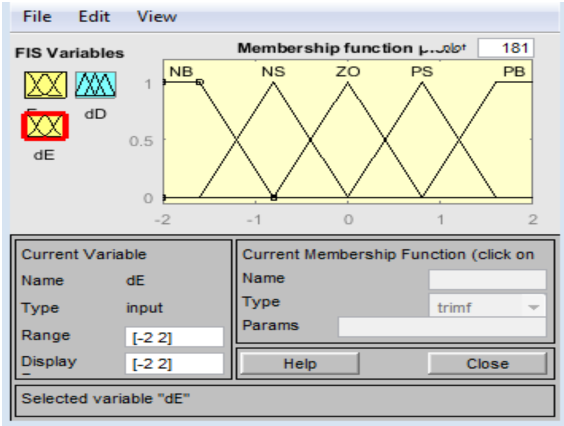

(b) Change in error (dE)

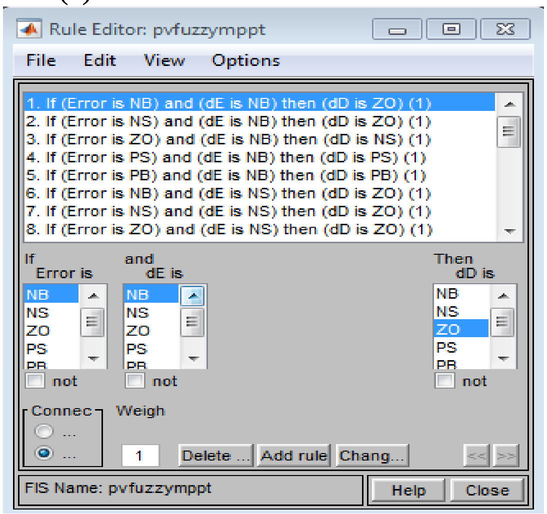

(c) Rules

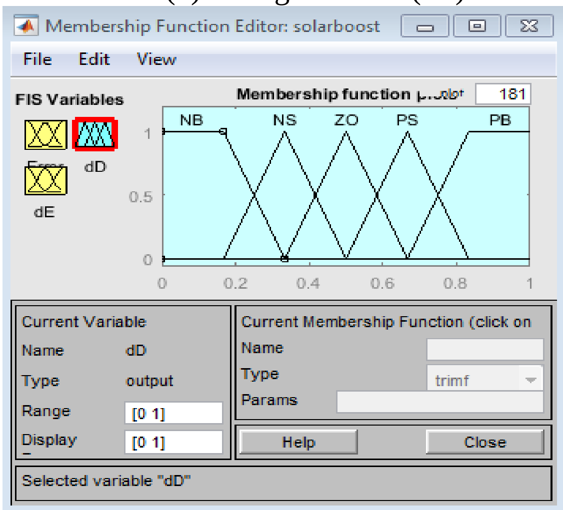

(d) Output MF (dD)

Figure 4.13: Fuzzy Membership Functions (MFs) and Rules

4.6 Partial shading of a P-V system using MATLAB

Figure 4.14 shows a P-V system implemented using Matlab Simulink which resembles an actual P-V plant with 12 modules. The plant has been divided into 3 groups each comprising 4 modules with incident irradiances of 1000 W / m^2,300 W / m^2 and 600 W / m^2,respectively. In addition, a combination of the Fuzzy logic and sliding mode controllers has been developed and tested, as shown in Figure 4.15.

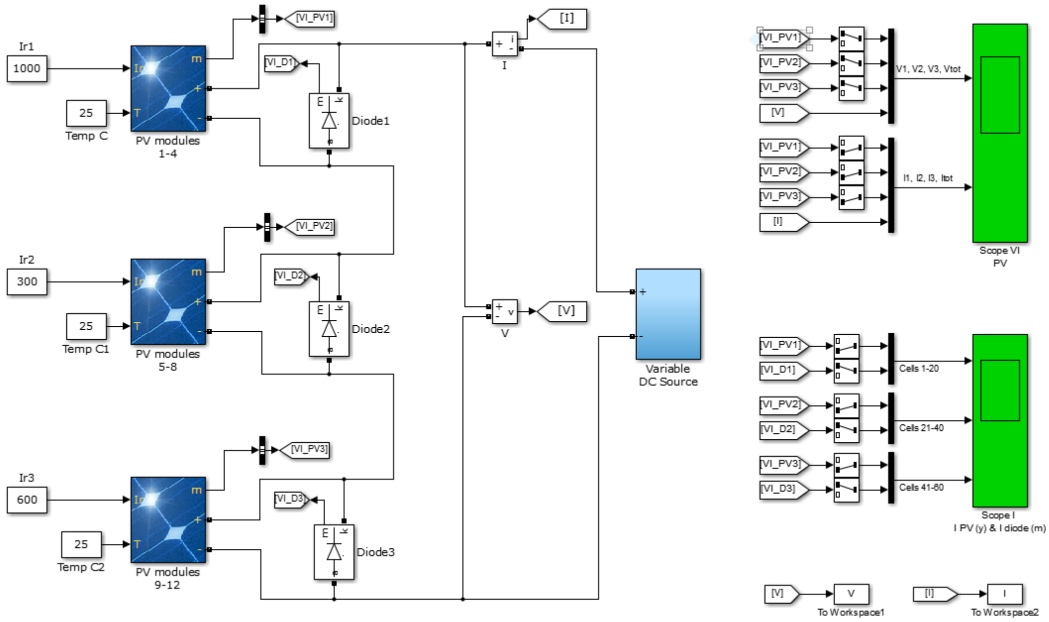

Figure 4.14: Partial shading of a PV module using Matlab

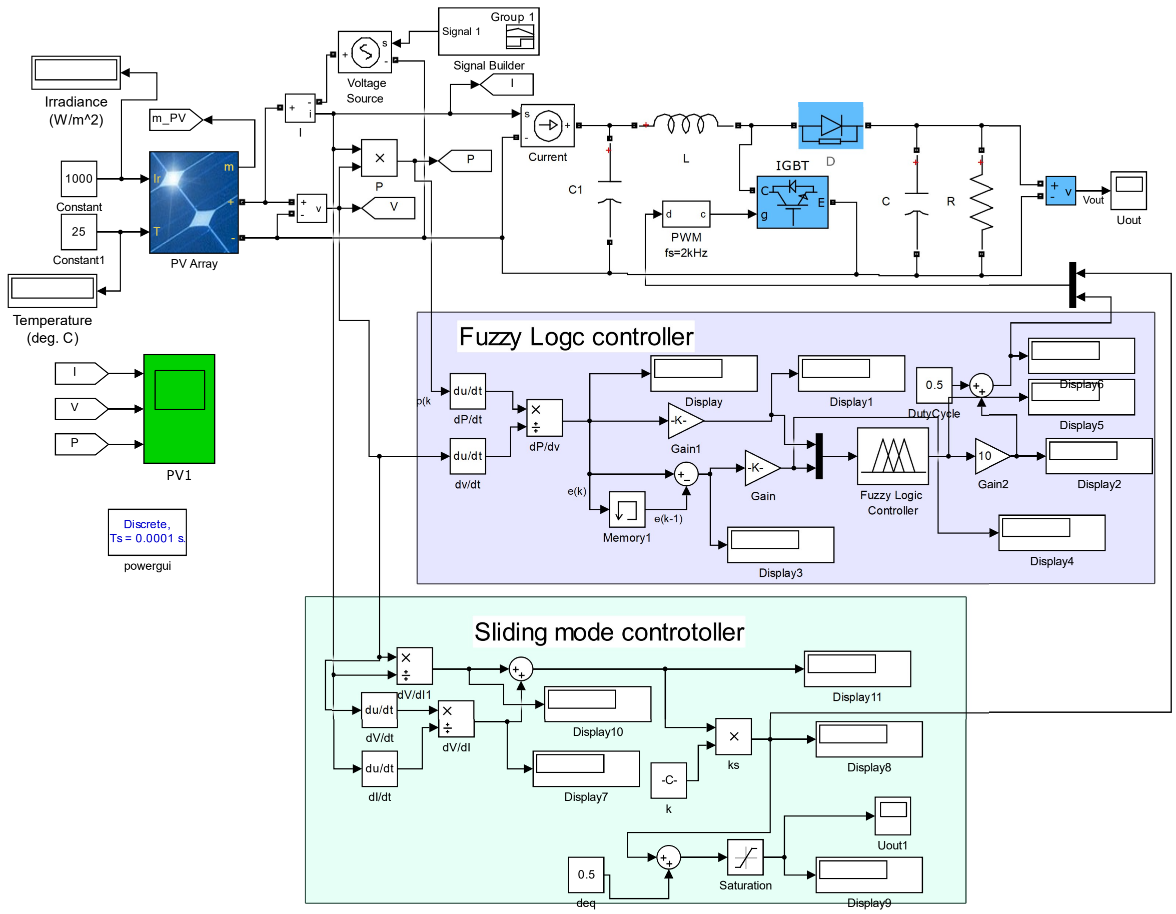

Figure 4.15: A hybrid Fuzzy Logic sliding mode Based MPPT Controller using Matlab

Chapter 5

Result Analysis and Discussion

Table 5.1 provides a summary of data for the poly-crystalline Solinc 60Wp, Kyocera KC130GT and Solinc 250Wp solar modules. The N_s, I_{sc}, I_{mpp}, V_{mpp}, P_{mpp}, and V_{oc} values for Kyocera KC130GT was extracted from the datasheet profile. However, the I_{sc}, I_{mpp}, V_{mpp}, P_{mpp}, and V_{oc} values for Solinc 60Wp and Solinc 250Wp were experimental data extracted using the Gsola XJCM-10A solar simulator as shown in Figures 5.1 and 5.2.

Table 5.1: Solinc 60Wp, Kyocera KC130GT and Solinc 250Wp photovoltaic modules data at STC

		Solar Module	
Parameters (Data Source)	Solinc 60 (Simulator)	KC130GT (Datasheet)	Solinc 250 (Simulator)
P_{mpp} (W)	61.1922	130.064	253.34
I_{mpp}(A)	3.6247	7.39	8.9389
V_{mpp}(V)	16.8821	17.6	28.342
I_{sc} (A)	3.7997	8.02	9.5006
V_{oc} (V)	21.462	21.9	36.061
N_s	36	36	60
A_o	1.6554	1.8274	1.7705
$I_{o_{opt}}$	2.851E-06	1.893E-05	1.7367E-05

The ideality factor optimal values (A_o) and saturation current optimal values ($I_{o_{opt}}$) that are also listed in Table (5.1) have been calculated using equations (3.28) and (3.16), respectively. These optimum values set the upper bound for A_o and their respective I_o and give the best replica of I_{sc}, V_{oc}, I_{mpp} and V_{mpp} points in I-V and P-V curves.

Graphical analysis of ideality factor A with respect to saturation current have been accomplished using equation (3.27) that give A_o value at the y-axis intercept as illustrated in

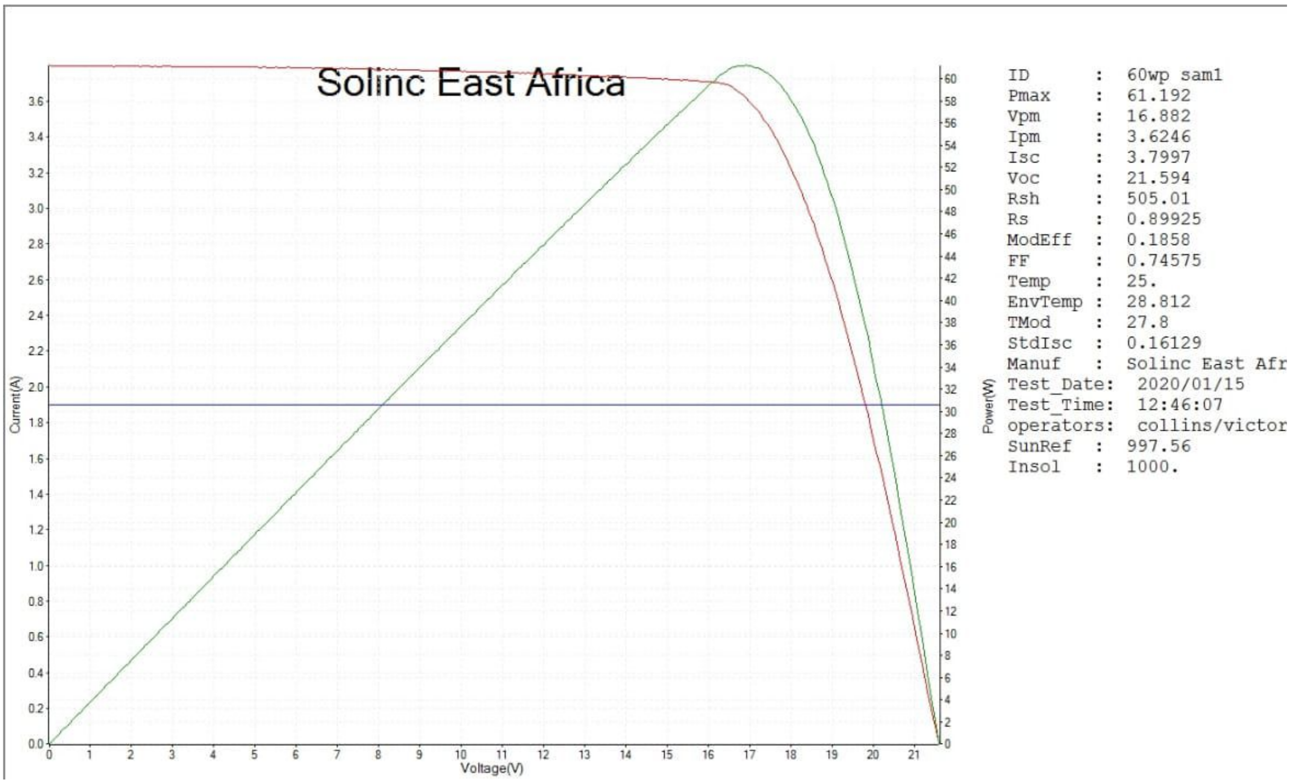

Figure 5.1: I-V and P-V curves for Solinc 60W using Gsola XJCM-10A solar simulator

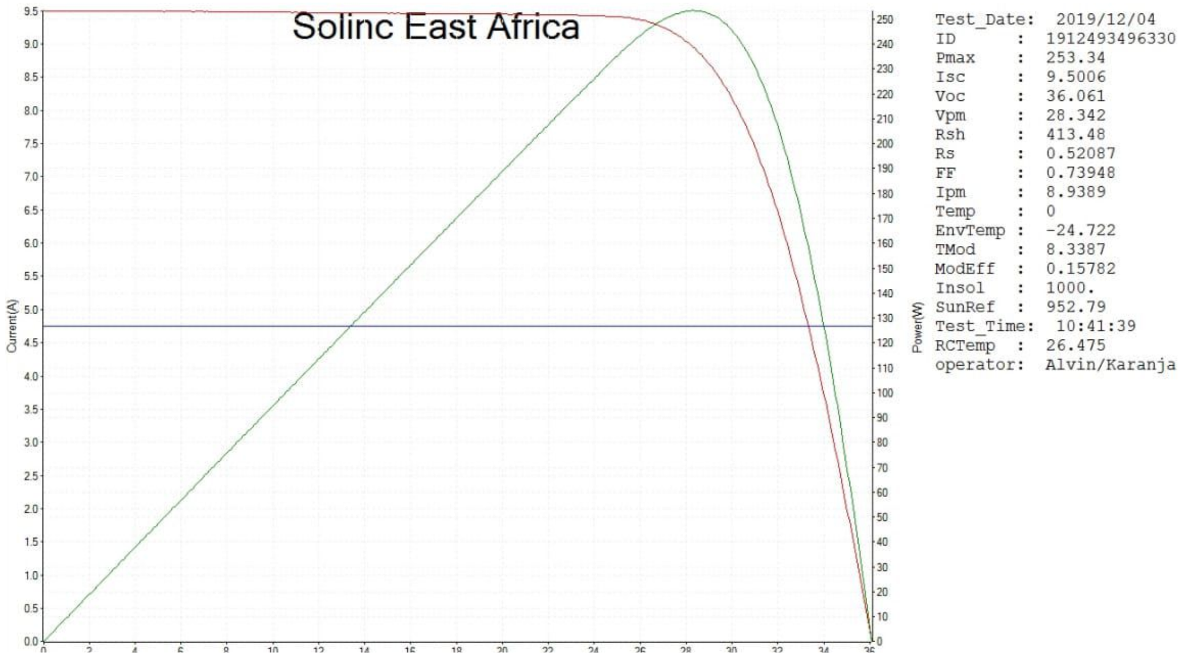

Figure 5.2: I-V and P-V curves for Solinc 250W using Gsola XJCM-10A solar simulator

Figure 5.3. The vertical-axis gives the optimal ideality factor values of 1.66, 1.83 and 1.77 for Solinc 60W, Kyocera KC130GT and Solinc 250W, respectively. These value agrees with the theoretical values shown in Table 5.1.

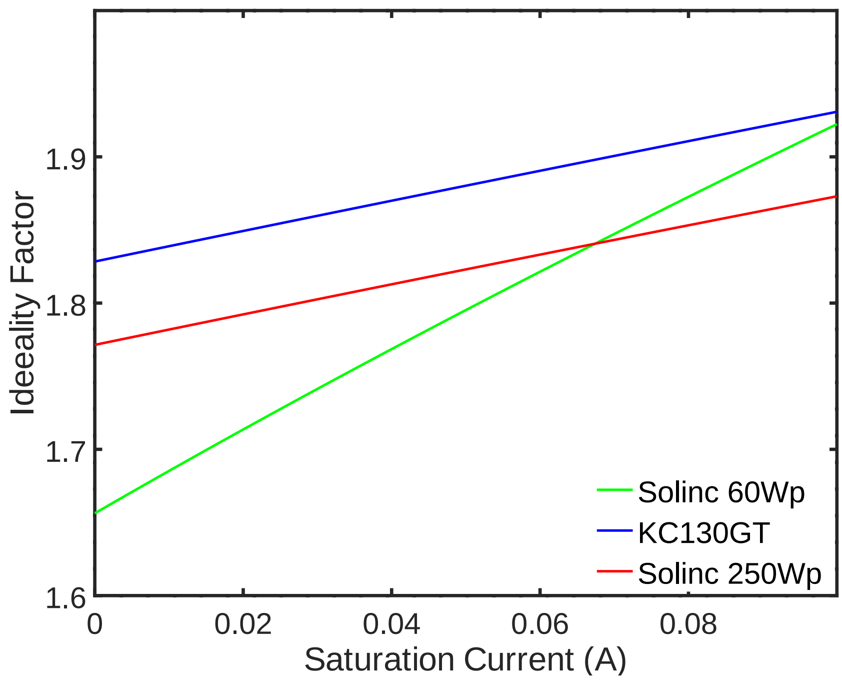

Figure 5.3: A graph of ideality factor against saturation current (A)

5.1 Extraction of five-model parameter for $A \leq A_o$

Table 5.2 gives a summary of extracted parameters for Solinc 60Wp, Kyocera KC130GT and Solinc 250Wp PV modules. The actual parameters have been extracted using algorithm shown in Figure 4.2. Figure 5.4 illustrates the relationship between R_{sh} and R_s using equation

Table 5.2: Extracted parameters for Solinc 60Wp, Kyocera KC130GT and Solinc 250Wp PV modules

Parameters	Solinc 60Wp	KC130GT	Solinc 250Wp
A	1.607	1.81	1.729
R_s	0.8998	0.2025	0.5208
R_{sh}	585.014	486.498	123.026
I_o	2.8484E-06	1.8933E-05	1.7367E-05
I_{ph}	3.8055	8.0233	9.5408
P_{mpp} (W)(Sim)	61.190	130.060	253.35
P_{mpp} (W) (expt)	61.192	130.064	253.34
Error % (W)	0.00360	0.00308	-0.00395

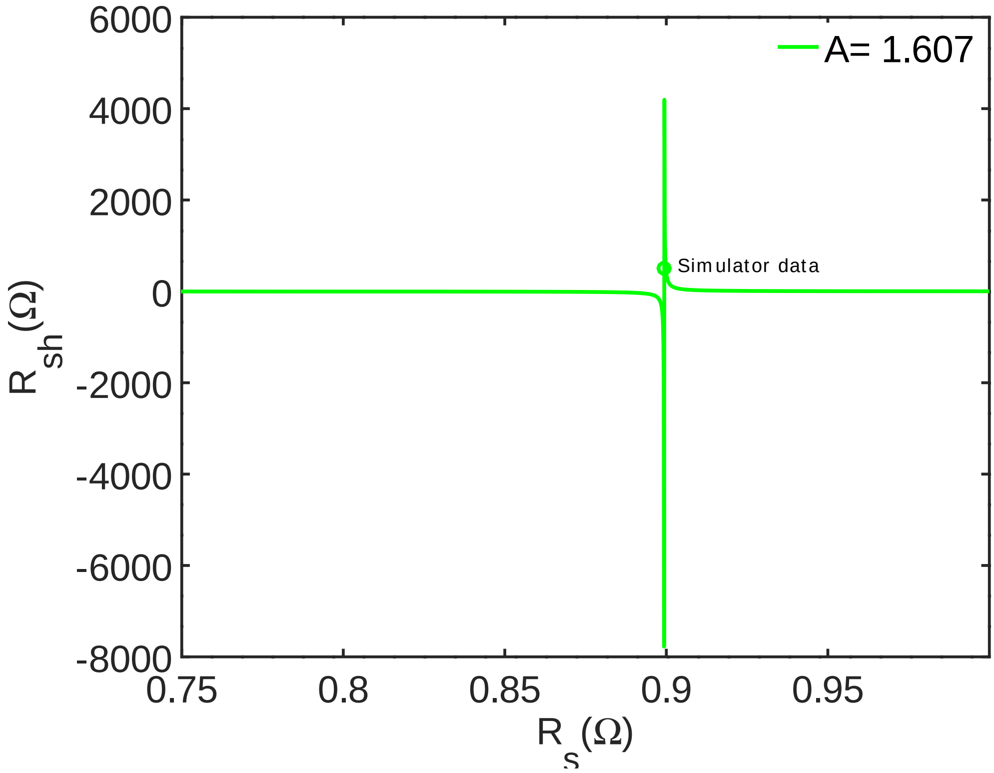

Figure 5.4: A graph of R_{sh} versus R_s for Solinc 60Wp

(3.39), for Solinc 60Wp. The ideality factor A=1.607 gives satisfactory values of $R_s = 0.8998\Omega$ and R_{sh} =585.014Ω, that are closer to the experimentally obtained results presented in Figure 5.1. The simulation has been done using arbitrarily selected range of R_s values from 0.75Ω to 1Ω. The R_s and R_{sh} data from the solar simulator has been used as the target point. From the graph, there are different values of R_s and R_{sh} pair that can be extracted in the neighborhood of solar simulator data. In Figure 5.4, R_s values below simulator data yield negative R_{sh} values.

Figure 5.5 has been plotted using KC130GT datasheet values, in which the range of R_s values have been arbitrarily selected between 0.1 to 0.3Ω. For KC130GT I-V plots, A = 1.81 produced satisfactory values of $R_s = 0.2025\Omega$ and $R_{sh} = 486.498\Omega$, respectively.

Figure 5.6 shows the R_{sh} versus R_S between 0 and 1Ω for Solinc 250Wp, where A = 1.729 provided R_s= 0.5208Ω and R_{sh} = 123.0236Ω that suit the simulator data.

The data in Table 5.2 has been used for plotting I-V and P-V curves. The curves have been plotted using GNU Octave open-source software code presented in appendix II.

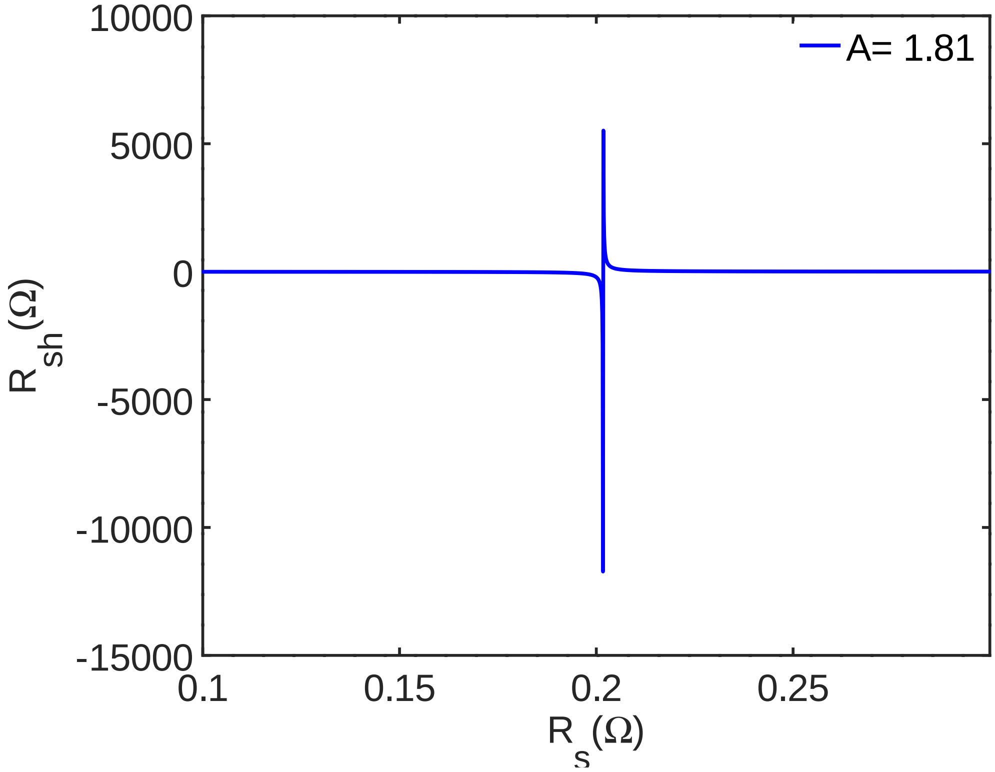

Figure 5.5: A graph of R_{sh} versus R_s for KC130GT

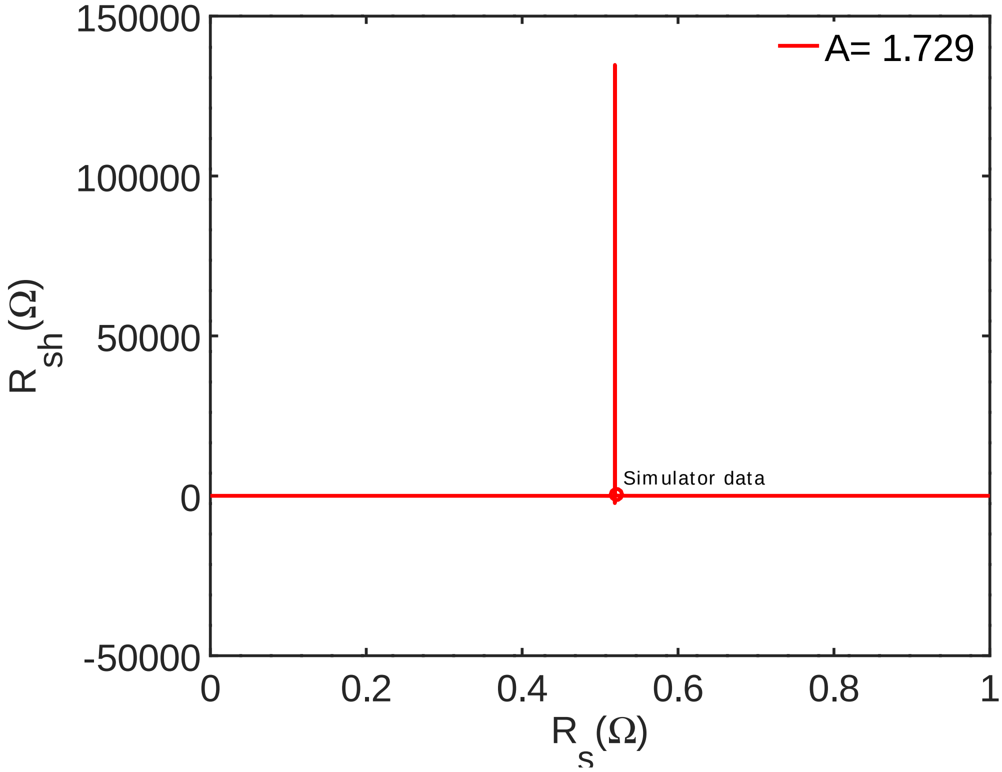

Figure 5.6: A graph of R_{sh} versus R_s for Solinc 250Wp

5.2 Analysis of I-V and P-V curves for $A \leq A_o$

Figures 5.7-5.9 display the I-V and P-V characteristic curves for Solinc 60Wp, Kyocera KC130GT and Solinc 250Wp PV modules, respectively. In both the I-V and P-V curves, the values in Tables 5.1 for A_0 and I_{opt} have been used to draw the boundary curves by assuming that $I_{ph} \approx I_{sc}$, $R_s \approx o$ and $R_{sh} \approx \infty$. However, the values in Tables 5.2 have been used to draw the best fit graphs for each PV modules.

Figure 5.7 (a) displays the I-V relationship for Solinc 60Wp, where the cardinal points (I_{sc}, P_{mpp} and V_{oc}) have been marked with small circles. The curves for ideality factors $A_o = 1.6554$ and $A = 1.607$ merge at I_{sc} but differ substantially at P_{mpp} and V_{oc} respectively. This imply that ideality factor values between 1.607 and 1.6554 provide sufficient data when implemented in algorithm of Figure 4.3. A similar observation has been made in Figure 5.7 (b) which illustrates power against voltage relationship, where the A_o and A curves converge at the starting point but differ at P_{mpp} and V_{oc}. The zoomed parts illustrates the differences at both P_{mpp} and V_{oc} points.

For Kyocera KC130GT solar module, the I-V and P-V curves shown in Figures 5.8 (a) and (b) reveal $A_o = 1.8274$ and $A = 1.81$ lines diverging at P_{mpp} and V_{oc} as illustrated by the zoomed parts. However, the two lines intersect at zero point of Figure 5.8 (b) P-V curve.

Figures 5.9 (a) and (b) display similar results for Solinc 250Wp. In the I-V curve of Figure 5.9 (a), the lines for $A_o = 1.7705$ and $A = 1.729$ converge at I_{sc} and V_{oc} but differ slightly as illustrated in the zoomed part. Likewise, the lines converge at zero point and V_{oc} in P-V curve of Figure 5.9 (b). However, the lines in both I-V and P-V graphs diverge significantly at P_{mpp}. Therefore, since the P_{mpp} from experimental data is embedded on the A_o line, while $A = 1.729$ gives reasonable R_s and R_{sh} from equation (3.39), then choosing A between $A_o = 1.7705$ and $A = 1.729$ gives acceptable results.

5.3 Extraction of five-model parameter for $A \geq A_o$

The parameters extracted for Solinc 60Wp, Kyocera KC130GT and Solinc 250Wp photovoltaic modules are given in Table 5.3 for $A \geq A_o$. Figure 5.10 shows R_{sh} against R_s graph for Solinc 60Wp. The values for R_s and R_{sh} pair, has been determined using equation (3.29),

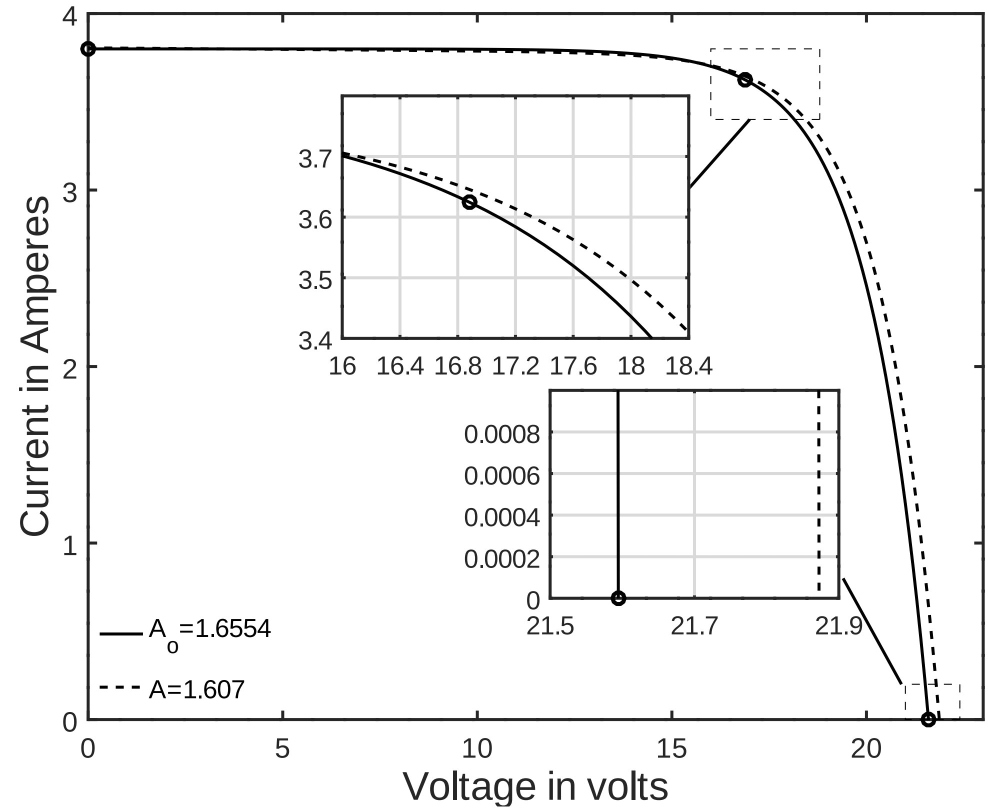

(a)

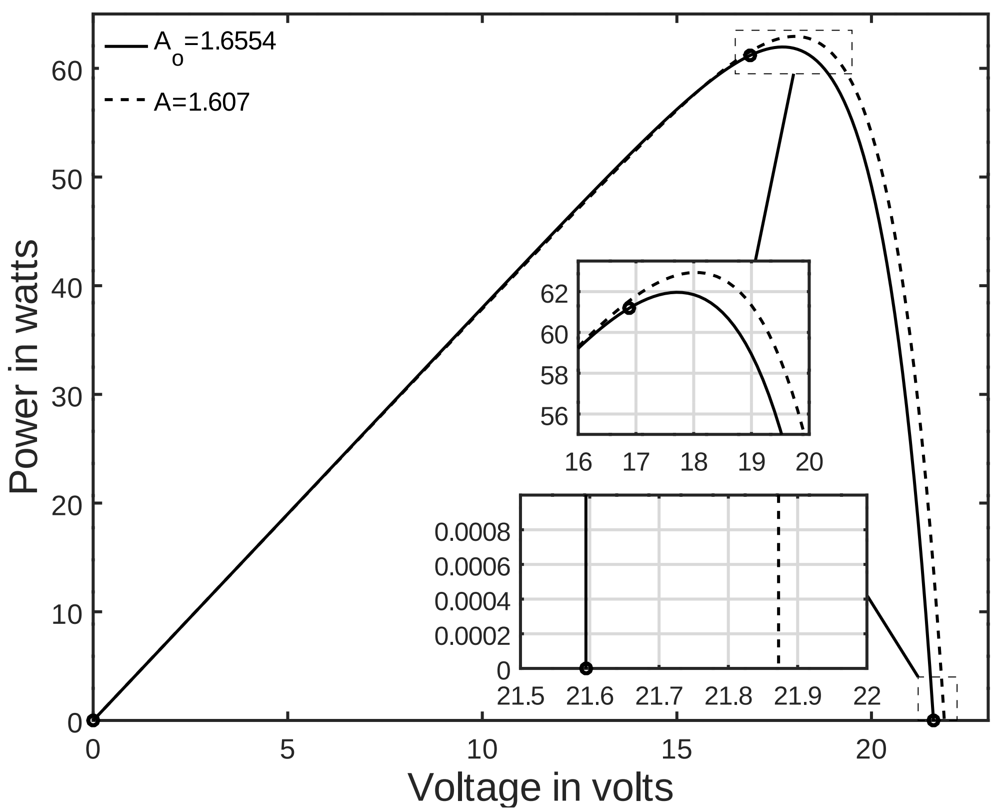

(b)

Figure 5.7: A graph of (a) current vs voltage (b) power vs voltage for Solinc 60Wp, $A \leq A_o$

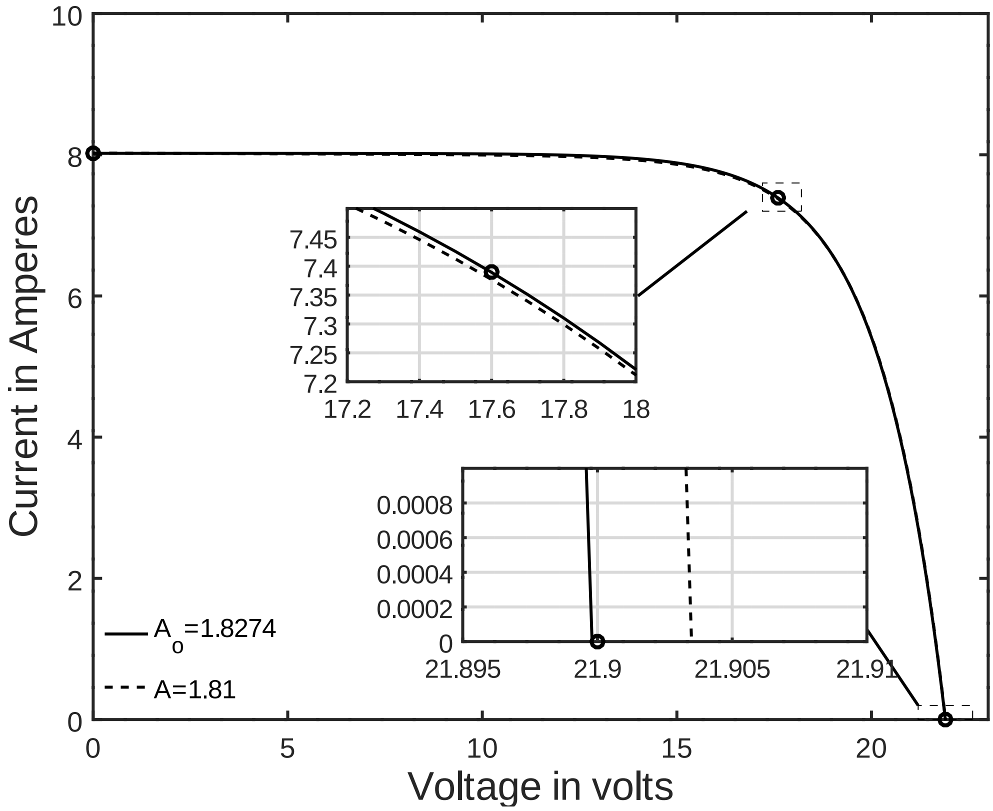

(a)

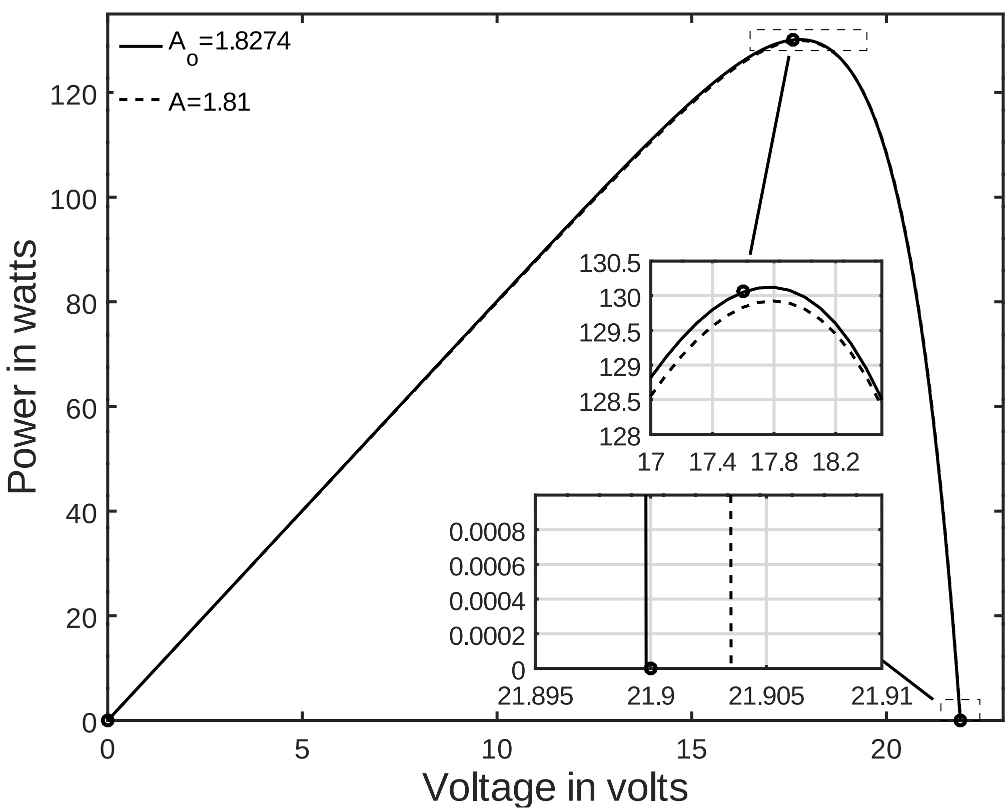

(b)

Figure 5.8: A graph of (a) current vs voltage (b) power vs voltage for KC130GT, $A \leq A_o$

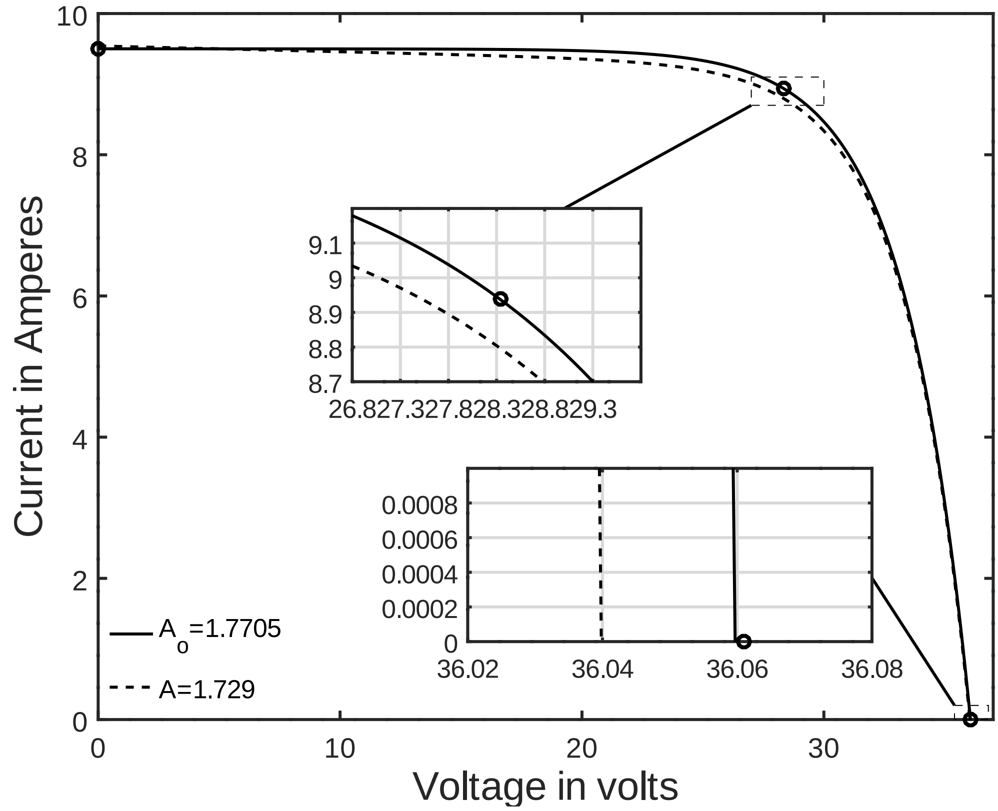

(a)

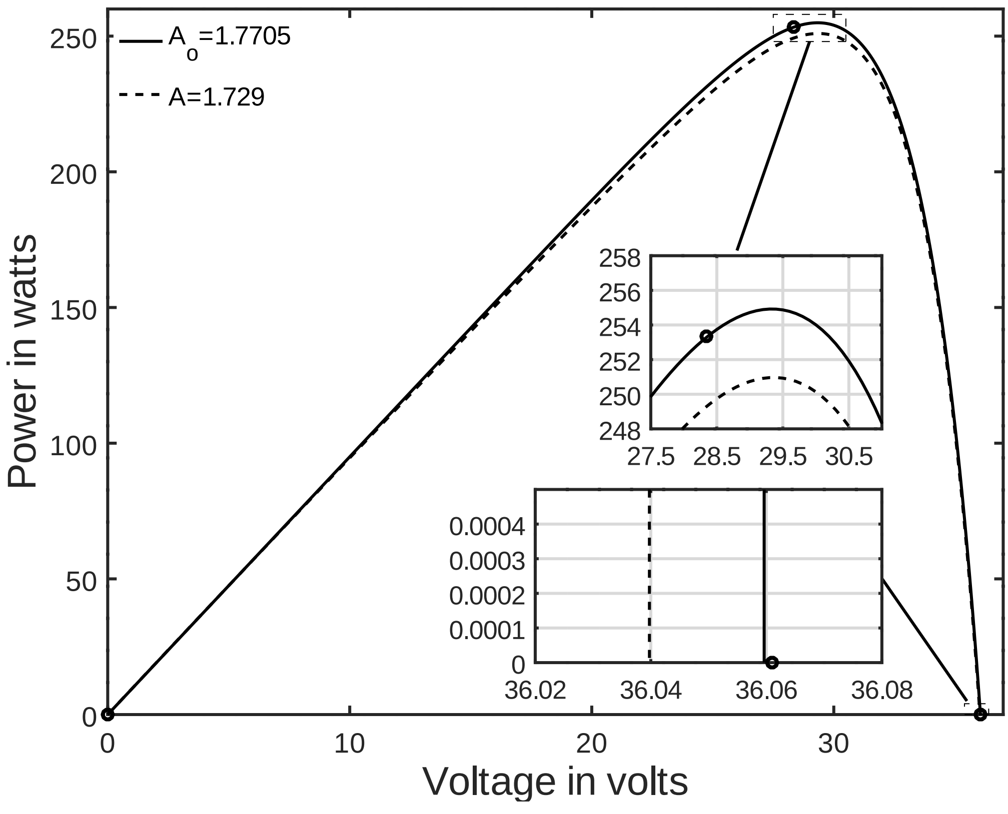

(b)

Figure 5.9: A graph of (a) current vs voltage (b) power vs voltage for Solinc 250Wp, $A \leq A_o$

while other parameters have been calculated using same equations as those used in section 5.2.

Table 5.3: Extracted parameters for Solinc 60Wp, Kyocera KC130GT and Solinc 250Wp photovoltaic modules for $A \geq A_o$

Parameters	Solinc 60Wp	KC130GT	Solinc 250Wp
A	1.978	1.98	1.92
$R_s(\Omega)$	0.8993	0.1912	0.2143
R_{sh} (Ω)	7043.3234	996.8652	349.4125
I_o (A)	2.8414E-05	5.1377E-05	4.8581E-05
I_{ph} (A)	3.8002	8.02154	9.50637
P_{mpp} (Sim)	61.193	130.060	253.350
P_{mpp} (expt)	61.192	130.064	253.340
Error % (W)	-0.00131	0.00308	-0.00395

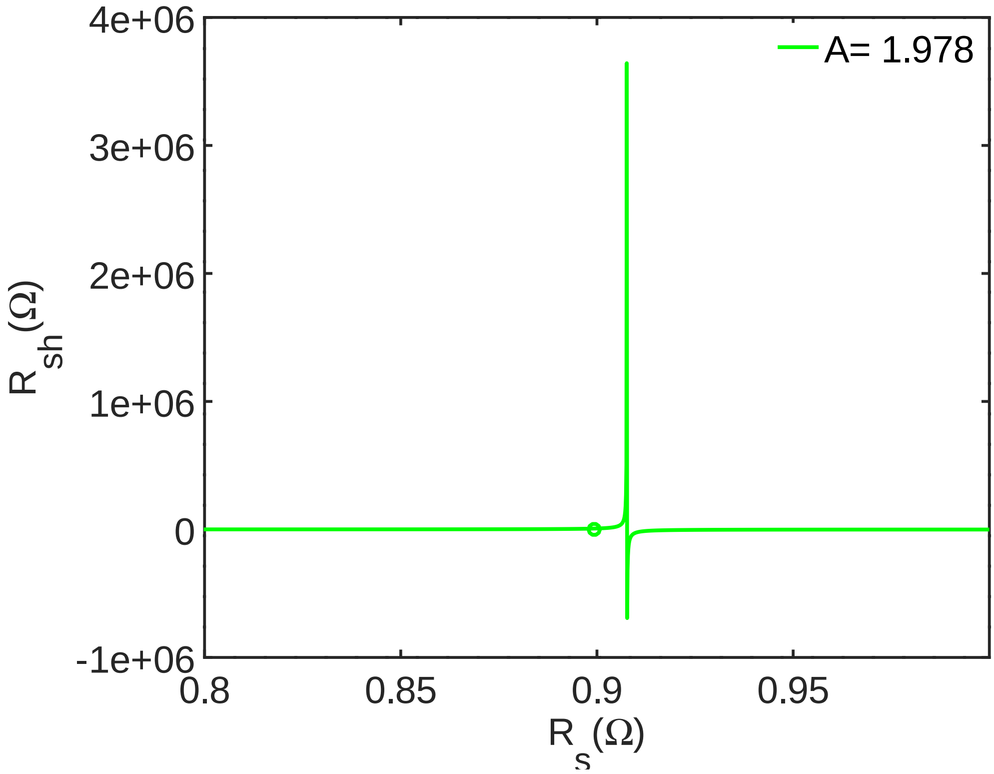

Figure 5.10: A graph of R_{sh} versus R_s for Solinc 60Wp

The ideality factor of $A = 1.978$ gives values of $R_s = 0.8993\Omega$ and $R_{sh} = 7043.323\Omega$. The simulation has been done using GNU Octave open-source software code presented in Appendix VI using arbitrarily selected R_s values from 0.8 to 1Ω. Figure 5.11 gives R_{sh} vs R_s curve for KC130GT, where the values of R_s have been chosen randomly between 0-0.4Ω. For the KC130GT parameter $A = 1.98$ provided values of $R_s = 0.1912\Omega$ and $R_{sh} = 996.865\Omega$, respectively.

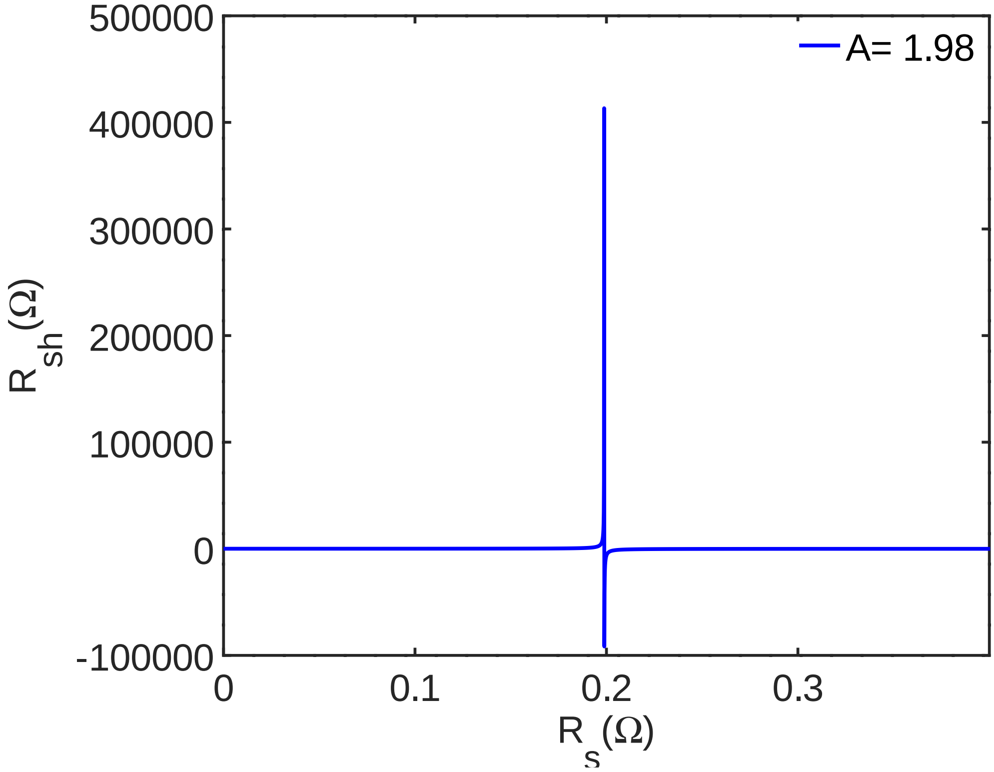

Figure 5.11: A graph of R_{sh} versus R_s for KC130GT

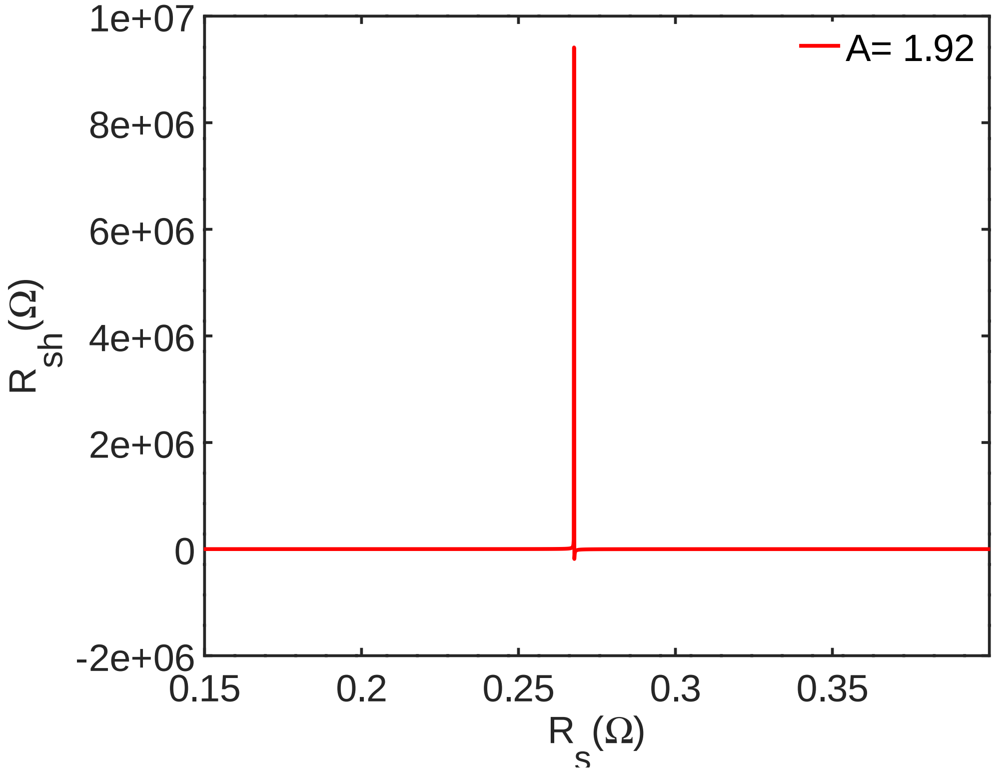

Figure 5.12: A graph of R_{sh} versus R_s for Solinc 250Wp

Figure 5.12 shows R_{sh} versus R_s for Solinc 250Wp, between 0 and 1Ω , where $A = 1.92$, $R_s = 0.2143\Omega$ and $R_{sh} = 349.413\Omega$ match the simulator results.

5.4 Analysis of I-V and P-V curves for $A \geq A_o$

Figures 5.13-5.15 show the characteristic curves for Solinc 60Wp, Kyocera KC130GT and Solinc 250Wp, respectively, for $A \geq A_o$.

The I-V curves shown in Figure 5.13 (a) and (b), for Solinc 60Wp, have been plotted using ideality factors of $A_o = 1.6554$ and $A = 1.978$. In Figure 5.13 (a) the lines representing the ideality factors $A_o = 1.6554$ and $A = 1.978$ merge only at I_{sc} but differ at P_{mpp} and V_{oc}. Similarly, in the P-V graph, the two lines meet at the starting point but differ notably at P_{mpp} and V_{oc} as illustrated in Figure 5.13 (b).

For the KC130GT PV module, the I-V and P-V curves shown in Figures 5.14 (a) and (b) consist of two lines for $A_o = 1.8274$ and $A = 1.98$ which diverge at P_{mpp}. The two lines, however, converge at both I_{sc} and V_{oc} with a small difference of 0.005V portrayed in the zoomed part.

Figures 5.15 (a) and (b) demonstrates similar results for Solinc 250Wp, where the lines for $A_o = 1.7705$ and $A = 1.92$ converge at I_{sc} and V_{oc} in I-V curve of Figure 5.15 (a) and converges at zero point and V_{oc} in P-V curve of Figure 5.15 (b). However, the lines conspicuously differ at P_{mpp} since the second live representing $A = 1.92$ has higher parasitic resistance values that reduce the output power.

5.5 Analysis of five-parameters using $0 \leq A \leq A_o$

Tables 5.4-5.6 give the five-model parameter data for Solinc 60Wp, Kyocera 130GT and Solinc 250Wp that have been obtained using four different approaches presented in algorithm 3 section 4.2.4. In addition, the simulated output power and errors are also reported in Tables 5.4-5.6 that represent how much the model's data deviate from the solar simulator's data shown in Figures 5.1 and 5.2. The following sections address the most feasible outcomes of the five-model parameters and provide more practical evidence for each approach that matches experimental results. Four approaches are listed here because they offer small percentage error.

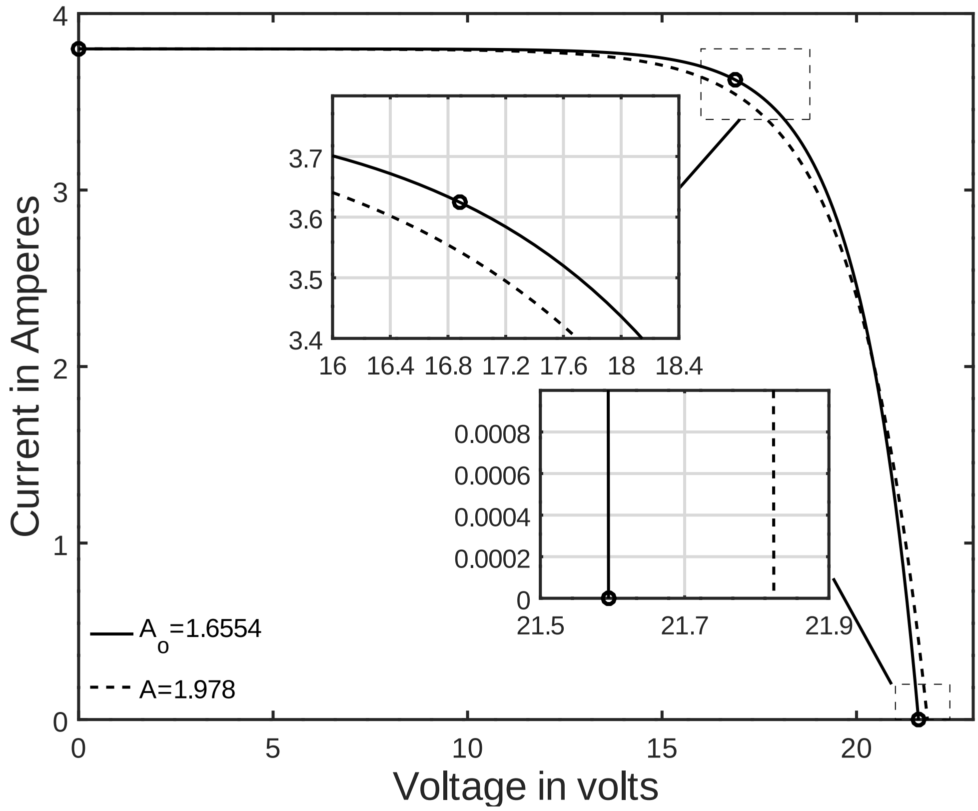

(a)

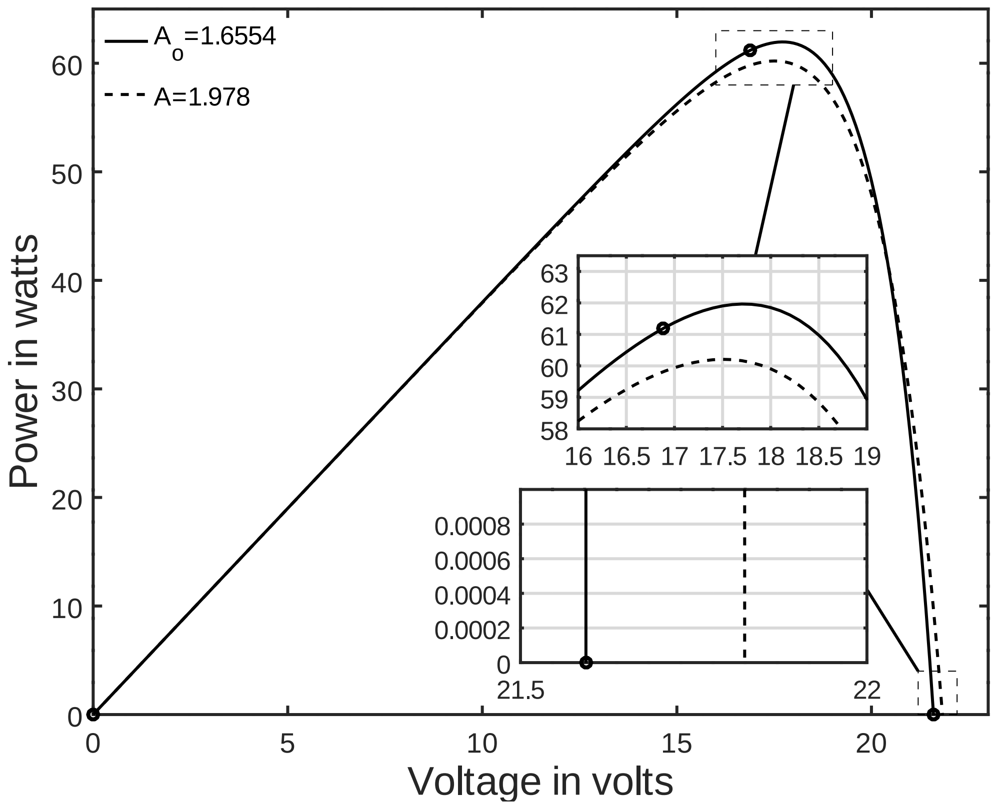

(b)

Figure 5.13: A graph of (a) current vs voltage (b) power vs voltage for Solinc 60Wp for $A \geq A_o$

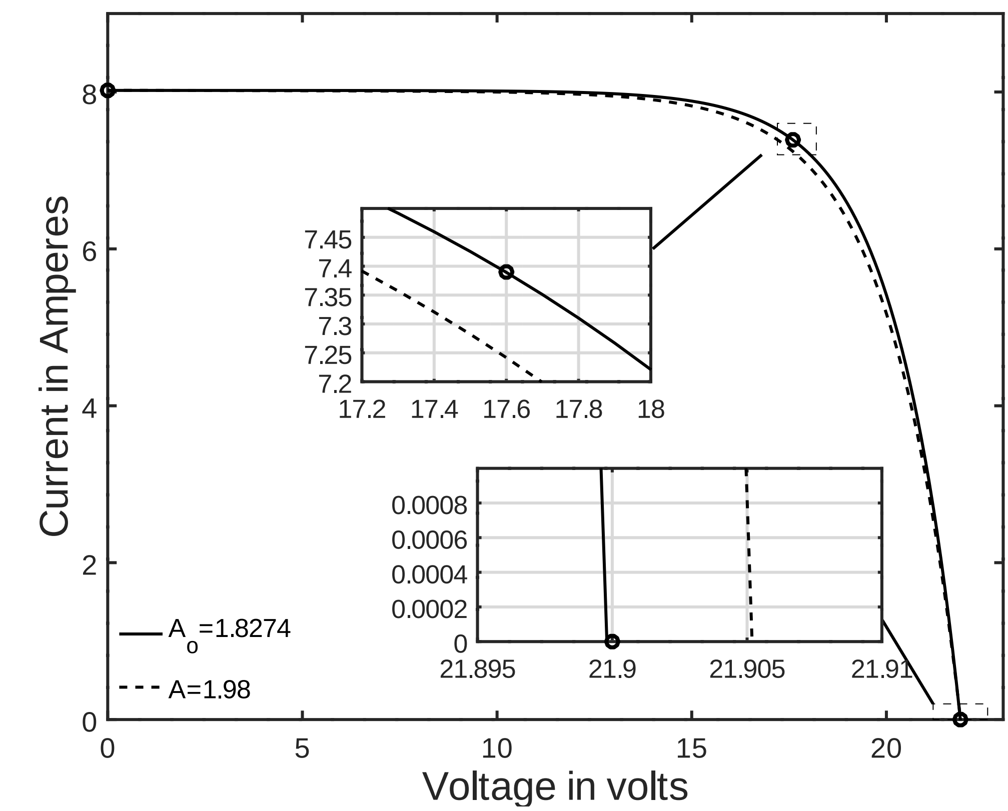

(a)

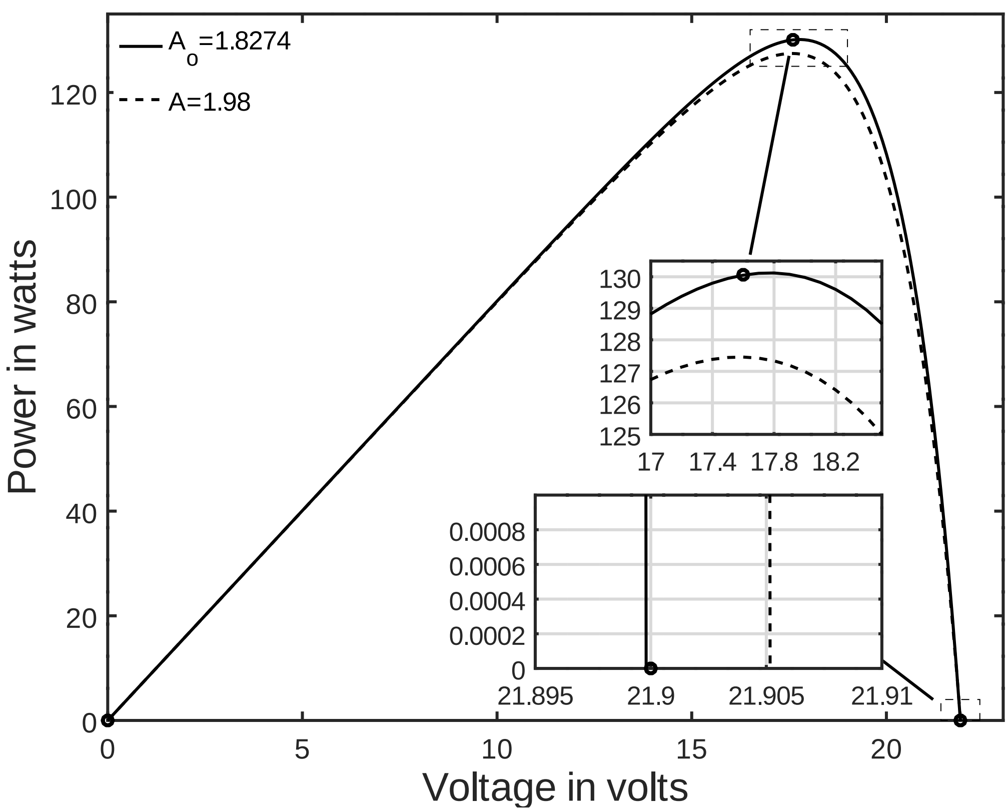

(b)

Figure 5.14: A graph of (a) current vs voltage (b) power vs voltage for KC130GT for $A \geq A_o$

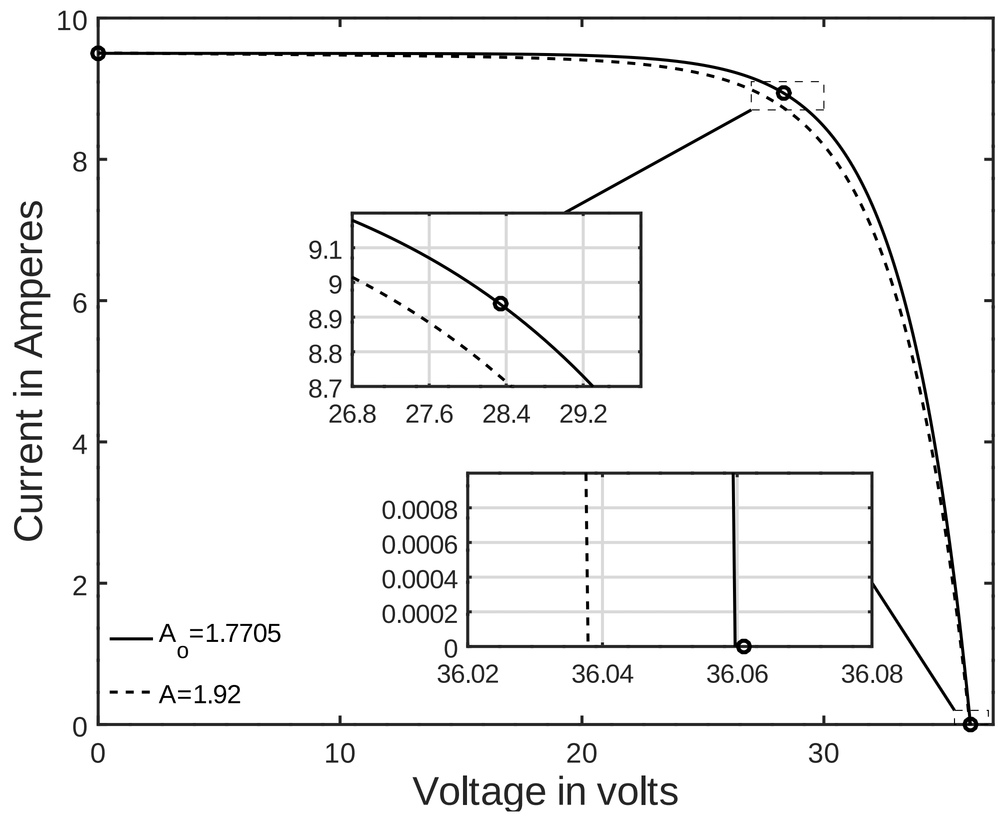

(a)

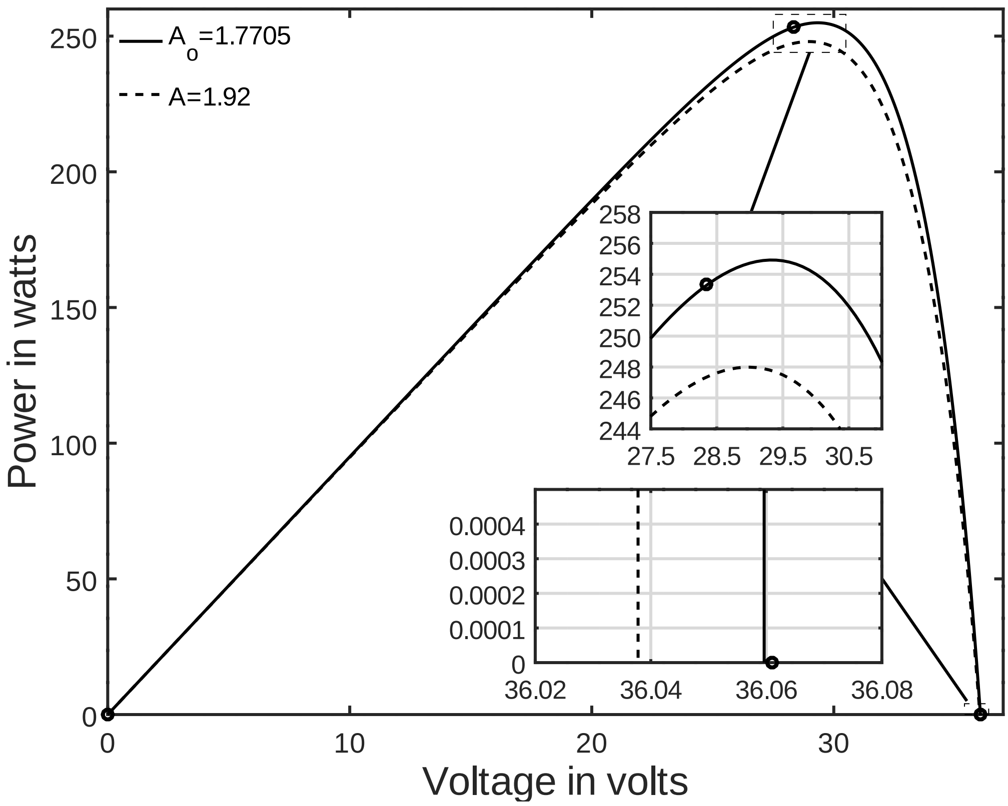

(b)

Figure 5.15: A graph of (a) current vs voltage (b) power vs voltage for Solinc 250Wp for $A \geq A_o$

Approach 1

The data shown in the Tables 5.4-5.6 in rows 2-6 summarizes the A, I_{ph}, R_s, R_{sh} and I_o extracted parameters, while rows 7-10 give the P_{mpp} data from the simulator and model in algorithm 3 and the errors. Approach 1 data are presented in column 1 based on open and short circuit points, where I_o is determined using equations (3.13), (3.15) or (3.23). This approach gives credible [Rs, Rsh] pair from equation (3.29), when compared to the data obtained from solar simulator as shown in Figures 5.1 and 5.2.

Approach 2

The data shown in Tables 5.4-5.6 in column 2, have been extracted using approach 2 data where I_o has been calculated using either equations (3.14) or (3.16) that are independent of R_s, R_{sh} pair. This approach gives satisfactory [R_s, R_{sh}] pair from equations (3.29), (3.30) (3.31), (3.32) and (3.38).

Approach 3

Again, the data shown in Tables 5.4-5.6 in column 3 have been obtained using approach 3 where I_o is determined using equation (3.19). This approach gives satisfactory [R_s, R_{sh}] pair only from equations (3.29), (3.30), (3.31) and (3.38).

Approach 4

The fourth approach data is listed in column 4 o f Tables 5.4 and 5.6 for Solinc 60Wp, KC130GT and Solinc 250Wp. In this case, I_o is determined using equation (3.20) that is independent of R_s, R_{sh} pair. This approach gives satisfactory [R_s, R_{sh}] pair only from equations (3.29), (3.30), (3.31) and (3.38).

Tables 5.4 - 5.6 give the extracted parameters and simulated data for Solinc 60Wp, KC130GT and Solinc 250Wp, respectively. The four approaches give appropriate percentage error for output power of less than 0.1 percent. The fourth method gives the least error of 0.0261 percent for Solinc 60Wp shown in Table 5.4 and 0.0479 % shown in Table 5.5 for KC130GT. However, the second approach gives the least output power error of 0.000042% for Solinc 250Wp. These data have been used to plot the I-V and P-V curves shown in Figures 5.14 - 5.16.

Table 5.4: Extracted parameters and simulated Data for Solinc 60Wp

Parameters	Approach 1	Approach 2	Approach 3	Approach 4
A	0.5	0.5	0.5	0.5
$I_{ph}(A)$	3.8109	3.8096	3.8099	3.8108
$R_s(\Omega)$	0.8893	0.8893	0.8893	0.8893
$R_{sh}(\Omega)$	546.399	607.297	582.141	487.236
$I_o(A)$	1.9657E-20	1.9974E-20	1.9821E-20	1.91E-20
$P_{mpp}(W)$ (Simulator)	61.1925	61.1925	61.1925	61.1925
$P_{mpp}(W)$(model)	61.2122	61.2142	61.2132	61.2085
Error	0.0197	0.0216	0.0207	0.0160
ΔP_{mpp} Error	0.0322	0.0353	0.0338	0.0261

Table 5.5: Extracted parameters and simulated data for KC130GT

Parameters	Approach 1	Approach 2	Approach 3	Approach 4
A	1.14	1.14	1.14	1.14
$I_{ph}(A)$	8.033278	8.028423	8.029375	8.031727
$R_s(\Omega)$	0.2112	0.2112	0.2112	0.2112
$R_{sh}(\Omega)$	329.701	462.108	413.603	233.151
$I_o(A)$	7.5054E-09	7.6567E-09	7.6066E-09	7.1768E-09
$P_{mpp}(W)$ (Simulator)	130.064	130.064	130.064	130.064
$P_{mpp}(W)$(model)	130.162	130.200	130.187	130.126
Error	0.0978	0.1364	0.1235	0.0623
ΔP_{mpp} Error	0.0752	0.1049	0.0950	0.0479

Table 5.6: Extracted parameters and simulated data for Solinc 250Wp

Parameters	Approach 1	Approach 2	Approach 3	Approach 4
A	0.6	0.6	0.6	0.6
$I_{ph}(A)$	9.5513	9.6003	9.6003	9.5509
$R_s(\Omega)$	0.5209	0.5208	0.5208	0.5209
$R_{sh}(\Omega)$	118.888	104.652	101.279	115.392
$I_o(A)$	1.073500E-16	1.110780E-16	1.077090E-16	1.045360E-16
$P_{mpp}(W)$ (Simulator)	253.3463	253.3463	253.3463	253.3463
$P_{mpp}(W)$(model)	253.3466	253.3464	253.3465	253.3535
Error	0.000255	0.000106	0.000165	0.007146
ΔP_{mpp} Error	0.000101	0.000042	0.000065	0.002821

5.6 Comparison of extracted parameters with other approaches in literature for KC130GT

The results obtained using the three analytical methods presented in this work has been compared with the results published by Orioli and Di Gangi (2013), Kler *et al.* (2018) and Zaimi *et al.* (2019) for KC130GT. Compared to other reported methods, the extracted parameters shown in the Table 5.7 provide satisfactory results for R_s and I_{ph}. However, other parameters differ due to the variation in approaches of evaluating the ideality factor.

Table 5.7: Extracted parameters and simulated data for KC130GT

Parameter	A	I_{ph}(A)	$R_s\Omega$	$R_{sh}\Omega$	I_o(A)
Method 1 $A \leq A_O$	1.81	8.0233	0.2025	486.498	1.6710E-05
Method 2 $A \geq A_o$	1.98	8.0215	0.1912	996.865	5.1377E-05
Method 3 $0 \leq A \leq A_o$	1.14	8.0333	0.2112	329.701	7.5054E-09
Orioli and Di Gangi (2013) method	1.35	8.02	0.35	84.000	7.0700E-09
Kler *et al.* (2018) method	1.0352	8.0390	0.206	86.978	9.0742E-10
Zaimi *et al.* (2019) Method	1.036	8.0317	0.16902	116.979	9.3085E-10

5.7 I-V and P-V curves for Solinc 60Wp, KC130GT and Solinc 250Wp modules using the four approaches

Figure 5.16 (a) displays the current-voltage relationship for Solinc 60Wp, where the zoomed sections demonstrate the four approaches at short circuit point, maximum power point and open circuit point. The curves converge at maximum power point but vary significantly at short circuit point and at open circuit point. Figure 5.16 (b) shows the P-V curve for Solinc 60Wp.

Figure 5.17 (a) and (b) show the I-V and P-V relationships for KC130GT, where the zoomed parts also display the variances of the four approaches at the cardinal points. The curves converge at the maximum power point but differ at other points.

Figure 5.18 (a) and (b) display the I-V and P-V curves for Solinc 250Wp, where the zoomed parts also show the differences between the four approaches at short circuit and open circuit. However, the curves converge remarkably at the maximum power.

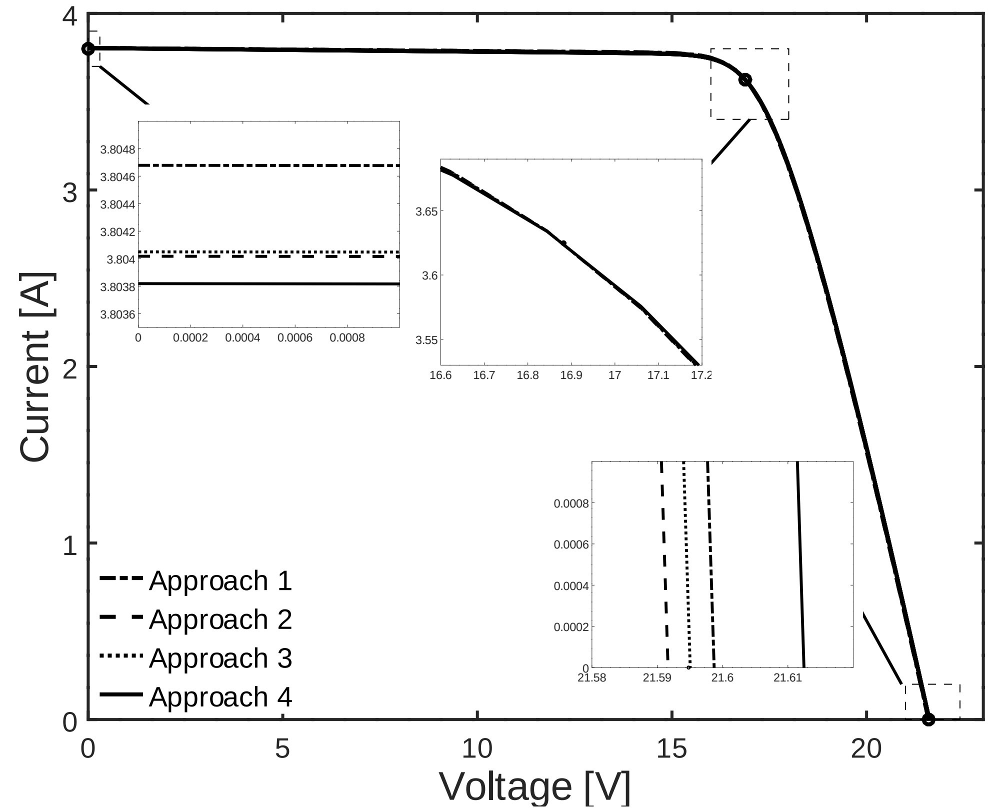

(a)

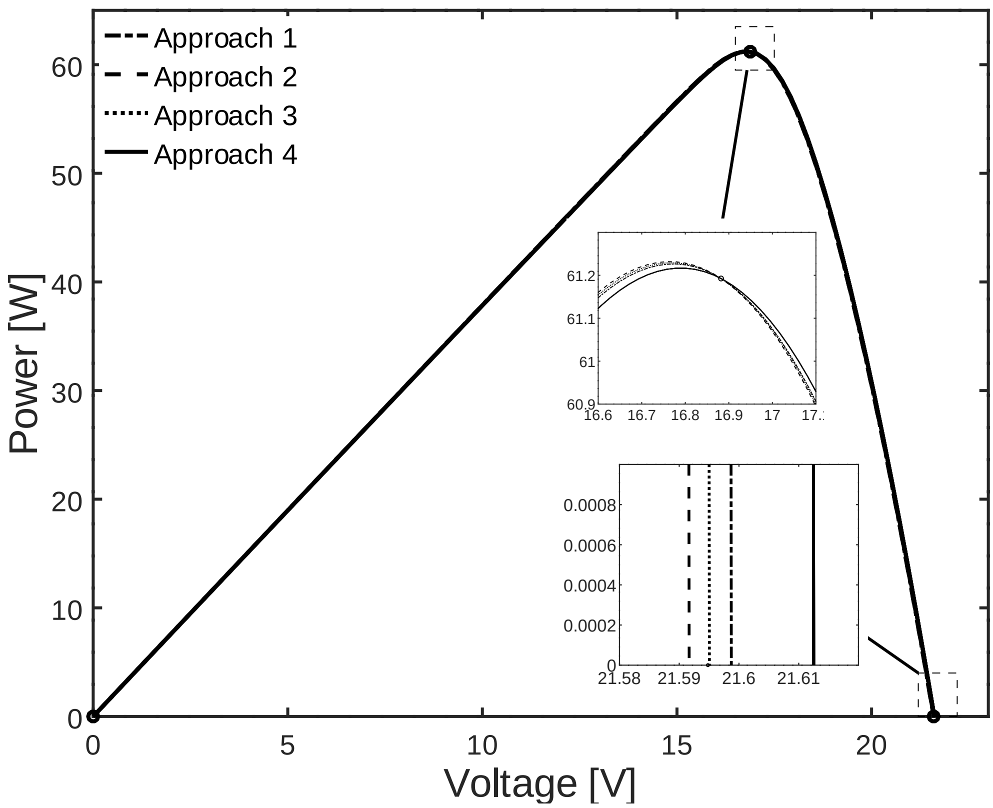

(b)

Figure 5.16: A graph of (a) current vs voltage (b) power vs voltage for Solinc 60Wp, $0 \leq A \leq A_o$

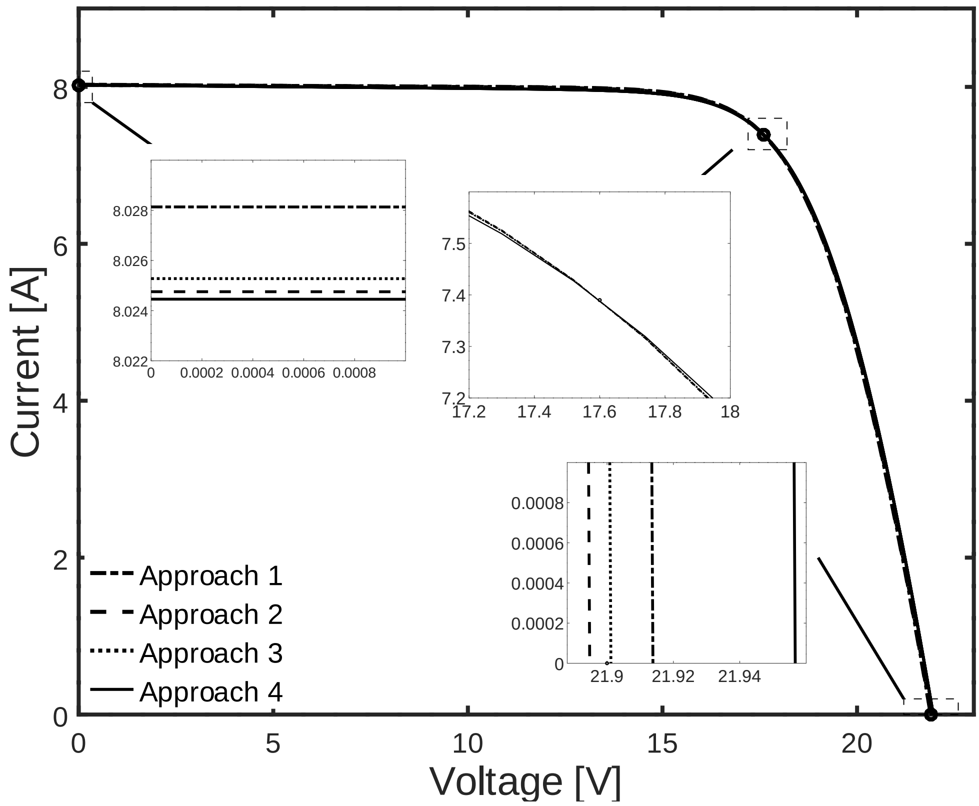

(a)

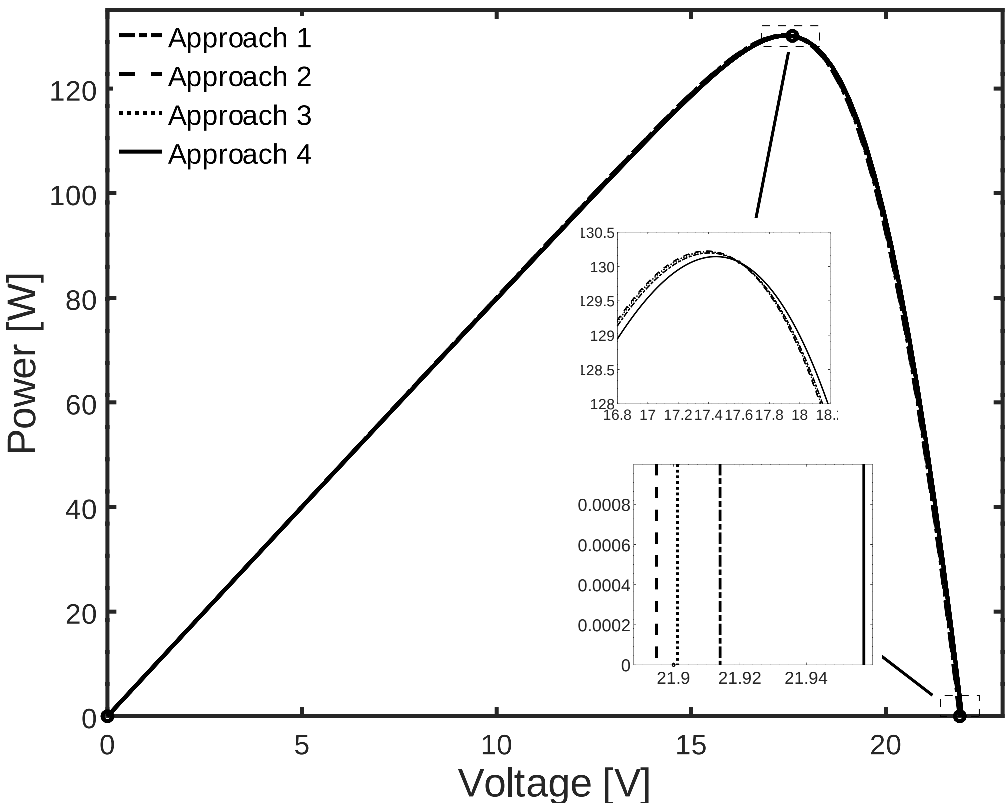

(b)

Figure 5.17: A graph of (a) current vs voltage (b) power vs voltage for KC130GT, $0 \leq A \leq A_o$

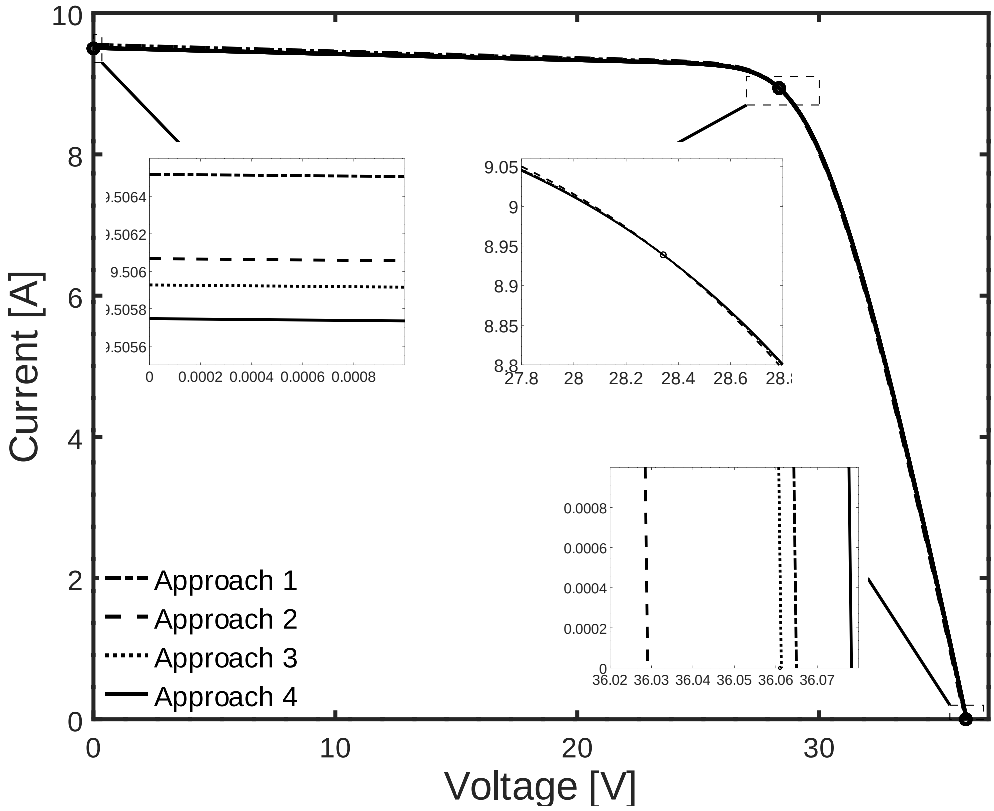

(a)

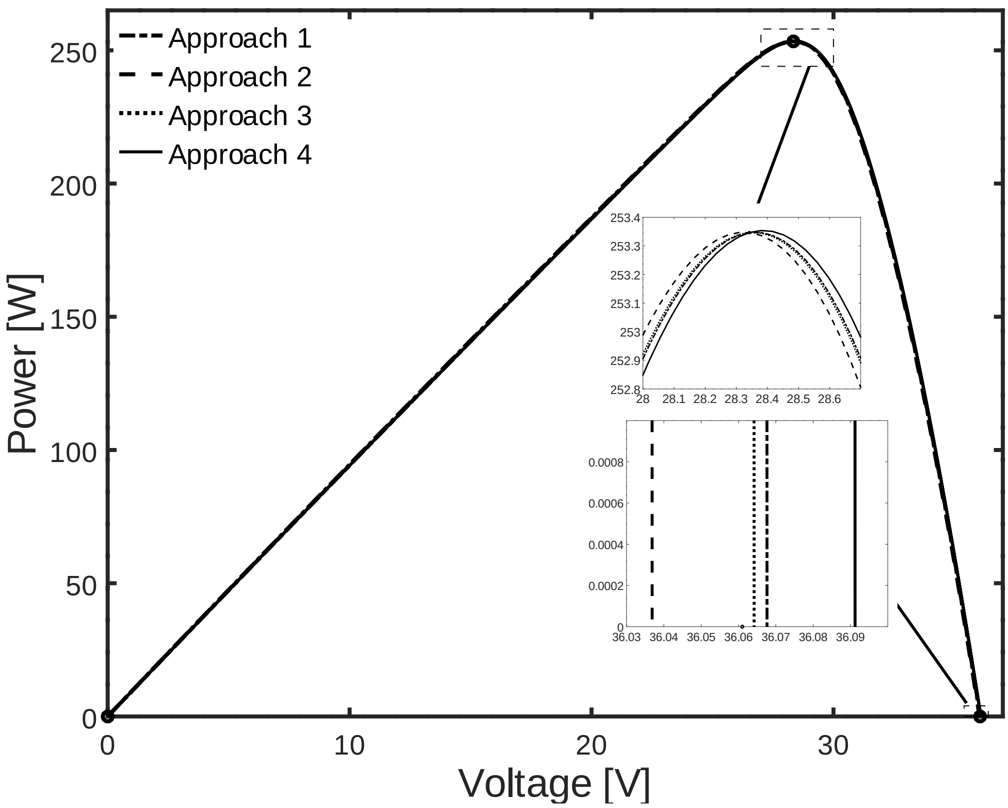

(b)

Figure 5.18: A graph of (a) current vs voltage (b) power vs voltage for Solinc 250Wp, $0 \leq A \leq A_o$

5.8 I-V and P-V characterization at ambient temperature, NOCT and actual irradiance

The Kyocera KC130GT has the ISO / IEC specification and has been selected to demonstrate the effects of irradiance and temperature on a single diode model's key parameters. The datasheet gives temperature coefficient of V_{oc} as -0.0821$V/^oC$ and temperature coefficient of I_{sc} as -0.00318$A/^oC$, that have been used as starting conditions to evaluate other parameters at various irradiances and temperatures.

Table 5.8 contains the calculated parameters and simulated values for the three cardinal point at irradiance of 200, 400 , 600, 800 and 1000W/m^2. These values have been extracted using equations (3.50) to (3.60) and have been applied to plot I-V and P-V curves at various irradiance as shown in Figures 5.19 and 5.20. The simulated values for I_{sc}, I_{mpp}, V_{mpp}, and V_{oc} at 800 and 1000W/m^2 match the datasheet values and all values at 200, 400 , 600, 800 and 1000W/m^2 a agrees with the values reported by Zaimi *et al.* (2019).

Table 5.9 give the calculated parameters and simulated values for the three cardinal point at different temperatures of 20, 25 , 30, 35 and 50^oC. These values have also been applied to plot I-V and P-V curves at various temperatures shown in Figures 5.21 and 5.22.

Table 5.8: Simulated data and extracted parameters values for KC130GT at air temperature of 20^oC and NOCT of 47^oC and different irradiance levels

Irradiance (W/m^2)	1000	800	600	400	200
I_{sc} (A)	8.0900	6.4720	4.8540	3.2360	1.6180
I_{mpp} (A)	7.420	5.936	4.452	2.968	1.484
V_{mpp} (V)	15.748	15.451	15.068	14.528	13.606
V_{oc} (V)	20.268	19.971	19.588	19.049	18.126
A	1.34	1.32	1.29	1.26	1.1
I_o (A)	1.968E-06	1.567E-06	1.112E-06	7.930E-07	1.008E-07
I_{ph} (A)	8.096	6.518	4.894	3.239	1.637
R_s (Ω)	0.158	0.201	0.301	0.362	1.151
R_{sh} (Ω)	756.718	234.393	447.274	890.984	516.337
P_{mpp} (W)	116.845	91.712	67.079	43.887	20.190
$\mathrm{P_{mpp}}$ (W)(sim)	116.842	91.711	67.078	43.881	20.190
Error	0.003173	0.000625	0.000669	0.005988	0.000138
$\Delta P_{mpp}\%$	0.00272	0.00068	0.00100	0.01364	0.00068

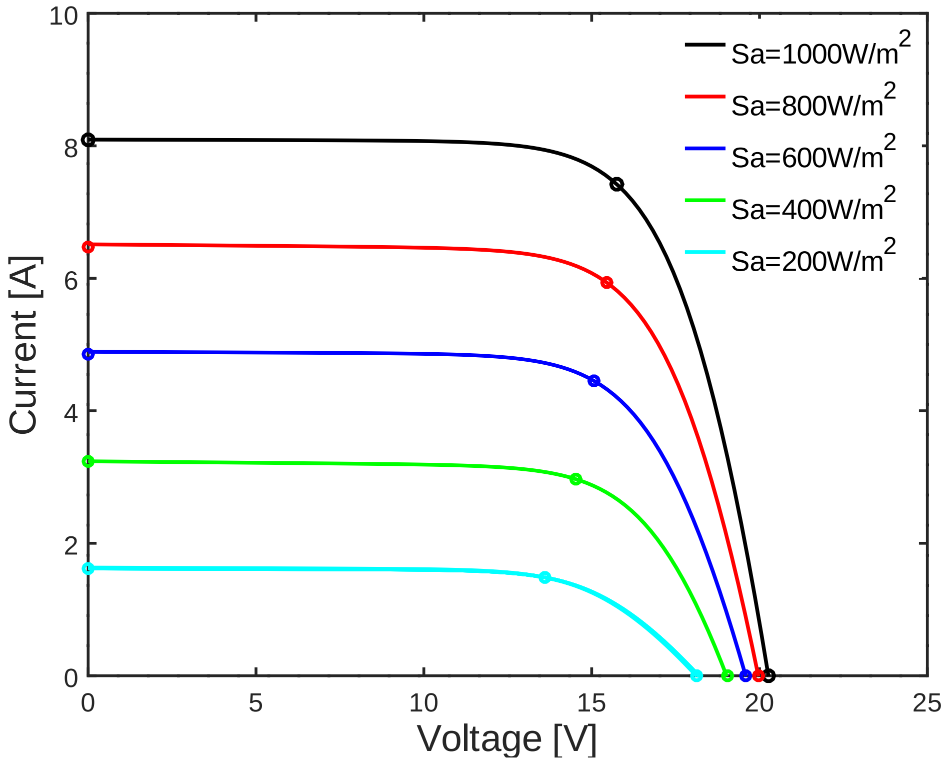

.

Figure 5.19: A graph of current versus voltage for KC130GT at different irradiance levels

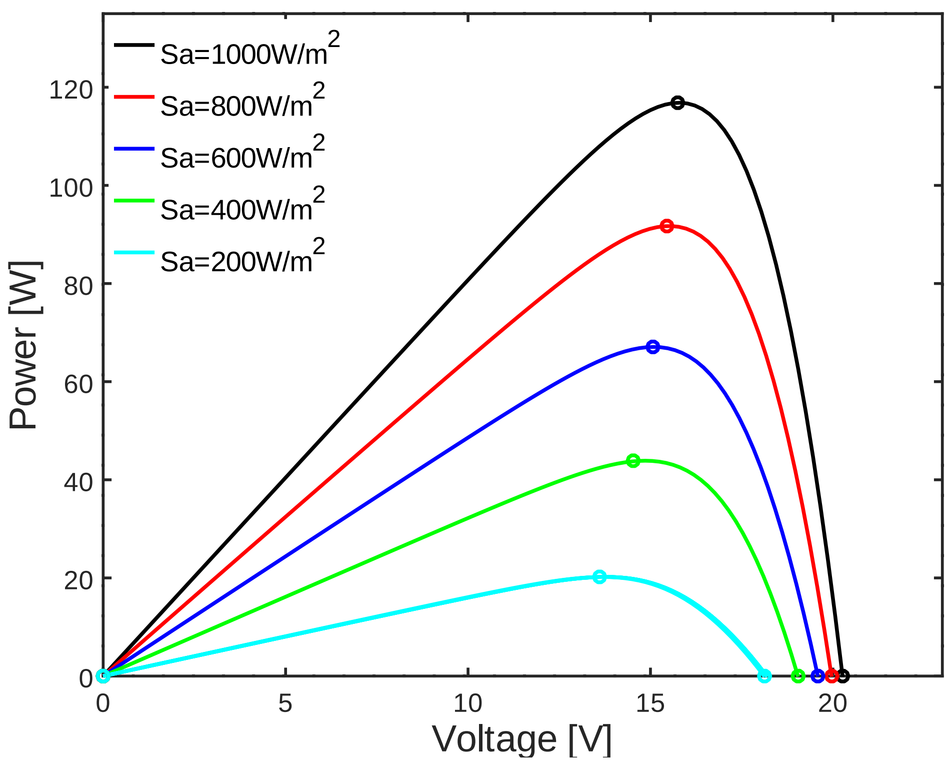

.

Figure 5.20: A graph of power versus voltage for KC130GT at different irradiance levels

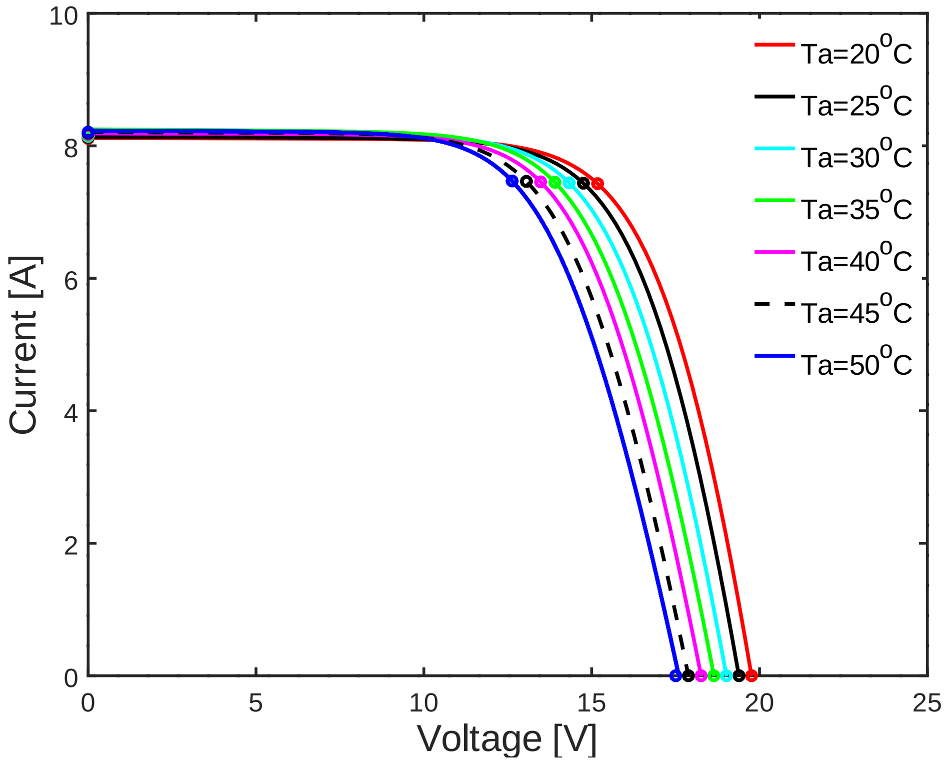

.

Figure 5.21: A graph of current versus voltage for KC130GT showing various temperatures curves at $1000W/m^2$

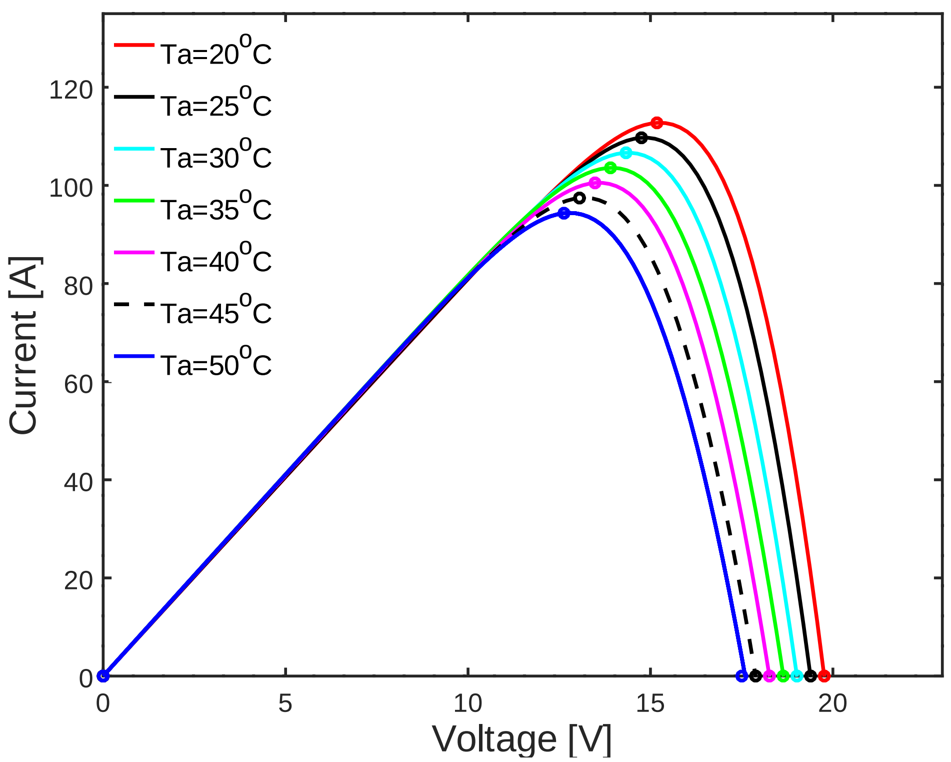

.

Figure 5.22: A graph of power versus voltage for KC130GT showing various temperatures curves at $1000W/m^2$

Table 5.9: Simulated data and extracted model parameters values for KC130GT photovoltaic module at various air and NOCT temperatures for $1000W/m^2$ irradiance level

Temperature (^oC)	20	25	30	35	40	45	50
NOCT (^oC)	53.75	58.75	63.75	68.75	73.75	78.75	83.75
T (Kelvin)	326.9	331.9	336.9	341.9	346.9	351.9	356.9
I_{sc} (A)	8.1114	8.1273	8.1432	8.1591	8.1750	8.1909	8.2068
I_{mpp} (A)	7.4288	7.4356	7.4423	7.4491	7.4558	7.4626	7.4693
V_{mpp} (V)	15.177	14.754	14.330	13.905	13.480	13.055	12.629
V_{oc} (V)	19.764	19.389	19.014	18.638	18.261	17.883	17.504
A	1.33	1.3	1.29	1.27	1.22	1.21	1.18
I_o $(A)(\times 10^{-6})$	3.5102	3.3329	3.9687	4.2352	3.1804	3.8383	3.3742
I_{ph} (A)	8.1176	8.1357	8.2258	8.255	8.1895	8.2079	8.2289
R_s (Ω)	0.165	0.182	0.202	0.224	0.237	0.248	0.279
R_{sh} (Ω)	928.065	625.585	234.484	309.163	832.145	691.047	666.96
P_{mpp} (W)	112.7463	109.7048	106.6482	103.5797	100.5042	97.4242	94.33
$\mathrm{P_{mpp}}$ (W)(sim)	112.7598	109.7099	106.6482	103.5799	100.5208	97.4693	94.393
Error	0.0134	0.0050	0.000016	0.000151	0.01658	0.04503	0.06333
$\Delta P_{mpp}\%$	0.0119	0.004595	0.000015	0.000146	0.0165	0.0462	0.0671

5.9 I-V and P-V Curves under Partial Shading

The incident of partial shading has been simulated using Matlab Simulink of Figure 4.14, where the first four solar modules have been subject to an irradiance of $1000W/m^2$. The next set of four modules have been subjected to an irradiance of $300W/m^2$ and the last set of four modules have been subjected to an irradiance of $600W/m^2$.

Figure 5.23 shows I-V and P-V curves for KC130GT module under partial shading condition, where the modules partially received different irradiance of $1000W/m^2$, $300W/m^2$ and $600W/m^2$. The curves show multiple maximum power points. The maximum power point with the highest value, marked with a red circular marker, shows the global MPP. The other maximum points represent the local MPPs, which give less output power. Tracking of global MPP has been targeted using the Fuzzy logic controller similar to the work reported by Zou *et al.* (2019). However, the sliding mode technique fails to track global MPP as suggested by Levron and Shmilovitz (2013).

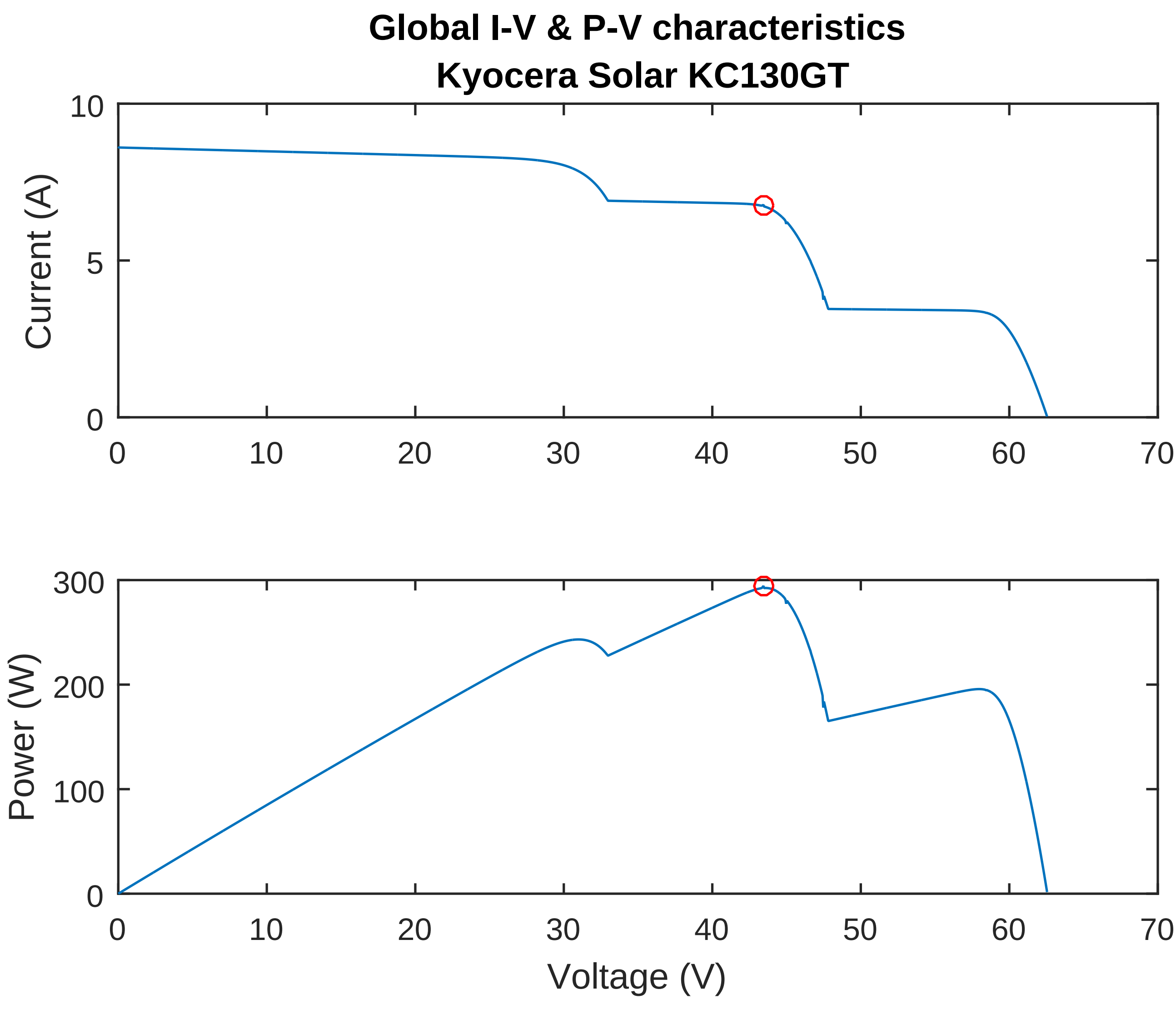

Figure 5.23: Graphs of current and power versus voltage for KC130GT showing local and global MPPs

Chapter 6

Conclusion and Recommendations

Throughout this work, the simulation and modeling of the characteristics of three different low-, medium- and high-power PV modules under various environmental conditions has been successfully accomplished. The study of photovoltaic systems has been carried out using a single diode model where three algorithms have been developed to extract its unknown parameters. The first two algorithms have been based on the threshold value of the ideal factor where the actual ideality factor has been chosen in the vicinity of the optimum value. Choosing the ideal factor close to its optimum value makes the process easy to execute and improves processing speed.

The first algorithm where A has been selected near A_o such that A is slightly less than A_o, the method gave output powers of 61.193W for Solinc 60Wp, 130.06W for KC130GT and 253.35W for Solinc 250Wp, with errors of 0.0036%, 0.00308% and -0.00395%, respectively. The second algorithm where A has been selected slightly above A_o, gave simulated output power of 61.193 for Solinc 60Wp, 130.06W for KC130GT and 253.35W for Solinc 250Wp, with errors of -0.00131%, 0.00308% and -0.00395%, respectively. The third algorithm is an improved Newton–Raphson numerical analysis method in which four separate approaches of deriving the unknown parameters have been used to obtain the preliminary data, and the Newton-Raphson method is henceforth used to estimate the most viable voltage and current values for I-V and P-V plots. The four approaches gave simulated output powers of 61.2122W,612142W, 61.612085W for Solinc60Wp, 130.162W,130.200W,130.187W and 130.126W for KC130GT and 253.3466W, 253.3464W, 253.3465W and 253.3535W for Solinc 25Wp. These four approaches gave negligible power errors of lees than 0.02% for Solinc 60Wp, less than 0.2% for KC130GT and less than0.002% for Solinc 250Wp. The third algorithm has less percentage compared to the first two algorithms.However the first two algorithm have less computational time since there fewer steps involved in their implementation.

The effects of temperature change and irradiance on model parameter have also been studied, in order to minimize the error commonly introduced when estimating the first and second order current and voltage coefficients. Simple procedures of arriving at the best five-model parameters at nominal cell operating temperature and actual irradiance have been introduced that depend on the short circuit current coefficient. There are new formulation of obtaining the V_{oc} and V_{mpp} at various irradiances and temperatures. This has been driven by the fact that the five extracted parameters depend on the three cardinal points, which are prone to errors when estimating the current and voltage coefficients. Such new methods include a reliable and clear analytical approach to determine the characteristics of I-V and P-V at all weather conditions. The new approach gave output powers of 20.19W at $200W/m^2$, 43.881W at $400W/m^2$, 67.078W at $600W/m^2$, 91.711W at $800W/m^2$ and 116.842W at $1000W/m^2$ at NOCT temperature of 47^oC for KC130GT. These values correspond to the change of irradiance at constant temperature.

Fuzzy logic and sliding mode MPPT controllers have also been studied and simulated. The Matlab-Simulink based systems that mimic an actual plant demonstrate the versatility of a high efficiency hybrid system that can work efficiently under all weather conditions, including partial shading instances. However, due to facility constraints, the MPPT model has not been implemented in an actual plant and remains to be research work for further studies. The system would require the use of powerful embedded system that can easily be implemented using FPGA, microcontroller or DSP chips.

References

Abbassi, R., Abbassi, A., Jemli, M., and Chebbi, S. (2018). Identification of unknown parameters of solar cell models: A comprehensive overview of available approaches. *Renewable and Sustainable Energy Reviews*, 90:453–474.

Abd Alhussain, H. and Yasin, N. (2020). Improved efficiency of photovoltaic module based on fuzzy logic MPPT technique. *MS&E*, 745(1):012006.

Abdel-Salam, M., El-Mohandes, M. T., and El-Ghazaly, M. (2020). An efficient tracking of mpp in PV systems using a newly-formulated P&O-MPPT method under varying irradiation levels. *Journal of Electrical Engineering & Technology*, 15(1):501–513.

Abo-Elyousr, F. K., Abdelshafy, A. M., and Abdelaziz, A. Y. (2020). MPPT-based particle swarm and cuckoo search algorithms for PV systems. In *Modern Maximum Power Point Tracking Techniques for Photovoltaic Energy Systems*, pages 379–400. Springer.

Ahmad, F. F., Ghenai, C., Hamid, A. K., and Bettayeb, M. (2020). Application of sliding mode control for maximum power point tracking of solar photovoltaic systems: A comprehensive review. *Annual Reviews in Control*.

Ahmad, J. (2010). A fractional open circuit voltage based maximum power point tracker for photovoltaic arrays. In *2010 2nd International Conference on Software Technology and Engineering*, volume 1, pages V1–247. IEEE.

Ahmad, R., Murtaza, A. F., and Sher, H. A. (2019). Power tracking techniques for efficient operation of photovoltaic array in solar applications–a review. *Renewable and Sustainable Energy Reviews*, 101:82–102.

Al-Diab, A. and Sourkounis, C. (2010). Variable step size P&O MPPT algorithm for PV systems. In *2010 12th International Conference on Optimization of Electrical and Electronic Equipment*, pages 1097–1102. IEEE.

Al-Majidi, S. D., Abbod, M. F., and Al-Raweshidy, H. S. (2019). Design of an efficient maximum power point tracker based on anfis using an experimental photovoltaic system data. *Electronics*, 8(8):858.

Alajmi, B. N., Ahmed, K. H., Finney, S. J., and Williams, B. W. (2010). Fuzzy-logic-control approach of a modified hill-climbing method for maximum power point in microgrid standalone photovoltaic system. *IEEE transactions on power electronics*, 26(4):1022–1030.

Ali, A., Almutairi, K., Malik, M. Z., Irshad, K., Tirth, V., Algarni, S., Zahir, M., Islam, S., Shafiullah, M., Shukla, N. K., *et al.* (2020). Review of online and soft computing maximum power point tracking techniques under non-uniform solar irradiation conditions. *Energies*, 13(12):3256.

Alik, R. and Jusoh, A. (2017). Modified perturb and observe (P&O) with checking algorithm under various solar irradiation. *Solar Energy*, 148:128–139.

Allahabadi, S., Iman-Eini, H., and Farhangi, S. (2019). Neural network based maximum power point tracking technique for PV arrays in mobile applications. In *2019 10th International Power Electronics, Drive Systems and Technologies Conference (PEDSTC)*, pages 701–706. IEEE.

Amalo, K. A., Birninkudu, S. I., Bukata, B. B., Salawudeen, A. T., and Ahmad, A. A. (2020). Cultured bat algorithm for optimized MPPT tracking under different shading conditions. In *2020 International Conference in Mathematics, Computer Engineering and Computer Science (ICMCECS)*, pages 1–8. IEEE.

Ataboev, O. K., Kabulov, R. R., Matchanov, N. A., and Egamov, S. R. (2019). Influence of temperature on the output parameters of a photovoltaic module based on amorphous hydrogenated silicon. *Applied Solar Energy*, 55(3):159–167.

Atay, B. K. and Eminoğlu, U. (2019). A new approach for parameter estimation of the single-diode model for photovoltaic cells/modules. *Turkish Journal of Electrical Engineering & Computer Sciences*, 27(4):3026–3039.

Atici, K., Sefa, I., and Altin, N. (2019). Grey wolf optimization based MPPT algorithm for solar PV system with sepic converter. In *2019 4th International Conference on Power Electronics and their Applications (ICPEA)*, pages 1–6. IEEE.

Avila, E., Pozo, N., Pozo, M., Salazar, G., and Domínguez, X. (2017). Improved particle swarm optimization based MPPT for PV systems under partial shading conditions. In *2017 IEEE Southern Power Electronics Conference (SPEC)*, pages 1–6. IEEE.

Bag, A., Subudhi, B., and Ray, P. K. (2018). An adaptive sliding mode control scheme for grid integration of a PV system. *CPSS Transactions on Power Electronics and Applications*, 3(4):362–371.

Bahari, M. I., Tarassodi, P., Naeini, Y. M., Khalilabad, A. K., and Shirazi, P. (2016). Modeling and simulation of hill climbing MPPT algorithm for photovoltaic application. In *2016 International Symposium on Power Electronics, Electrical Drives, Automation and Motion (SPEEDAM)*, pages 1041–1044. IEEE.

Barreto, R. A. (2018). Fossil fuels, alternative energy and economic growth. *Economic Modelling*, 75:196–220.

Basha, C. and Rani, C. (2020). Different conventional and soft computing MPPT techniques for solar PV systems with high step-up boost converters: A comprehensive analysis. *Energies*, 13(2):371.

Basha, C. H., Bansal, V., Rani, C., Brisilla, R., and Odofin, S. (2020). Development of cuckoo search MPPT algorithm for partially shaded solar PV sepic converter. In *Soft Computing for Problem Solving*, pages 727–736. Springer.

Batzelis, E. (2019). Non-iterative methods for the extraction of the single-diode model parameters of photovoltaic modules: A review and comparative assessment. *Energies*, 12(3):358.

Belhachat, F. and Larbes, C. (2018). A review of global maximum power point tracking techniques of photovoltaic system under partial shading conditions. *Renewable and Sustainable Energy Reviews*, 92:513–553.

Belhachat, F. and Larbes, C. (2019). Comprehensive review on global maximum power point tracking techniques for PV systems subjected to partial shading conditions. *Solar Energy*, 183:476–500.

Belkaid, A., Colak, I., and Kayisli, K. (2017). Implementation of a modified P&O-MPPT algorithm adapted for varying solar radiation conditions. *Electrical Engineering*, 99(3):839–846.

Beltran, A., Hughes, C., and Das, S. (2019). Improved maximum power point tracking of partially shaded PV arrays using particle swarm optimization with zone initialization. In *2019 IEEE 46th Photovoltaic Specialists Conference (PVSC)*, pages 0663–0667. IEEE.

Bendib, B., Krim, F., Belmili, H., Almi, M., and Boulouma, S. (2014). Advanced fuzzy MPPT controller for a stand-alone PV system. *Energy Procedia*, 50(2014):383–392.

Bensaha, A., Benkouider, F., and Cheknane, A. (2020). Design and size optimization of the PV modules for stand-alone photovoltaic systems. In *ICREEC 2019*, pages 167–172. Springer.

Bhan, V., Hashmani, A. A., and Shaikh, M. M. (2019). A new computing perturb-and-observe-type algorithm for MPPT in solar photovoltaic systems and evaluation of its performance against other variants by experimental validation. *Scientia Iranica*, 26(Special Issue on machine learning, data analytics, and advanced optimization techniques in modern power systems [Transactions on Computer Science & Engineering and Electrical Engineering (D)]):3656–3671.

Bielecki, A., Ernst, S., Skrodzka, W., and Wojnicki, I. (2020). The externalities of energy production in the context of development of clean energy generation. *Environmental Science and Pollution Research*, pages 1–25.

Bingöl, O. and Özkaya, B. (2019). A comprehensive overview of soft computing based MPPT techniques for partial shading conditions in PV systems. *Mühendislik Bilimleri ve Tasarım Dergisi*, 7(4):926–939.

Bouchriha, I., Ghanem, A. B., and Nouri, K. (2019). MPPT control of a photovoltaic system based on sliding mode control. In *2019 International Conference on Advanced Systems and Emergent Technologies (IC_ASET)*, pages 12–16. IEEE.

Boukenoui, R. and Mellit, A. (2019). Applications of improved versions of fuzzy logic based maximum power point tracking for controlling photovoltaic systems. In *Solar Photovoltaic Power Plants*, pages 143–164. Springer.

Bratcu, A. I., Munteanu, I., Bacha, S., and Raison, B. (2008). Maximum power point tracking of grid-connected photovoltaic arrays by using extremum seeking control. *Journal of Control Engineering and Applied Informatics*, 10(4):3–12.

Brockway, P. E., Owen, A., Brand-Correa, L. I., and Hardt, L. (2019). Estimation of global final-stage energy-return-on-investment for fossil fuels with comparison to renewable energy sources. *Nature Energy*, 4(7):612–621.

Brunton, S. L., Rowley, C. W., Kulkarni, S. R., and Clarkson, C. (2010). Maximum power point tracking for photovoltaic optimization using ripple-based extremum seeking control. *IEEE transactions on power electronics*, 25(10):2531–2540.

Carrero, C., Rodriguez, J., Ramirez, D., and Platero, C. (2010). Simple estimation of PV modules loss resistances for low error modelling. *Renewable Energy*, 35(5):1103–1108.

Castaner, L. and Silvestre, S. (2002). *Modelling photovoltaic systems using PSpice*. John Wiley and Sons.

Celik, A. N. and Acikgoz, N. (2007). Modelling and experimental verification of the operating current of mono-crystalline photovoltaic modules using four-and five-parameter models. *Applied energy*, 84(1):1–15.

Chaibi, Y., Salhi, M., and El-Jouni, A. (2019). Sliding mode controllers for standalone PV systems: Modeling and approach of control. *International Journal of Photoenergy*, 2019.

Chan, D. S. and Phang, J. C. (1987). Analytical methods for the extraction of solar-cell single- and double-diode model parameters from IV characteristics. *IEEE Transactions on Electron devices*, 34(2):286–293.

Charaabi, A., Barambones, O., Zaidi, A., and Zanzouri, N. (2020). A novel two stage controller for a DC-DC boost converter to harvest maximum energy from the PV power generation. In *Actuators*, volume 9, page 29. Multidisciplinary Digital Publishing Institute.

Chenni, R., Makhlouf, M., Kerbache, T., and Bouzid, A. (2007). A detailed modeling method for photovoltaic cells. *Energy*, 32(9):1724–1730.

Chin, C. S., Neelakantan, P., Yang, S. S., Chua, B. L., and Tze Kin Teo, K. (2011). Effect of partially shaded conditions on photovoltaic array's maximum power point tracking. *International Journal of Simulation–Systems, Science & Technology*, 12(3).

Chin, V. J., Salam, Z., and Ishaque, K. (2015). Cell modelling and model parameters estimation techniques for photovoltaic simulator application: A review. *Applied Energy*, 154:500–519.

Chouay, Y. and Ouassaid, M. (2019). An experimental artificial neural network based mpp tracking for solar photovoltaic systems. In *International Conference Europe Middle East & North Africa Information Systems and Technologies to Support Learning*, pages 533–542. Springer.

Chu, C.-C. and Chen, C.-L. (2009). Robust maximum power point tracking method for photovoltaic cells: A sliding mode control approach. *Solar Energy*, 83(8):1370–1378.

Cubas, J., Pindado, S., and Farrahi, A. (2013). New method for analytical photovoltaic parameter extraction. In *2013 International Conference on Renewable Energy Research and Applications (ICRERA)*, pages 873–877. IEEE.

da Rocha, M. V., Sampaio, L. P., and da Silva, S. A. O. (2020). Comparative analysis of MPPT algorithms based on bat algorithm for PV systems under partial shading condition. *Sustainable Energy Technologies and Assessments*, 40:100761.

Dadfar, S., Samad, S., and Nakamura, H. (2020). Variable step size perturb and observe MPPT controller by applying θ-modified krill herd algorithm-sliding mode controller to increase accuracy in photovoltaic system. *Journal of Cleaner Production*, page 122243.

Daraban, S., Petreus, D., and Morel, C. (2014). A novel MPPT (maximum power point tracking) algorithm based on a modified genetic algorithm specialized on tracking the global maximum power point in photovoltaic systems affected by partial shading. *Energy*, 74:374–388.

De Brito, M. A. G., Galotto, L., Sampaio, L. P., e Melo, G. d. A., and Canesin, C. A. (2012). Evaluation of the main MPPT techniques for photovoltaic applications. *IEEE transactions on industrial electronics*, 60(3):1156–1167.

De Soto, W., Klein, S. A., and Beckman, W. A. (2006). Improvement and validation of a model for photovoltaic array performance. *Solar energy*, 80(1):78–88.

Debnath, D., Soren, N., Pandey, A. D., and Barbhuiya, N. H. (2020). Improved grey wolf assists MPPT approach for solar photovoltaic system under partially shaded and gradually atmospheric changing condition. *International Energy Journal*, 20(1).

Derri, M., Bouzi, M., Lagrat, I., and Baba, Y. (2016). Fuzzy sliding mode control for photovoltaic system. *International Journal of Power Electronics and Drive Systems*, 7(3):964.

Dey, B. K., Khan, I., Mandal, N., and Bhattacharjee, A. (2016). Mathematical modelling and characteristic analysis of solar PV cell. In *2016 IEEE 7th Annual Information Technology, Electronics and Mobile Communication Conference (IEMCON)*, pages 1–5. IEEE.

Dharshan, B., Rajasekar, N., and Sankarkumar, R. S. (2020). Adaptability analysis of particle swarm optimization variants in maximum power tracking for solar PV systems. In *Intelligent Computing Techniques for Smart Energy Systems*, pages 397–409. Springer.

Dileep, G. and Singh, S. (2017). Application of soft computing techniques for maximum power point tracking of SPV system. *Solar Energy*, 141:182–202.

Dincer, I. (2000). Renewable energy and sustainable development: a crucial review. *Renewable and sustainable energy reviews*, 4(2):157–175.

Divyasharon, R., Banu, R. N., and Devaraj, D. (2019). Artificial neural network based MPPT with cuk converter topology for PV systems under varying climatic conditions. In *2019 IEEE International Conference on Intelligent Techniques in Control, Optimization and Signal Processing (INCOS)*, pages 1–6. IEEE.

Dixit, S. (2020). Solar technologies and their implementations: A review. *Materials Today: Proceedings*.

Dongue, S. B., Njomo, D., Tamba, J. G., and Ebengai, L. (2012). Modeling of electrical response of illuminated crystalline photovoltaic modules using four-and five-parameter models. *International Journal of Emerging Technology and Advanced Engineering*, 2(11):612–619.

Duan, Q., Leng, J., Duan, P., Hu, B., and Mao, M. (2015). An improved variable step PO and global scanning MPPT method for PV systems under partial shading condition. In *2015 7th international conference on intelligent human-machine systems and cybernetics*, volume 1, pages 382–386. IEEE.

Duan, Q., Mao, M., Duan, P., and Hu, B. (2017). An intelligent algorithm for maximum power point tracking in photovoltaic system under partial shading conditions. *Transactions of the Institute of Measurement and Control*, 39(2):244–256.

Ebhota, W. S. and Jen, T.-C. (2020). Fossil fuels environmental challenges and the role of solar photovoltaic technology advances in fast tracking hybrid renewable energy system. *International Journal of Precision Engineering and Manufacturing-Green Technology*, 7(1):97–117.

El Achouby, H., Zaimi, M., Ibral, A., and Assaid, E. (2018). New analytical approach for modelling effects of temperature and irradiance on physical parameters of photovoltaic solar module. *Energy conversion and management*, 177:258–271.

El-Helw, H. M., Magdy, A., and Marei, M. I. (2017). A hybrid maximum power point tracking technique for partially shaded photovoltaic arrays. *IEEE access*, 5:11900–11908.

Elobaid, L. M., Abdelsalam, A. K., and Zakzouk, E. E. (2015). Artificial neural network-based photovoltaic maximum power point tracking techniques: a survey. *IET Renewable Power Generation*, 9(8):1043–1063.

Eltamaly, A. M. and Abdelaziz, A. Y. (2019). *Modern Maximum Power Point Tracking Techniques for Photovoltaic Energy Systems*. Springer.

Eltamaly, A. M., Al-Saud, M., Abokhalil, A. G., and Farh, H. M. (2020). Simulation and experimental validation of fast adaptive particle swarm optimization strategy for photovoltaic global peak tracker under dynamic partial shading. *Renewable and Sustainable Energy Reviews*, 124:109719.

Eltamaly, A. M., Farh, H. M., and Othman, M. F. (2018). A novel evaluation index for the photovoltaic maximum power point tracker techniques. *Solar Energy*, 174:940–956.

Esram, T., Kimball, J. W., Krein, P. T., Chapman, P. L., and Midya, P. (2006). Dynamic maximum power point tracking of photovoltaic arrays using ripple correlation control. *IEEE Transactions on power electronics*, 21(5):1282–1291.

Eydi, M., Hosseini Sabzevari, S. I., and Ghazi, R. (2020). A novel strategy of maximum power point tracking for photovoltaic panels based on fuzzy logic algorithm. *Advances in Electrical and Electronic Engineering*, 18(1):1–10.

Farah, L., Haddouche, A., and Haddouche, A. (2020). Comparison between proposed fuzzy logic and anfis for MPPT control for photovoltaic system. *International Journal of Power Electronics and Drive Systems*, 11(2):1065.

Fares, A. M., Zalam, B. A. A., El Nashar, S. G., and Aka, H. (2013). Comparison between different algorithms for maximum ppt in photovoltaic systems and its implementation on microcontroller. *Journal of Energy Technologies and Policy*, 3(5):62–72.

Femia, N., Petrone, G., Spagnuolo, G., and Vitelli, M. (2005). Optimization of perturb and observe maximum power point tracking method. *IEEE transactions on power electronics*, 20(4):963–973.

García Vera, Y. E., Dufo-López, R., and Bernal-Agustín, J. L. (2019). Energy management in microgrids with renewable energy sources: A literature review. *Applied Sciences*, 9(18):3854.

Garraoui, R., Hamed, M. B., and Sbita, L. (2015). A robust optimization technique based on first order sliding mode approach for photovoltaic power systems. *International Journal of Automation and Computing*, 12(6):620–629.

Ghani, F., Rosengarten, G., Duke, M., and Carson, J. (2014). The numerical calculation of single-diode solar-cell modelling parameters. *Renewable Energy*, 72:105–112.

Goel, S. and Sharma, R. (2017). Performance evaluation of stand alone, grid connected and hybrid renewable energy systems for rural application: A comparative review. *Renewable and Sustainable Energy Reviews*, 78:1378–1389.

Gunerhan, H., Hepbasli, A., and Giresunlu, U. (2008). Environmental impacts from the solar energy systems. *Energy Sources, Part A: Recovery, Utilization, and Environmental Effects*, 31(2):131–138.

Guo, L., Meng, Z., Sun, Y., and Wang, L. (2018). A modified cat swarm optimization based maximum power point tracking method for photovoltaic system under partially shaded condition. *Energy*, 144:501–514.

Hanitsch, R., Schulz, D., and Siegfried, U. (2001). Shading effects on output power of grid connected photovoltaic generator systems. *Rev. Energ. Ren.: Power Engineering*, pages 93–99.

Hansen, J. S. (2011). *GNU Octave: Beginner's Guide: Become a Proficient Octave User by Learning this High-level Scientific Numerical Tool from the Ground Up*. Packt Publishing Ltd.

Hashim, N. and Salam, Z. (2019). Critical evaluation of soft computing methods for maximum power point tracking algorithms of photovoltaic systems. *International Journal of Power Electronics and Drive Systems*, 10(1):548.

Hassan, S., Abdelmajid, B., Mourad, Z., Aicha, S., and Abdenaceur, B. (2017). An advanced MPPT based on artificial bee colony algorithm for MPPT photovoltaic system under partial shading condition. *International Journal of Power Electronics and Drive Systems*, 8(2):647.

Hejri, M., Mokhtari, H., Azizian, M. R., and Söder, L. (2013). An analytical-numerical approach for parameter determination of a five-parameter single-diode model of photovoltaic cells and modules. *International Journal of Sustainable Energy*, 35(4):396–410.

Hu, Y., Chen, H., Xu, R., Yu, D., and Li, R. (2012). Maximum power point tracking under shadowed conditions. In *Zhongguo Dianji Gongcheng Xuebao(Proceedings of the Chinese Society of Electrical Engineering)*, volume 32, pages 14–26. Chinese Society for Electrical Engineering.

Hua, C., Lin, J., and Shen, C. (1998). Implementation of a dsp-controlled photovoltaic system with peak power tracking. *IEEE Transactions on Industrial Electronics*, 45(1):99–107.

Huang, C., Wang, L., Long, H., Luo, X., and Wang, J.-H. (2019). A hybrid global maximum power point tracking method for photovoltaic arrays under partial shading conditions. *Optik*, 180:665–674.

Huang, C., Zhang, Z., Wang, L., Song, Z., and Long, H. (2017). A novel global maximum power point tracking method for PV system using jaya algorithm. In *2017 IEEE Conference on Energy Internet and Energy System Integration (EI2)*, pages 1–5. IEEE.

Huang, Y.-P. and Hsu, S.-Y. (2016). A performance evaluation model of a high concentration photovoltaic module with a fractional open circuit voltage-based maximum power point tracking algorithm. *Computers & Electrical Engineering*, 51:331–342.

Huang, Y.-P., Huang, M.-Y., and Ye, C.-E. (2020). A fusion firefly algorithm with simplified propagation for photovoltaic MPPT under partial shading conditions. *IEEE Transactions on Sustainable Energy*.

Humada, A. M., Hojabri, M., Mekhilef, S., and Hamada, H. M. (2016). Solar cell parameters extraction based on single and double-diode models: A review. *Renewable and Sustainable Energy Reviews*, 56:494–509.

Huynh, P. and Cho, B. H. (1996). Design and analysis of a microprocessor-controlled peak-power-tracking system [for solar cell arrays]. *IEEE Transactions on Aerospace and Electronic Systems*, 32(1):182–190.

Ibrahim, A. E., Nor, N. M., Nawi, I. B. M., Mohd, F. R., and Mohd, K. N. (2019). Genetic algorithm to improve power output of photovoltaic system under partial shaded condition. *International Journal of Power Electronics and Drive Systems*, 10(4):2182.

Jiang, J.-A., Huang, T.-L., Hsiao, Y.-T., Chen, C.-H., *et al.* (2005). Maximum power tracking for photovoltaic power systems. *Tamkang Journal of Science and Engineering*, 8(2):147.

Jiang, L. L., Maskell, D. L., and Patra, J. C. (2013). A novel ant colony optimization-based maximum power point tracking for photovoltaic systems under partially shaded conditions. *Energy and Buildings*, 58:227–236.

Jordehi, A. R. (2016). Parameter estimation of solar photovoltaic PV cells: A review. *Renewable and Sustainable Energy Reviews*, 61:354–371.

Karagoz, M. and Demirel, H. (2017). A novel MPPT method for PV arrays based on modified bat algorithm with partial shading capability.

Kaundinya, D. P., Balachandra, P., and Ravindranath, N. H. (2009). Grid-connected versus stand-alone energy systems for decentralized power—a review of literature. *Renewable and Sustainable Energy Reviews*, 13(8):2041–2050.

Kennerud, K. L. (1969). Analysis of performance degradation in CdS solar cells. *IEEE Transactions on aerospace and electronic systems*, (6):912–917.

Khan, M. F. N., Ali, G., Khan, A. K., *et al.* (2019). A review of estimating solar photovoltaic cell parameters. In *2019 2nd International Conference on Computing, Mathematics and Engineering Technologies (iCoMET)*, pages 1–6. IEEE.

Khatib, T. and Muhsen, D. H. (2020). Optimal sizing of standalone photovoltaic system using improved performance model and optimization algorithm. *Sustainability*, 12(6):2233.

Khatibi, A., Razi Astaraei, F., and Ahmadi, M. H. (2019). Generation and combination of the solar cells: A current model review. *Energy Science & Engineering*, 7(2):305–322.

Khezzar, R., Zereg, M., and Khezzar, A. (2014). Modeling improvement of the four parameter model for photovoltaic modules. *Solar Energy*, 110:452–462.

Kinattingal, S., Simon, S. P., Nayak, P. S. R., *et al.* (2020). MPPT in PV systems using ant colony optimisation with dwindling population. *IET Renewable Power Generation*, 14(7):1105–1112.

Kittner, N., Gheewala, S. H., and Kammen, D. M. (2016). Energy return on investment (eroi) of mini-hydro and solar PV systems designed for a mini-grid. *Renewable Energy*, 99:410–419.

Kler, D., Rana, K., and Kumar, V. (2018). A nonlinear pid controller based novel maximum power point tracker for PV systems. *Journal of the Franklin Institute*, 355(16):7827–7864.

Kolluru, V. R., Patjoshi, R. K., and Panigrahi, R. (2019). A comprehensive review on maximum power tracking of a photovoltaic system under partial shading conditions. *International Journal of Renewable Energy Research (IJRER)*, 9(1):175–185.

Krein, P. T. (1999). Ripple correlation control, with some applications. In *ISCAS'99. Proceedings of the 1999 IEEE International Symposium on Circuits and Systems VLSI (Cat. No. 99CH36349)*, volume 5, pages 283–286. IEEE.

Kruglykhin, P., Gusev, A., and Kievets, A. (2020). The effect of partial shading on the i–v photovoltaic cell characteristics. In *AIP Conference Proceedings*, volume 2212, page 020030. AIP Publishing LLC.

Kumar, N., Hussain, I., Singh, B., and Panigrahi, B. K. (2017a). MPPT in dynamic condition of partially shaded PV system by using WODE technique. *IEEE Transactions on Sustainable Energy*, 8(3):1204–1214.

Kumar, N., Hussain, I., Singh, B., and Panigrahi, B. K. (2017b). Rapid MPPT for uniformly and partial shaded PV system by using jayade algorithm in highly fluctuating atmospheric conditions. *IEEE Transactions on Industrial Informatics*, 13(5):2406–2416.

Lasnier, F. and Juen, W. Y. (2017). The sizing of stand-alone photovoltaic systems using the simulation technique. *International Energy Journal*, 12(1).

Lei, P., Li, Y., Chen, Q., and Seem, J. E. (2010). Extremum seeking control based integration of MPPT and degradation detection for photovoltaic arrays. In *Proceedings of the 2010 American Control Conference*, pages 3536–3541. IEEE.

Levron, Y. and Shmilovitz, D. (2013). Maximum power point tracking employing sliding mode control. *IEEE Transactions on Circuits and Systems I: Regular Papers*, 60(3):724–732.

Leyva, R., Alonso, C., Queinnec, I., Cid-Pastor, A., Lagrange, D., and Martinez-Salamero, L. (2006). MPPT of photovoltaic systems using extremum-seeking control. *IEEE transactions on aerospace and electronic systems*, 42(1):249–258.

Leyva, R., Artillan, P., Cabal, C., Estibals, B., and Alonso, C. (2011). Dynamic performance of maximum power point tracking circuits using sinusoidal extremum seeking control for photovoltaic generation. *International Journal of Electronics*, 98(4):529–542.

Li, C.-h., Zhu, X.-j., Cao, G.-y., Hu, W.-q., Sui, S., and Hu, M.-r. (2009). A maximum power point tracker for photovoltaic energy systems based on fuzzy neural networks. *Journal of Zhejiang University-Science A*, 10(2):263–270.

Li, H., Peng, J., Liu, W., Huang, Z., and Lin, K.-C. (2014). A newton-based extremum seeking MPPT method for photovoltaic systems with stochastic perturbations. *International Journal of Photoenergy*, 2014.

Li, X., Li, Y., Seem, J. E., and Lei, P. (2011). Maximum power point tracking for photovoltaic systems using adaptive extremum seeking control. In *Dynamic Systems and Control Conference*, volume 54754, pages 803–810.

Liu, F., Tait, S., Schellart, A., Mayfield, M., and Boxall, J. (2020). Reducing carbon emissions by integrating urban water systems and renewable energy sources at a community scale. *Renewable and Sustainable Energy Reviews*, 123:109767.

Liu, X. and Lopes, L. A. (2004). An improved perturbation and observation maximum power point tracking algorithm for PV arrays. In *2004 IEEE 35th Annual Power Electronics Specialists Conference (IEEE Cat. No. 04CH37551)*, volume 3, pages 2005–2010. IEEE.

Lu, L., Weng, Q., Xie, Y., Guo, H., and Li, Q. (2019). An assessment of global electric power consumption using the defense meteorological satellite program-operational linescan system nighttime light imagery. *Energy*, 189:116351.

Ma, T., Yang, H., and Lu, L. (2014). Development of a model to simulate the performance characteristics of crystalline silicon photovoltaic modules/strings/arrays. *Solar Energy*, 100:31–41.

Macaulay, J. and Zhou, Z. (2018). A fuzzy logical-based variable step size P&O MPPT algorithm for photovoltaic system. *Energies*, 11(6):1340.

Mahdi, A., Mahamad, A., Saon, S., Tuwoso, T., Elmunsyah, H., and Mudjanarko, S. (2020). Maximum power point tracking using perturb and observe, fuzzy logic and anfis. *SN Applied Sciences*, 2(1):89.

Mäki, A. and Valkealahti, S. (2014). Differentiation of multiple maximum power points of partially shaded photovoltaic power generators. *Renewable energy*, 71:89–99.

Manickam, C., Raman, G. P., Raman, G. R., Ganesan, S. I., and Chilakapati, N. (2016). Fireworks enriched P&O algorithm for GMPPT and detection of partial shading in PV systems. *IEEE Transactions on Power Electronics*, 32(6):4432–4443.

Mao, M., Duan, Q., Duan, P., and Hu, B. (2018). Comprehensive improvement of artificial fish swarm algorithm for global MPPT in PV system under partial shading conditions. *Transactions of the Institute of Measurement and Control*, 40(7):2178–2199.

Mao, M., Zhang, L., Duan, Q., Oghorada, O., Duan, P., and Hu, B. (2017). A two-stage particle swarm optimization algorithm for MPPT of partially shaded PV arrays. *International Journal of Green Energy*, 14(8):694–702.

McEvoy, A., Markvart, T., Castañer, L., Markvart, T., and Castaner, L. (2003). *Practical handbook of photovoltaics: fundamentals and applications*. Elsevier.

Meinhardt, M. and Cramer, G. (2000). Past, present and future of grid connected photovoltaic- and hybrid-power-systems. In *2000 Power Engineering Society Summer Meeting (Cat. No. 00CH37134)*, volume 2, pages 1283–1288. IEEE.

Meral, M. E. and Dincer, F. (2011). A review of the factors affecting operation and efficiency of photovoltaic based electricity generation systems. *Renewable and Sustainable Energy Reviews*, 15(5):2176–2184.

Mertens, K. (2018). *Photovoltaics: fundamentals, technology, and practice*. John Wiley & Sons.

Midya, P., Krein, P. T., Turnbull, R. J., Reppa, R., and Kimball, J. (1996). Dynamic maximum power point tracker for photovoltaic applications. In *PESC Record. 27th Annual IEEE Power Electronics Specialists Conference*, volume 2, pages 1710–1716. IEEE.

Mikkili, S., Bollipo, R. B., and Bonthagarla, P. K. (2020). A critical review on PV MPPT techniques: Classical, intelligent and optimization. *IET Renewable Power Generation*.

Miqoi, S., El Ougli, A., Boutouba, M., and Tidhaf, B. (2017). Fuzzy sliding mode control for maximum power point tracking of a photovoltaic pumping system. *Journal of Electrical Systems*, 13(1):95–114.

Mohanty, M., Selvakumar, S., Koodalsamy, C., and Simon, S. (2019). Global maximum operating point tracking for PV system using fast convergence firefly algorithm. *Turkish Journal of Electrical Engineering & Computer Sciences*, 27(6).

Mohanty, S., Subudhi, B., and Ray, P. K. (2016). A grey wolf-assisted perturb & observe MPPT algorithm for a PV system. *IEEE Transactions on Energy Conversion*, 32(1):340–347.

Mosaad, M. I., abed el Raouf, M. O., Al-Ahmar, M. A., and Banakher, F. A. (2019). Maximum power point tracking of PV system based cuckoo search algorithm; review and comparison. *Energy Procedia*, 162:117–126.

Motahhir, S., Chouder, A., El Hammoumi, A., Benyoucef, A. S., El Ghzizal, A., Kichou, S., Kara, K., Sanjeevikumar, P., and Silvestre, S. (2020a). Optimal energy harvesting from a multistrings PV generator based on artificial bee colony algorithm. *IEEE Systems Journal*.

Motahhir, S., El Hammoumi, A., and El Ghzizal, A. (2020b). The most used MPPT algorithms: Review and the suitable low-cost embedded board for each algorithm. *Journal of cleaner production*, 246:118983.

Nafeh, A. E.-S. A., Fahmy, F. H., Mahgoub, O. A., and El-Zahab, E. M. A. (1998). Developed algorithm of maximum power tracking for stand-alone photovoltaic system. *Energy Sources*, 20(1):45–53.

Neville, R. C. (1995). *Solar energy conversion: the solar cell*. Elsevier.

Nguyen, D. D. and Lehman, B. (2006). Modeling and simulation of solar PV arrays under changing illumination conditions. In *2006 IEEE Workshops on Computers in Power Electronics*, pages 295–299. IEEE.

Nie, X., Wang, W., and Nie, H. (2017). Chaos quantum-behaved cat swarm optimization algorithm and its application in the PV MPPT. *Computational Intelligence and Neuroscience*, 2017.

Noguchi, T., Togashi, S., and Nakamoto, R. (2002). Short-current pulse-based maximum-power-point tracking method for multiple photovoltaic-and-converter module system. *IEEE Transactions on Industrial electronics*, 49(1):217–223.

Nugraha, D. A., Lian, K.-L., *et al.* (2019). A novel MPPT method based on cuckoo search algorithm and golden section search algorithm for partially shaded PV system. *Canadian Journal of Electrical and Computer Engineering*, 42(3):173–182.

Ogliari, E. and Leva, S. (2019). *Computational Intelligence in Photovoltaic Systems*. MDPI.

Orioli, A. and Di Gangi, A. (2013). A procedure to calculate the five-parameter model of crystalline silicon photovoltaic modules on the basis of the tabular performance data. *Applied Energy*, 102:1160–1177.

Otieno, C. A., Nyakoe, G. N., and Wekesa, C. W. (2009). A neural fuzzy based maximum power point tracker for a photovoltaic system. In *AFRICON 2009*, pages 1–6. IEEE.

Owusu-Nyarko, I., Elgenedy, M. A., and Ahmed, K. (2019). Combined temprature and irradiation effects on the open circuit voltage and short circuit current constants for enhancing their related PV-MPPT algorithms. In *2019 IEEE Conference on Power Electronics and Renewable Energy (CPERE)*, pages 343–348. IEEE.

Ozturk, M. and Dincer, I. (2019). Comparative environmental impact assessment of various fuels and solar heat for a combined cycle. *International Journal of Hydrogen Energy*, 44(10):5043–5053.

Perera, F. (2018). Pollution from fossil-fuel combustion is the leading environmental threat to global pediatric health and equity: solutions exist. *International journal of environmental research and public health*, 15(1):16.

Phang, J., Chan, D., and Phillips, J. (1984a). Accurate analytical method for the extraction of solar cell model parameters. *Electronics Letters*, 20(10):406–408.

Phang, J. C. H., Chan, D. S. H., and Phillips, J. R. (1984b). Accurate analytical method for the extraction of solar cell model parameters. *Electronics Letters*, 20(10):406–408.

Priyadarshi, N., Ramachandaramurthy, V. K., Padmanaban, S., and Azam, F. (2019). An ant colony optimized MPPT for standalone hybrid PV-wind power system with single cuk converter. *Energies*, 12(1):167.

Psarros, G., Batzelis, E., and Papathanassiou, S. (2014). Analysis of local mpps on the PV curve of a partially shaded PV string. *EU PVSEC*, pages 3383–3389.

Qais, M. H., Hasanien, H. M., and Alghuwainem, S. (2020). Parameters extraction of three-diode photovoltaic model using computation and harris hawks optimization. *Energy*, 195:117040.

Raghavendra, K. V. G., Zeb, K., Muthusamy, A., Krishna, T., Kumar, S., Kim, D.-H., Kim, M.-S., Cho, H.-G., and Kim, H.-J. (2020). A comprehensive review of DC–DC converter topologies and modulation strategies with recent advances in solar photovoltaic systems. *Electronics*, 9(1):31.

Ram, J. P., Babu, T. S., and Rajasekar, N. (2017). A comprehensive review on solar PV maximum power point tracking techniques. *Renewable and Sustainable Energy Reviews*, 67:826–847.

Ramyar, A., Iman-Eini, H., and Farhangi, S. (2016). Global maximum power point tracking method for photovoltaic arrays under partial shading conditions. *IEEE Transactions on Industrial Electronics*, 64(4):2855–2864.

Raugei, M., Fullana-i Palmer, P., and Fthenakis, V. (2012). The energy return on energy investment (eroi) of photovoltaics: Methodology and comparisons with fossil fuel life cycles. *Energy Policy*, 45:576–582.

Rauschenbach, H. S. (1971). Electrical output of shadowed solar arrays. *IEEE Transactions on Electron Devices*, 18(8):483–490.

Rauschenbach, H. S. (2012). Solar cell array design handbook: The principles and technology of photovoltaic energy conversion. *Springer Science and Business Media.*

Reis, L., Camacho, J., and Novacki, D. (2017). The newton raphson method in the extraction of parameters of PV modules. In *Proceedings of the International Conference on Renewable Energies and Power Quality (ICREPQ'17), Malaga, Spain*, pages 4–6.

Robles-Campos, H. R., Azuaje-Berbecí, B. J., Scheller, C. J., Angulo, A., and Mancilla-David, F. (2019). Detailed modeling of large scale photovoltaic power plants under partial shading conditions. *Solar Energy*, 194:485–498.

Saha, C., Agbu, N., Jinks, R., and Huda, M. (2018). Review article of the solar PV parameters estimation using evolutionary algorithms. *MOJ Solar and Photoenergy Systems*, 2(2):66–78.

Salam, Z., Ahmed, J., and Merugu, B. S. (2013). The application of soft computing methods for MPPT of PV system: A technological and status review. *Applied energy*, 107:135–148.

Sandali, A., Oukhoya, T., and Cheriti, A. (2014). Modeling and design of PV grid connected system using a modified fractional short-circuit current MPPT. In *2014 International Renewable and Sustainable Energy Conference (IRSEC)*, pages 224–229. IEEE.

Saravanan, S. and Babu, N. R. (2016). Maximum power point tracking algorithms for photovoltaic system–a review. *Renewable and Sustainable Energy Reviews*, 57:192–204.

Schwingshackl, C., Petitta, M., Wagner, J. E., Belluardo, G., Moser, D., Castelli, M., Zebisch, M., and Tetzlaff, A. (2013). Wind effect on PV module temperature: Analysis of different techniques for an accurate estimation. *Energy Procedia*, 40:77–86.

Segev, G., Mittelman, G., and Kribus, A. (2012). Equivalent circuit models for triple-junction concentrator solar cells. *Solar Energy Materials and Solar Cells*, 98:57–65.

Sera, D., Teodorescu, R., and Rodriguez, P. (2007). PV panel model based on datasheet values. In *2007 IEEE international symposium on industrial electronics*, pages 2392–2396. IEEE.

Seyedmahmoudian, M., Mekhilef, S., Rahmani, R., Yusof, R., and Renani, E. T. (2013). Analytical modeling of partially shaded photovoltaic systems. *Energies*, 6(1):128–144.

Shang, L., Guo, H., and Zhu, W. (2020). An improved MPPT control strategy based on incremental conductance algorithm. *Protection and Control of Modern Power Systems*, 5(1):1–8.

Sharma, A., Pachauri, R., Sharma, A., and Raj, N. (2019). Extraction of the solar PV module parameters using chicken swarm optimization technique. In *2019 Women Institute of Technology Conference on Electrical and Computer Engineering (WITCON ECE)*, pages 45–48. IEEE.

Shengqing, L., Fujun, L., Jian, Z., Wen, C., and Donghui, Z. (2020). An improved MPPT control strategy based on incremental conductance method. *Soft Computing*, pages 1–8.

Sher, H. A., Murtaza, A. F., Noman, A., Addoweesh, K. E., Al-Haddad, K., and Chiaberge, M. (2015). A new sensorless hybrid MPPT algorithm based on fractional short-circuit current measurement and P&O MPPT. *IEEE Transactions on sustainable energy*, 6(4):1426–1434.

Shockley, W. (1949). The theory of p-n junctions in semiconductors and p-n junction transistors. *Bell System Technical Journal*, 28(3):435–489.

Silvestre, S. and Chouder, A. (2008). Effects of shadowing on photovoltaic module performance. *Progress in Photovoltaics: Research and applications*, 16(2):141–149.

soufyane Benyoucef, A., Chouder, A., Kara, K., Silvestre, S., *et al.* (2015). Artificial bee colony based algorithm for maximum power point tracking (MPPT) for PV systems operating under partial shaded conditions. *Applied Soft Computing*, 32:38–48.

Subroto, R. K., Ardhenta, L., and Maulana, E. (2017). A novel of adaptive sliding mode controller with observer for DC/DC boost converters in photovoltaic system. In *2017 5th International Conference on Electrical, Electronics and Information Engineering (ICEEIE)*, pages 9–14. IEEE.

Sze, S. M. and Ng, K. K. (2006). *Physics of semiconductor devices*. John wiley & sons.

Taghizadeh-Hesary, F., Yoshino, N., and Inagaki, Y. (2019). Empirical analysis of factors influencing the price of solar modules. *International Journal of Energy Sector Management*.

Tajuddin, M. F. N., Ayob, S. M., Salam, Z., and Saad, M. S. (2013). Evolutionary based maximum power point tracking technique using differential evolution algorithm. *Energy and Buildings*, 67:245–252.

Takun, P., Kaitwanidvilai, S., and Jettanasen, C. (2010). Maximum power point tracking using fuzzy logic control for photovoltaic systems. In *World Congress on Engineering 2012. July 4-6, 2012. London, UK.*, volume 2189, pages 986–990. International Association of Engineers.

Titri, S., Kaced, K., and Larbes, C. (2019). Maximum power point tracking based on the bio inspired bat algorithm. In *International Conference in Artificial Intelligence in Renewable Energetic Systems*, pages 22–29. Springer.

Titri, S., Larbes, C., Toumi, K. Y., and Benatchba, K. (2017). A new MPPT controller based on the ant colony optimization algorithm for photovoltaic systems under partial shading conditions. *Applied Soft Computing*, 58:465–479.

Tjahjono, A., Anggriawan, D. O., Habibi, M. N., and Prasetyono, E. (2020). Modified grey wolf optimization for maximum power point tracking in photovoltaic system under partial shading conditions. *International Journal on Electrical Engineering and Informatics*, 12(1):94–104.

Twidell, J. and Weir, T. (2015). *Renewable energy resources*. Routledge.

Ulinuha, A. and Zulfikri, A. (2020). Enhancement of solar photovoltaic using maximum power point tracking based on hill climbing optimization algorithm. In *Journal of Physics: Conference Series*, volume 1517, page 012096.

Vemuru, S., Singh, P., and Niamat, M. (2012). Modeling impact of bypass diodes on photovoltaic cell performance under partial shading. In *2012 IEEE International Conference on Electro/Information Technology*, pages 1–5. IEEE.

Verma, P., Garg, R., and Mahajan, P. (2020). Asymmetrical interval type-2 fuzzy logic control based MPPT tuning for PV system under partial shading condition. *ISA transactions*.

Vieira, R. G., de Araújo, F. M., Dhimish, M., and Guerra, M. I. (2020). A comprehensive review on bypass diode application on photovoltaic modules. *Energies*, 13(10):2472.

Villalva, M. G., Gazoli, J. R., and Ruppert Filho, E. (2009). Comprehensive approach to modeling and simulation of photovoltaic arrays. *IEEE Transactions on power electronics*, 24(5):1198–1208.

Walker, G. (2001). Evaluating MPPT converter topologies using a matlab PV model. *Journal of Electrical and Electronics Engineering, Australia*, 21(1):49.

Walker, S., Sooriyaarachchi, N., Liyanage, N., Abeynayake, P., and Abeyratne, S. (2011). Comparative analysis of speed of convergence of MPPT techniques. In *2011 6th International Conference on Industrial and Information Systems*, pages 522–526. IEEE.

Won, C.-Y., Kim, D.-H., Kim, S.-C., Kim, W.-S., and Kim, H.-S. (1994). A new maximum power point tracker of photovoltaic arrays using fuzzy controller. In *Proceedings of 1994 Power Electronics Specialist Conference-PESC'94*, volume 1, pages 396–403. IEEE.

Wu, Z., Yu, D., and Kang, X. (2018). Application of improved chicken swarm optimization for MPPT in photovoltaic system. *Optimal Control Applications and Methods*, 39(2):1029–1042.

Würfel, P. and Würfel, U. (2016). *Physics of solar cells: from basic principles to advanced concepts*. John Wiley & Sons.

Xiao, W. and Dunford, W. G. (2004). A modified adaptive hill climbing MPPT method for photovoltaic power systems. In *2004 IEEE 35th annual power electronics specialists conference (IEEE Cat. No. 04CH37551)*, volume 3, pages 1957–1963. Ieee.

Xu, D., Dai, Y., Yang, C., and Yan, X. (2019). Adaptive fuzzy sliding mode command-filtered backstepping control for islanded PV microgrid with energy storage system. *Journal of the Franklin Institute*, 356(4):1880–1898.

Yang, B., Li, W., Zhao, Y., and He, X. (2010). Design and analysis of a grid-connected photovoltaic power system. *IEEE transactions on power electronics*, 25(4):992–1000.

Yau, H.-T. and Chen, C.-L. (2012). Fuzzy sliding mode controller design for maximum power point tracking control of a solar energy system. *Transactions of the Institute of Measurement and Control*, 34(5):557–565.

Yau, H.-T., Lin, C.-J., and Wu, C.-H. (2013). Sliding mode extremum seeking control scheme based on pso for maximum power point tracking in photovoltaic systems. *International Journal of Photoenergy*, 2013.

Yau, H.-T. and Wu, C.-H. (2011). Comparison of extremum-seeking control techniques for maximum power point tracking in photovoltaic systems. *Energies*, 4(12):2180–2195.

Yetayew, T. T., Jyothsna, T., and Kusuma, G. (2016). Evaluation of incremental conductance and firefly algorithm for PV MPPT application under partial shade condition. In *2016 IEEE 6th International Conference on Power Systems (ICPS)*, pages 1–6. IEEE.

Yousri, D., Babu, T. S., Allam, D., Ramachandaramurthy, V., Beshr, E., Eteiba, M., *et al.* (2019a). Fractional chaos maps with flower pollination algorithm for partial shading mitigation of photovoltaic systems. *Energies*, 12(18):3548.

Yousri, D., Babu, T. S., Allam, D., Ramachandaramurthy, V. K., and Etiba, M. B. (2019b). A novel chaotic flower pollination algorithm for global maximum power point tracking for photovoltaic system under partial shading conditions. *IEEE Access*, 7:121432–121445.

Zaimi, M., El Achouby, H., Ibral, A., and Assaid, E. (2019). Determining combined effects of solar radiation and panel junction temperature on all model-parameters to forecast peak power and photovoltaic yield of solar panel under non-standard conditions. *Solar Energy*, 191:341–359.

Zazo, H., Del Castillo, E., Reynaud, J. F., and Leyva, R. (2012). MPPT for photovoltaic modules via newton-like extremum seeking control. *Energies*, 5(8):2652–2666.

Zeb, K., Islam, S. U., Din, W. U., Khan, I., Ishfaq, M., Busarello, T. D. C., Ahmad, I., and Kim, H. J. (2019). Design of fuzzy-pi and fuzzy-sliding mode controllers for single-phase two-stages grid-connected transformerless photovoltaic inverter. *Electronics*, 8(5):520.

Zhang, P. and Sui, H. (2020). Maximum power point tracking technology of photovoltaic array under partial shading based on adaptive improved differential evolution algorithm. *Energies*, 13(5):1254.

Zheng, D., Li, J., Wu, W., Yu, H., Du, J., Sun, W., Xiao, S., and Shao, Z. (2020). The study for MPPT of photovoltaic system based on terminal sliding mode control method. *E&ES*, 467(1):012089.

Zou, Y., Yan, F., Wang, X., and Zhang, J. (2019). An efficient fuzzy logic control algorithm for photovoltaic maximum power point tracking under partial shading condition. *Journal of the Franklin Institute*.

Appendix I

Ideality factor vs saturation current code (Figure 5.3)

```
clc
clear
output_precision(15)
T=298;
k=1.38065*10^(-23);
q=1.6022*10^(-19);
Vth=(k*T)/q
%ideality factor (A) vs Satution Current (Io)
Ippt=[3.5719 7.39 8.9389];
Vppt=[17 17.6 28.342];
Isc =[3.8008 8.02 9.5006];
Voc =[21.462 21.9 36.061];
Nsc =[36 36 60];
c={'g','b','r'};
for i=[1 2 3];
Io=[0:0.001:0.1];
n=(Voc(i)-Vppt(i))./((log(Isc(i)+Io)-log(Isc(i)+Io-Ippt(i)))*Nsc(i)*Vth);
figure 1
plot(Io,n, c(i),"linewidth", 1.5)
hleg=legend('Solinic 60Wp','KC130GT', 'Solnic 250W',"location","southeast");
legend boxoff
set (hleg, "fontsize", 18);
set(gca, "linewidth", 2)
set(gca, "fontsize", 18)
xlim ([0, 0.1]);
ylim ([1.6, 2]);
xlabel('Saturation Current (n)', "fontsize", 20);
ylabel('Ideeality Factor', "fontsize", 20);
hold on;
clear n;
end
```

Appendix II

R_{sh} against R_s Code for $A \leq A_o$ (Figure 5.4)

```
clc
clear
output_precision(8)
Ippt=3.6247;
Vppt=16.8821;
Isc=3.7997;
Voc=21.5948;
Nsc=36;
T=298.15;
k=1.3806503*10^(-23);
q=1.6021764*10^(-19);
Vth=(k*T)/q
no =(Voc-Vppt)./(Nsc*Vth*log(Isc./(Isc-Ippt)))
Io = Isc/(exp(Voc./(no*Vth*Nsc)))
n=1.607
Rsr=[0:0.0001:1];
B=Rsr.*Ippt;
C=Vppt+(Rsr.*Ippt);
D=Io*exp(C./(n*Nsc*Vth));
F=Io*exp(Voc./(n*Nsc*Vth));
num=Voc-Vppt-B;
den = Ippt+D-F;
Rsr;
Rshr=num./den;
figure
plot(Rsr, Rshr,  "g","linewidth", 2)
hleg = legend('n= 1.607');
legend boxoff
set (hleg, "fontsize", 20);
set(gca, "linewidth", 1.5)
set(gca, "fontsize", 20)
xlim ([0.75, 1]);
xlabel('R_s(\Omega)', "fontsize", 20);
ylabel('R_{sh}(\Omega)', "fontsize", 20);
hold
Rshr=(Voc-Vppt-(Rsr.*Ippt))./(Ippt+(Io*exp((Vppt+(Rsr.*Ippt))./(n*
    Nsc*Vth)))-(Io*exp(Voc./(n*Nsc*Vth))));
```

```
figure
plot(Rsr, Rshr, "g","linewidth", 2)
hleg = legend('n= 1.607');
legend boxoff
set (hleg, "fontsize", 20);
set(gca, "linewidth", 1.5)
set(gca, "fontsize", 20)
xlim ([0.75, 1]);
xlabel('R_s(\Omega)', "fontsize", 20);
ylabel('R_{sh}(\Omega)', "fontsize", 20);
hold
plot(0.8993,505.013218,'o','LineWidth',2,'MarkeRsrize',6,'Color','g'
    )
Rsr=0.8998
Rshr=(Voc-Vppt-(Rsr.*Ippt))./(Ippt+(Io*exp((Vppt+(Rsr.*Ippt))./(n*
    Nsc*Vth)))-(Io*exp(Voc./(n*Nsc*Vth))))
Io = Isc/(exp(Voc./(n*Vth*Nsc)))
Iph=Isc+(Isc*Rsr)./Rshr
```

Appendix III

I-V Curve Code for $n \leq A_o$ (Figure 5.7 (a))

```
clc
clear
T=298.15;
k=1.3806503*10^(-23);
q=1.6021764*10^(-19);
Vth=(k*T)/q
Ippt=3.6247;
Vppt=16.8821;
Isc=3.7997;
Voc=21.5948;
Nsc = 36;
V=[0:0.1:1000];
n=[1.6554 1.607];
Io=[2.8481E-06 1.8624E-06];
Iph=[3.7997 3.80554];
Rshr =  [64437.533 585.0140];
Rsr = [0.001 0.8998];
c={'k','k--'};
for i=[1 2];
I=Iph(i)+Io(i)-Io(i)*exp((V+(I.*Rsr(i)))./(n(i)*Vth*Nsc))-((V+(I.*
   Rsr(i)))./Rshr(i));
figure(4)
plot(V,I, c{i},"linewidth", 1.5);
hleg = legend('n_o=1.6554','n=1.607',"location", "southwest");
set (hleg, "fontsize", 13);
legend boxoff
axis([0 23 0 4]);
set(gca, "linewidth", 1.5)
set(gca, "fontsize", 14)
xlabel('Voltage in volts', "fontsize", 20);
ylabel('Current in Amperes', "fontsize", 20);
%grid minor on;
hold on;
clear I;
end
figure(4)
```

```
plot([0 Vppt Voc ],[Isc Ippt 0 ],'o','LineWidth',2,'MarkeRsrize',6,'
    Color','k')
rectangle ("position", [16, 3.4, 2.8, 0.4],"linestyle","--");
rectangle ("position", [21, 0, 1.4, 0.2],"linestyle","--");
line([17 15.4], [3.4 3],"linewidth",1.5)
line([20.9 19.4], [0.2 0.8],"linewidth",1.5)
axes ('position', [0.35,0.55,0.3,0.28]);
for i=[1 2];
R=15<V & V<23;
I=Iph(i)+Io(i)-Io(i)*exp((V+(I.*Rsr(i)))./(n(i)*Vth*Nsc))-((V+(I.*
    Rsr(i)))./Rshr(i));
plot(V(R),I(R), c{i},"linewidth", 1.5);
set (gca, "xlim", [16 18.4], "ylim", [3.4 3.8])
set(gca,'XTick', 16:0.4:18.4)
set(gca, "linewidth", 1.5)
set(gca, "fontsize", 13)
hold on;
grid on;
clear I;
end
figure(4)
plot([0 Vppt Voc ],[Isc Ippt 0 ],'o','LineWidth',2,'MarkeRsrize',6,'
    Color','k')
axes ('position', [0.53, 0.25,0.25,0.24]);
for i=[1 2];
R=15<V & V<23;
I=Iph(i)+Io(i)-Io(i)*exp((V+(I.*Rsr(i)))./(n(i)*Vth*Nsc))-((V+(I.*
    Rsr(i)))./Rshr(i));
plot(V(R), I(R), c{i},"linewidth", 1.5);
set (gca, "xlim", [21.5 21.9], "ylim", [0 0.001])
set(gca,'XTick', 21.5:0.2:21.9)
set(gca, "linewidth", 1.5)
set(gca, "fontsize", 13)
hold on;
grid on;
clear I;
end
figure(4)
plot([0 Vppt Voc ],[Isc Ippt 0],'o','LineWidth',2,'MarkeRsrize',6,'
    Color','k')
```

Appendix IV

P-V curve code for $A \leq A_o$ (Figure 5.9 (b))

```
clc
clear
T=298.15;
k=1.3806503*10^(-23);
q=1.6021764*10^(-19);
Vth=(k*T)/q
Nsc = 36;
V=[0:0.1:1000];
n=[1.6554 1.607];
Io=[2.8481E-06 1.8624E-06];
Iph=[3.7997 3.80554];
Rshr =  [64437.533 585.0140];
Rsr = [0.001 0.8998];
c={'k','g'};
for i=[1 2];
I=Iph(i)+Io(i)-Io(i)*exp((V+(I.*Rsr(i)))./(n(i)*Vth*Nsc))-((V+(I.*
    Rsr(i)))./Rshr(i));
P = V.*I;
figure(2)
plot(V,P, c{i},"linewidth", 1.5);
hleg = legend('n_o=1.6554','n=1.607',"location", "northwest");
set (hleg, "fontsize", 13);
legend boxoff
axis([0 23 0 65]);
set(gca, "linewidth", 1.5)
set(gca, "fontsize", 14)
xlabel('Voltage in volts', "fontsize", 20);
ylabel('Power in watts', "fontsize", 20);
hold on;
clear I;
end
rectangle ("position", [16.5, 59.5, 3, 4],"linestyle","--");
rectangle ("position", [21.2, 0, 1, 4],"linestyle","--");
line([17 18], [42 59.5],"linewidth",1.5)
line([21.2 19.8], [4 12],"linewidth",1.5)
axes ('position', [0.55,0.44,0.2,0.2]);
for i=[1 2];
```

```
R=10<V & V<23;
I=Iph(i)+Io(i)-Io(i)*exp((V+(I.*Rsr(i)))./(n(i)*Vth*Nsc))-((V+(I.*
    Rsr(i)))./Rshr(i));
P = V.*I;
plot(V(R),P(R), c{i},"linewidth", 1.5);
set (gca, "xlim", [16 20], "ylim", [55 63.5])
set(gca, "linewidth", 1.5)
set(gca, "fontsize", 13)
hold on;
grid on;
clear I;
end
axes ('position', [0.5,0.17,0.3,0.2]);
set(gca, "linewidth", 1.5)
for i=[1 2];
R=10<V & V<22;
I=Iph(i)+Io(i)-Io(i)*exp((V+(I.*Rsr(i)))./(n(i)*Vth*Nsc))-((V+(I.*
    Rsr(i)))./Rshr(i));
P = V.*I;
plot(V(R),P(R), c{i},"linewidth", 1.5);
set (gca, "xlim", [21.5 22], "ylim", [0 0.001])
set(gca, "linewidth", 1.5)
set(gca, "fontsize", 13)
hold on;
grid on;
clear I;
end
```

Appendix V

R_{sh} against R_s Code for $A \geq A_o$ (Figure 5.8)

```
clc
clear
output_precision(8)
Ippt=3.6247;
Vppt=16.8821;
Isc=3.7997;
Voc=21.5948;
Nsc=36;
T=298.15;
k=1.3806503*10^(-23);
q=1.6021764*10^(-19);
Vth=(k*T)/q
no =(Voc-Vppt)./(Nsc*Vth*log(Isc./(Isc-Ippt)))
Io = Isc/(exp(Voc./(no*Vth*Nsc)))
n=1.978
Rsr=[0:0.0001:1];
Rshr=(Vppt+Ippt*Rsr)./(Isc-Ippt-(Io*(exp((Vppt+Ippt*Rsr)./(n*Nsc*Vth))-1)));
figure
plot(Rsr, Rshr, "g","linewidth", 2)
hleg = legend('n= 1.978');
legend boxoff
set (hleg, "fontsize", 20);
set(gca, "linewidth", 1.5)
set(gca, "fontsize", 20)
xlim ([0.8, 1]);
xlabel('R_s(\Omega)', "fontsize", 20);
ylabel('R_{sh}(\Omega)', "fontsize", 20);
hold
plot(0.8993,505.013218,'o','LineWidth',2,'MarkeRsrize',6,'Color','g')
Rsr=0.8993
Rshr=(Vppt+Ippt*Rsr)./(Isc-Ippt-(Io*(exp((Vppt+Ippt*Rsr)./(n*Nsc*Vth))-1)))
Io = Isc/(exp(Voc./(n*Vth*Nsc)))
Iph=Isc+(Isc*Rsr)./Rshr
```

Appendix VI

I-V Curve Code for $A \geq A_o$ (Figure 5.11 (a))

```
clc
clear
T=298.15;
k=1.3806503*10^(-23);
q=1.6021764*10^(-19);
Vth=(k*T)/q
Ippt=3.6247;
Vppt=16.8821;
Isc=3.7997;
Voc=21.5948;
Nsc = 36;
V=[0:0.1:1000];
n=[1.6554 1.978];
Io=[2.8481E-06 2.8414E-05];
Iph=[3.7997 3.8002];
Rshr = [64437.533 7043.3234];
Rsr = [0.001 0.8993];
c={'k','k--'};
for i=[1 2];
I=Iph(i)+Io(i)-Io(i)*exp((V+(I.*Rsr(i)))./(n(i)*Vth*Nsc))-((V+(I.*Rsr(i)))./Rshr(i));
figure(4)
plot(V,I, c{i},"linewidth", 1.5);
hleg = legend('n_o=1.6554','n=1.978',"location", "southwest");
set (hleg, "fontsize", 13);
legend boxoff
axis([0 23 0 4]);
set(gca, "linewidth", 1.5)
set(gca, "fontsize", 14)
xlabel('Voltage in volts', "fontsize", 20);
ylabel('Current in Amperes', "fontsize", 20);
%grid minor on;
hold on;
clear I;
end
figure(4)
```

```
plot([0 Vppt Voc ],[Isc Ippt 0 ],'o','LineWidth',2,'MarkeRsrize',6,'
    Color','k')
rectangle ("position", [16, 3.4, 2.8, 0.4],"linestyle","--");
rectangle ("position", [21, 0, 1.4, 0.2],"linestyle","--");
line([17 15.4], [3.4 3],"linewidth",1.5)
line([20.9 19.4], [0.2 0.8],"linewidth",1.5)
axes ('position', [0.35,0.55,0.3,0.28]);
for i=[1 2];
R=15<V & V<23;
I=Iph(i)+Io(i)-Io(i)*exp((V+(I.*Rsr(i)))./(n(i)*Vth*Nsc))-((V+(I.*
    Rsr(i)))./Rshr(i));
plot(V(R),I(R), c{i},"linewidth", 1.5);
set (gca, "xlim", [16 18.4], "ylim", [3.4 3.8])
set(gca,'XTick', 16:0.4:18.4)
set(gca, "linewidth", 1.5)
set(gca, "fontsize", 13)
hold on;
grid on;
clear I;
end
figure(4)
plot([0 Vppt Voc ],[Isc Ippt 0 ],'o','LineWidth',2,'MarkeRsrize',6,'
    Color','k')
axes ('position', [0.53, 0.25,0.25,0.24]);
for i=[1 2];
R=15<V & V<23;
I=Iph(i)+Io(i)-Io(i)*exp((V+(I.*Rsr(i)))./(n(i)*Vth*Nsc))-((V+(I.*
    Rsr(i)))./Rshr(i));
plot(V(R), I(R), c{i},"linewidth", 1.5);
set (gca, "xlim", [21.5 21.9], "ylim", [0 0.001])
set(gca,'XTick', 21.5:0.2:21.9)
set(gca, "linewidth", 1.5)
set(gca, "fontsize", 13)
hold on;
grid on;
clear I;
end
figure(4)
plot([0 Vppt Voc ],[Isc Ippt 0 ],'o','LineWidth',2,'MarkeRsrize',6,'
    Color','k')
```

Appendix VII

P-V Curve Code for $A \geq A_o$ (Figure 5.11 (b))

```
clc
clear
T=298.15;
k=1.3806503*10^(-23);
q=1.6021764*10^(-19);
Vth=(k*T)/q
Ippt=3.6247;
Vppt=16.8821;
Isc=3.7997;
Voc=21.5948;
Pmpp=Ippt*Vppt
Nsc = 36;
V=[0:0.1:1000];
n=[1.6554 1.978];
Io=[2.8481E-06 2.8414E-05];
Iph=[3.7997 3.8002];
Rshr = [64437.533 7043.3234];
Rsr = [0.001 0.8993];
c={'k','k--'};
for i=[1 2];
I=Iph(i)+Io(i)-Io(i)*exp((V+(I.*Rsr(i)))./(n(i)*Vth*Nsc))-((V+(I.*Rsr(i)))./Rshr(i));
P = V.*I;
figure(2)
plot(V,P, c{i},"linewidth", 1.5);
hleg = legend('n_o=1.6554','n=1.978',"location", "northwest");
set (hleg, "fontsize", 13);
legend boxoff
axis([0 23 0 65]);
set(gca, "linewidth", 1.5)
set(gca, "fontsize", 14)
xlabel('Voltage in volts', "fontsize", 20);
ylabel('Power in watts', "fontsize", 20);
hold on;
clear I;
end
figure (2)
```

```
plot([0 Vppt Voc ],[0 Pmpp 0 ],'o','LineWidth',2,'MarkeRsrize',5,'
    Color','k')
rectangle ("position", [16, 58, 3, 5],"linestyle","--");
rectangle ("position", [21.2, 0, 1, 4],"linestyle","--");
line([17 18], [42 58],"linewidth",1.5)
line([21.2 19.8], [4 12],"linewidth",1.5)
axes ('position', [0.55,0.44,0.25,0.2]);
for i=[1 2];
R=10<V & V<23;
I=Iph(i)+Io(i)-Io(i)*exp((V+(I.*Rsr(i)))./(n(i)*Vth*Nsc))-((V+(I.*
    Rsr(i)))./Rshr(i));
P = V.*I;
plot(V(R),P(R), c{i},"linewidth", 1.5);
set (gca, "xlim", [16 19], "ylim", [58 63.5])
set(gca,'XTick', 16:0.5:19)
set(gca, "linewidth", 1.5)
set(gca, "fontsize", 13)
hold on;
grid on;
clear I;
end
figure (2)
plot([0 Vppt Voc ],[0 Pmpp 0 ],'o','LineWidth',2,'MarkeRsrize',5,'
    Color','k')
axes ('position', [0.5,0.17,0.3,0.2]);
set(gca, "linewidth", 1.5)
for i=[1 2];
R=10<V & V<22;
I=Iph(i)+Io(i)-Io(i)*exp((V+(I.*Rsr(i)))./(n(i)*Vth*Nsc))-((V+(I.*
    Rsr(i)))./Rshr(i));
P = V.*I;
plot(V(R),P(R), c{i},"linewidth", 1.5);
set (gca, "xlim", [21.5 22], "ylim", [0 0.001])
set(gca,'XTick', 21.5:0.5:22)
set(gca, "linewidth", 1.5)
set(gca, "fontsize", 13)
hold on;
grid on;
clear I;
end
figure (2)
plot([0 Vppt Voc ],[0 Pmpp 0 ],'o','LineWidth',2,'MarkeRsrize',5,'
    Color','k')
```

Appendix VIII

I-V curve code for $0 \leq A \leq A_o$ (Figure 5.14 (a))

```
clc
clear all
output_precision(8)
Ippt=3.6247;
Vppt=16.8821;
Iscn=3.7997;
vocstc=21.5948;
Nsc = 36;
Pmax_e = Vppt*Ippt;
Kv = -0.123*vocstc;
Ki = -0.00318*Iscn;
T=298.15;
k=1.3806503*10^(-23);
q=1.6021764*10^(-19);
Vth=(k*T)/q;
%Method 1
Rsrinc=0.0001;
to1=0.001;
n_top=100;
nimax=2;
Rsr_max=(vocstc-Vppt)./Ippt;
Rshr_min=Vppt/(Iscn-Ippt)-Rsr_max;
Rshr=Rshr_min;
perror=Inf;
ni=0;
Rsr=0.8891;
a=0.5;
while (perror¿to1)&&(Rshr¿0)&&(ni<nimax)
Iph=(Rsr+Rshr)/Rshr*Iscn;
ni=ni+1 ;
Isc=Iscn;
Voc=vocstc;
A=a;
Io=(Iph*Rshr-Voc)./(Rshr*(exp(Voc/(n*Nsc*Vth))-1));%method 1
Rsr=Rsr+Rsrinc;
Rshr=(Vppt+Ippt*Rsr)./(Iph-Ippt-(Io*(exp((Vppt+Ippt*Rsr)./(n*Nsc*Vth
    ))-1)));
```

```
clear V
clear I
V=0:vocstc/n_top:23;
I=zeros(1,size(V,2));
for w=1: size(V,2)
x(w)=Iph-Io*(exp((V(w)+I(w)*Rsr)/Vth/Nsc/n)-1)-(V(w)+I(w)*Rsr)/Rshr-I(w);
while (abs(x(w))¿0.001)
x(w)=Iph-Io*(exp((V(w)+I(w)*Rsr)/Vth/Nsc/n)-1)-(V(w)+I(w)*Rsr)/Rshr-I(w);
xlin(w)=-Io*Rsr/Vth/Nsc/n*exp((V(w)+I(w)*Rsr)./Vth/Nsc/n)-Rsr/Rshr-1;
I_(w)=I(w)-x(w)/xlin(w);
I(w)=I_(w);
end
end
P = (Iph-Io*(exp((V+I.*Rsr)/Vth/Nsc/n)-1)-(V+I.*Rsr)/Rshr).*V;
Pmax_m = max(P)
perror = (Pmax_m-Pmax_e);
end
figure(3)
hold on
axis([0 23 0 4]);
plot(V,I,'LineWidth',1,"k") %
%Method 2
Rsrinc=0.0001;
tol=0.001;
n_top=100;
nimax=2;
Rsr_max=(vocstc-Vppt)./Ippt;
Rshr_min=Vppt/(Iscn-Ippt)-Rsr_max;
Rshr=Rshr_min;
perror=Inf;
ni=0;
Rsr=0.8891;
a=0.5;
while (perror¿tol)&&(Rshr¿0)&&(ni<nimax)
Iph=(Rsr+Rshr)/Rshr*Iscn;
ni=ni+1 ;
Isc=Iscn;
Voc=vocstc;

Io=Isc./exp(Voc./(n*Nsc*Vth));%method 2
Rsr=Rsr+Rsrinc;
Rshr=(Vppt+Ippt*Rsr)./(Iph-Ippt-(Io*(exp((Vppt+Ippt*Rsr)./(n*Nsc*Vth))-1))); %equation 27
clear V
clear I
V=0:vocstc/n_top:23;
I=zeros(1,size(V,2));
```

```
for w=1: size(V,2)
x(w)=Iph-Io*(exp((V(w)+I(w)*Rsr)/Vth/Nsc/n)-1)-(V(w)+I(w)*Rsr)/Rshr-I(w);
while (abs(x(w))¿0.001)
x(w)=Iph-Io*(exp((V(w)+I(w)*Rsr)/Vth/Nsc/n)-1)-(V(w)+I(w)*Rsr)/Rshr-I(w);
xlin(w)=-Io*Rsr/Vth/Nsc/n*exp((V(w)+I(w)*Rsr)./Vth/Nsc/n)-Rsr/Rshr-1;
I_(w)=I(w)-x(w)/xlin(w);
I(w)=I_(w);
end
end
P = (Iph-Io*(exp((V+I.*Rsr)/Vth/Nsc/n)-1)-(V+I.*Rsr)/Rshr).*V;
Pmax_m = max(P)
perror = (Pmax_m-Pmax_e);
end
figure(3)
hold on
axis([0 23 0 4]);
plot(V,I,'LineWidth',1,"r") %
%Method 3
Rsrinc=0.0001;
to1=0.001;
n_top=100;
nimax=2;
Rsr_max=(vocstc-Vppt)./Ippt;
Rshr_min=Vppt/(Iscn-Ippt)-Rsr_max;
Rshr=Rshr_min;
perror=Inf;
ni=0;
Rsr=0.8891;
n=0.5;
while (perror¿to1)&&(Rshr¿0)&&(ni<nimax)
Iph=(Rsr+Rshr)/Rshr*Iscn;
ni=ni+1 ;
Isc=Iscn;
Voc=vocstc;

Io=(Vppt-Voc+Ippt*Rshr+Ippt*Rsr)./(Rshr*(exp(Voc./(n*Nsc*Vth))-exp((Vppt+Ippt*Rsr)./(n*Nsc*Vth))))
%method 3
Rsr=Rsr+Rsrinc;
Rshr=(Vppt+Ippt*Rsr)./(Iph-Ippt-(Io*(exp((Vppt+Ippt*Rsr)./(n*Nsc*Vth))-1)));
clear V
clear I
V=0:vocstc/n_top:23;
I=zeros(1,size(V,2));
for w=1: size(V,2)
```

```
x(w)=Iph-Io*(exp((V(w)+I(w)*Rsr)/Vth/Nsc/n)-1)-(V(w)+I(w)*Rsr)/Rshr-I(w);
while (abs(x(w))¿0.001)
x(w)=Iph-Io*(exp((V(w)+I(w)*Rsr)/Vth/Nsc/n)-1)-(V(w)+I(w)*Rsr)/Rshr-I(w);
xlin(w)=-Io*Rsr/Vth/Nsc/n*exp((V(w)+I(w)*Rsr)./Vth/Nsc/n)-Rsr/Rshr-1;
I_(w)=I(w)-x(w)/clin(w);
I(w)=I_(w);
end
end
P = (Iph-Io*(exp((V+I.*Rsr)/Vth/Nsc/n)-1)-(V+I.*Rsr)/Rshr).*V;
Pmax_m = max(P)
perror = (Pmax_m-Pmax_e);
end
figure(3)
hold on
axis([0 23 0 4]);
plot(V,I,'LineWidth',1,"g") %
%Method 4
Rsrinc=0.0001;
tol=0.001;
n_top=1000;
nimax=2;
Rsr_max=(vocstc-Vppt)./Ippt;
Rshr_min=Vppt/(Iscn-Ippt)-Rsr_max;
Rshr=Rshr_min;
perror=Inf;
ni=0;
Rsr=0.8891;
n=0.5;
c={'w','w', 'w', 'w'};
for i=[1 2 3 4];
while (perror¿tol)&&(Rshr¿0)&&(ni<nimax)
Iph=(Rsr+Rshr)/Rshr*Iscn;
ni=ni+1 ;
Isc=Iscn;
Voc=vocstc;

Io=Ippt./(exp(Voc./(n*Nsc*Vth))-exp(Vppt./(n*Nsc*Vth))) %Method 4
Rsr=Rsr+Rsrinc;
Rshr=(Vppt+Ippt*Rsr)./(Iph-Ippt-(Io*(exp((Vppt+Ippt*Rsr)./(n*Nsc*Vth))-1)));
clear V
clear I
V=0:vocstc/n_top:23;
I=zeros(1,size(V,2));
for w=1: size(V,2)
x(w)=Iph-Io*(exp((V(w)+I(w)*Rsr)/Vth/Nsc/n)-1)-(V(w)+I(w)*Rsr)/Rshr-I(w);
```

```
while (abs(x(w))¿0.001)
x(w)=Iph-Io*(exp((V(w)+I(w)*Rsr)/Vth/Nsc/n)-1)-(V(w)+I(w)*Rsr)/Rshr-I(w);
xlin(w)=-Io*Rsr/Vth/Nsc/n*exp((V(w)+I(w)*Rsr)./Vth/Nsc/n)-Rsr/Rshr-1;
I_(w)=I(w)-x(w)/xlin(w);
I(w)=I_(w);
end
end
P = (Iph-Io*(exp((V+I.*Rsr)/Vth/Nsc/n)-1)-(V+I.*Rsr)/Rshr).*V;
Pmax_m = max(P)
perror = (Pmax_m-Pmax_e);
end
figure(3)
hold on
set(gca, "linewidth", 1.5)
set(gca, "fontsize", 14)
xlabel('Voltage [V]',"fontsize", 20);
ylabel('Current [A]',"fontsize", 20);
axis([0 23 0 4]);
plot(V,I, c(i),'LineWidth',1.5,'Color','b') %
hleg=legend('Approach 1','Approach 2','Approach 3','Approach 4',"location","southwest");
set (hleg, "fontsize", 14);
legend boxoff
%plot([0 Vppt vocstc ],[Iscn Ippt 0 ],'o','LineWidth',2,'MarkeRsrize',5,'Color','b')
box
end
figure (3)
plot([0 Vppt vocstc ],[Iscn Ippt 0 ],'o','LineWidth',2,'MarkeRsrize',5,'Color','b')
rectangle ("position", [16, 3.4, 2, 0.4],"linestyle","--");
rectangle ("position", [21, 0, 1.4, 0.2],"linestyle","--");
box
```

Appendix IX

P-V curve code for $0 \leq A \leq A_o$ (Figure 5.14 (b))

```
clc
clear all
output_precision(8)
Ippt=3.6247;
Vppt=16.8821;
Iscn=3.7997;
vocstc=21.5948;
Nsc = 36;
Pmax_e = Vppt*Ippt;
T=298.15;
k=1.3806503*10^(-23);
q=1.6021764*10^(-19);
Vth=(k*T)/q
%Method 1
Rsrinc=0.0001;
tol=0.001;
n_top=100;
nimax=2;
Rsr_max=(vocstc-Vppt)./Ippt;
Rshr_min=Vppt/(Iscn-Ippt)-Rsr_max;
Rshr=Rshr_min;
perror=Inf;
ni=0;
Rsr=0.8891;
n=0.5;
while (perror¿tol)&&(Rshr¿0)&&(ni<nimax)
Iph=(Rsr+Rshr)/Rshr*Iscn;
ni=ni+1 ;
Isc=Iscn;
Voc=vocstc;

Io=(Iph*Rshr-Voc)./(Rshr*(exp(Voc/(n*Nsc*Vth))-1));
Rsr=Rsr+Rsrinc;
Rshr=(Vppt+Ippt*Rsr)./(Iph-Ippt-(Io*(exp((Vppt+Ippt*Rsr)./(n*Nsc*Vth))-1)));
clear V
clear I
```

```
V=0:vocstc/n_top:34;
I=zeros(1,size(V,2));
for w=1: size(V,2)
x(w)=Iph-Io*(exp((V(w)+I(w)*Rsr)/Vth/Nsc/n)-1)-(V(w)+I(w)*Rsr)/Rshr-I(w);
while (abs(x(w))¿0.001)
x(w)=Iph-Io*(exp((V(w)+I(w)*Rsr)/Vth/Nsc/n)-1)-(V(w)+I(w)*Rsr)/Rshr-I(w);
xlin(w)=-Io*Rsr/Vth/Nsc/n*exp((V(w)+I(w)*Rsr)./Vth/Nsc/n)-Rsr/Rshr-1;
I_(w)=I(w)-x(w)/clin(w);
I(w)=I_(w);
end
end
P = (Iph-Io*(exp((V+I.*Rsr)/Vth/Nsc/n)-1)-(V+I.*Rsr)/Rshr).*V;
Pmax_m = max(P)
perror = (Pmax_m-Pmax_e);
end
figure(4)
hold on
axis([0 23 0 65]);
plot(V,P,'LineWidth',1.5,"k") %
%Method 2
Rsrinc=0.0001;
tol=0.001;
n_top=100;
nimax=2;
Rsr_max=(vocstc-Vppt)./Ippt;
Rshr_min=Vppt/(Iscn-Ippt)-Rsr_max;
Rshr=Rshr_min;
perror=Inf;
ni=0;
Rsr=0.8891;
n=0.5;
while (perror¿tol)&&(Rshr¿0)&&(ni<nimax)
Iph=(Rsr+Rshr)/Rshr*Iscn;
ni=ni+1 ;
Isc=Iscn;
Voc=vocstc;

Io=Isc./exp(Voc./(n*Nsc*Vth));
Rsr=Rsr+Rsrinc;
Rshr=(Vppt+Ippt*Rsr)./(Iph-Ippt-(Io*(exp((Vppt+Ippt*Rsr)./(n*Nsc*Vth))-1)));
clear V
clear I
V=0:vocstc/n_top:34;
I=zeros(1,size(V,2));
for w=1: size(V,2)
```

```
x(w)=Iph-Io*(exp((V(w)+I(w)*Rsr)/Vth/Nsc/n)-1)-(V(w)+I(w)*Rsr)/Rshr-I(w);
while (abs(x(w))¿0.001)
x(w)=Iph-Io*(exp((V(w)+I(w)*Rsr)/Vth/Nsc/n)-1)-(V(w)+I(w)*Rsr)/Rshr-I(w);
xlin(w)=-Io*Rsr/Vth/Nsc/n*exp((V(w)+I(w)*Rsr)./Vth/Nsc/n)-Rsr/Rshr-1;
I_(w)=I(w)-x(w)/clin(w);
I(w)=I_(w);
end
end
P = (Iph-Io*(exp((V+I.*Rsr)/Vth/Nsc/n)-1)-(V+I.*Rsr)/Rshr).*V;
Pmax_m = max(P)
perror = (Pmax_m-Pmax_e);
end
figure(4)
hold on
axis([0 23 0 65]);
plot(V,P,'LineWidth',1.5,"r") %
%Method 3
Rsrinc=0.0001;
to1=0.001;
n_top=100;
nimax=2;
Rsr_max=(vocstc-Vppt)./Ippt;
Rshr_min=Vppt/(Iscn-Ippt)-Rsr_max;
Rshr=Rshr_min;
perror=Inf;
ni=0;
Rsr=0.8891;
a=0.5;
while (perror¿to1)&&(Rshr¿0)&&(ni<nimax)
Iph=(Rsr+Rshr)/Rshr*Iscn;
ni=ni+1 ;
Isc=Iscn;
Voc=vocstc;
A=a;
Io=(Vppt-Voc+Ippt*Rshr+Ippt*Rsr)./(Rshr*(exp(Voc./(n*Nsc*Vth))-exp((Vppt+Ippt*Rsr)./(n*Nsc*Vth))))
Rsr=Rsr+Rsrinc;
Rshr=(Vppt+Ippt*Rsr)./(Iph-Ippt-(Io*(exp((Vppt+Ippt*Rsr)./(n*Nsc*Vth))-1)));
clear V
clear I
V=0:vocstc/n_top:34;
I=zeros(1,size(V,2));
for w=1: size(V,2)
x(w)=Iph-Io*(exp((V(w)+I(w)*Rsr)/Vth/Nsc/n)-1)-(V(w)+I(w)*Rsr)/Rshr-I(w);
while (abs(x(w))¿0.001)
```

```
x(w)=Iph-Io*(exp((V(w)+I(w)*Rsr)/Vth/Nsc/n)-1)-(V(w)+I(w)*Rsr)/Rshr-I(w);
xlin(w)=-Io*Rsr/Vth/Nsc/n*exp((V(w)+I(w)*Rsr)./Vth/Nsc/n)-Rsr/Rshr-1;
I_(w)=I(w)-x(w)/clin(w);
I(w)=I_(w);
end
end
P = (Iph-Io*(exp((V+I.*Rsr)/Vth/Nsc/n)-1)-(V+I.*Rsr)/Rshr).*V;
Pmax_m = max(P)
perror = (Pmax_m-Pmax_e);
end
figure(4)
hold on
axis([0 23 0 65]);
plot(V,P,'LineWidth',1.5,"g") %
%Method 4
Rsrinc=0.0001;
tol=0.001;
n_top=100;
nimax=2;
Rsr_max=(vocstc-Vppt)./Ippt;
Rshr_min=Vppt/(Iscn-Ippt)-Rsr_max;
Rshr=Rshr_min;
perror=Inf;
ni=0;
Rsr=0.8891;
a=0.5;
c={'w','w', 'w', 'w'};
for i=[1 2 3 4];
while (perror¿tol)&&(Rshr¿0)&&(ni<nimax)
Iph=(Rsr+Rshr)/Rshr*Iscn;
ni=ni+1 ;
Isc=Iscn;
Voc=vocstc;
A=a;
Io=Ippt./(exp(Voc./(n*Nsc*Vth))-exp(Vppt./(n*Nsc*Vth)))
Rsr=Rsr+Rsrinc;
Rshr=(Vppt+Ippt*Rsr)./(Iph-Ippt-(Io*(exp((Vppt+Ippt*Rsr)./(n*Nsc*Vth))-1)));
clear V
clear I
V=0:vocstc/n_top:34;
I=zeros(1,size(V,2));
for w=1: size(V,2)
x(w)=Iph-Io*(exp((V(w)+I(w)*Rsr)/Vth/Nsc/n)-1)-(V(w)+I(w)*Rsr)/Rshr-I(w);
while (abs(x(w))¿0.001)
x(w)=Iph-Io*(exp((V(w)+I(w)*Rsr)/Vth/Nsc/n)-1)-(V(w)+I(w)*Rsr)/Rshr-I(w);
```

```
xlin(w)=-Io*Rsr/Vth/Nsc/n*exp((V(w)+I(w)*Rsr)./Vth/Nsc/n)-Rsr/Rshr-1;
I_(w)=I(w)-x(w)/clin(w);
I(w)=I_(w);
end
end
P = (Iph-Io*(exp((V+I.*Rsr)/Vth/Nsc/n)-1)-(V+I.*Rsr)/Rshr).*V;
Pmax_m = max(P)
perror = (Pmax_m-Pmax_e);
end
figure(4)
hold on
set(gca, "linewidth", 1.5)
set(gca, "fontsize", 14)
xlabel('Voltage [V]',"fontsize", 20);
ylabel('Power [W]',"fontsize", 20);
axis([0 23 0 65]);
plot(V,P, c(i),'LineWidth',1.5,'Color','b') %
hleg = legend('Approach 1', 'Approach 2','Approach 3','Approach 4',"location", "northwest");
set (hleg, "fontsize", 14);
legend boxoff
%plot([0 Vppt vocstc ],[Iscn Ippt 0 ],'o','LineWidth',2,'MarkeRsrize',5,'Color','b')
box
end
figure (4)
plot([0 Vppt vocstc ],[0 Pmax_e 0 ],'o','LineWidth',2,'MarkeRsrize',5,'Color','b')
rectangle ("position", [16.5, 59.5, 1, 4],"linestyle","--");
rectangle ("position", [21.2, 0, 1, 4],"linestyle","--");
box
```

Appendix X

Data Analysis Code for KC130GT at Various Irradiances (Table 5.7)

```
clc
clear all
output_precision(8)
T=298.15;
Ta=302.15;
Iscn = 8.02;
vocstc = 21.9;
Ippt = 7.39;
Vppt = 17.6;
Pmax_e = Vppt*Ippt;
Kv = -0.0821;
Ki = 0.00318;
Nsc = 36;
T=298.15;
k=1.3806503*10^(-23);
q=1.6021764*10^(-19);
Vth=(k*T)/q
Gn=1000;
G=1000
n=1.34;
Ion=Iscn/(exp(vocstc/(n*Vth*Ns)))
Voc=(log(Iscn)-log(Ion))*(n*Vth*Ns)
Ta=320.15;
dT=Ta-T;
Isc=(Iscn+Ki*dT)*G/Gn
Vth1=(k*Ta)/q
Eg=1.12;
n=1.34;
Ion1=Ion*[Ta/T]^3*(exp(q*Eg/(k*n)*((1/T)-(1/Ta))))
Voc=(log(Isc)-log(Ion1))*(n*Vth1*Nsc)
Io=Isc/(exp(Voc/(n*Vth1*Ns)))
Voc2=vocstc+Kv*dT+(1.1811e-3*(G-Gn))+(-1.8544e-6*(G-Gn)^2)
Ki=0.00135;
Ippt1=(Ippt+Ki*dT)*G/Gn
no=(vocstc-Vppt)./(Vth*Nsc*log(Iscn./(Iscn-Ippt)));
```

```
Vppto=Voc-(no*Vth1*Nsc*log(Isc/(Isc-Ippt1)))
Vppt4=Vppt+(-140e-3*dT)+(-9.6801e-5*(G-Gn))+(-2.73215e-6*(G-Gn)^2)
Ion3=Isc/(exp(Voc/(n*Vth1*Nsc)))
%@800
G=800
n=1.34;
Ta=320.15;
dT=Ta-T;
Isc=(Iscn+Ki*dT)*G/Gn
Vth1=(k*Ta)/q
Eg=1.12;
n=1.34;
Ion=Iscn/(exp(vocstc/(n*Vth*Ns)))
Ion1=Ion*[Ta/T]^3*(exp(q*Eg/(k*n)*((1/T)-(1/Ta))))
Voc=(log(Isc)-log(Ion1))*(n*Vth1*Ns)
Voc2=vocstc+Kv*dT+(1.1811e-3*(G-Gn))+(-1.8544e-6*(G-Gn)^2)
Io=Isc/(exp(Voc/(n*Vth1*Ns)))
Ki= 0.00135;
Ippt1=(Ippt+Ki*dT)*G/Gn
no=(vocstc-Vppt)./(Vth*Nsc*log(Iscn./(Iscn-Ippt)));
Vppto=Voc-(no*Vth1*Nsc*log(Isc/(Isc-Ippt1)))%equation 26
Vppt4=Vppt+(-140e-3*dT)+(-9.6801e-5*(G-Gn))+(-2.73215e-6*(G-Gn)^2)
Ion3=Isc/(exp(Voc/(n*Vth1*Nsc)))

%@600
G=600
n=1.34;
Ta=320.15;
dT=Ta-T;
Isc=(Iscn+Ki*dT)*G/Gn
Vth1=(k*Ta)/q
Eg=1.12;
n=1.34;
Ion=Iscn/(exp(vocstc/(n*Vth*Ns)))
Ion1=Ion*[Ta/T]^3*(exp(q*Eg/(k*n)*((1/T)-(1/Ta))))
Voc=(log(Isc)-log(Ion1))*(n*Vth1*Ns)
Voc2=vocstc+Kv*dT+(1.1811e-3*(G-Gn))+(-1.8544e-6*(G-Gn)^2)
Io=Isc/(exp(Voc/(n*Vth1*Ns)))
Ki= 0.00135;
Ippt1=(Ippt+Ki*dT)*G/Gn
no=(vocstc-Vppt)./(Vth*Ns*log(Iscn./(Iscn-Ippt)));
Vppto=Voc-(no*Vth1*Ns*log(Isc/(Isc-Ippt1)))%equation 26
Vppt4=Vppt+(-140e-3*dT)+(-9.6801e-5*(G-Gn))+(-2.73215e-6*(G-Gn)^2)
%@400
G=400
n=1.34;
Ta=320.15;
dT=Ta-T;
Isc=(Iscn+Ki*dT)*G/Gn
Vth1=(k*Ta)/q
```

```
Eg=1.12;
n=1.34;
Ion=Iscn/(exp(vocstc/(n*Vth*Ns)))
Ion1=Ion*[Ta/T]^3*(exp(q*Eg/(k*n)*((1/T)-(1/Ta))))
Voc=(log(Isc)-log(Ion1))*(n*Vth1*Ns)
Voc2=vocstc+Kv*dT+(1.1811e-3*(G-Gn))+(-1.8544e-6*(G-Gn)^2)
Io=Isc/(exp(Voc/(n*Vth1*Ns)))
Ki= 0.00135;
Ippt1=(Ippt+Ki*dT)*G/Gn
no=(vocstc-Vppt)./(Vth*Ns*log(Iscn./(Iscn-Ippt)));
Vppto=Voc-(no*Vth1*Ns*log(Isc/(Isc-Ippt1)))%equation 26
Vppt4=Vppt+(-140e-3*dT)+(-9.6801e-5*(G-Gn))+(-2.73215e-6*(G-Gn)^2)
%@200
G=200
n=1.34;
Ta=320.15;
dT=Ta-T;
Isc=(Iscn+Ki*dT)*G/Gn
Vth1=(k*Ta)/q
Eg=1.12;
n=1.34;
Ion=Iscn/(exp(vocstc/(n*Vth*Nsc)))
Ion1=Ion*[Ta/T]^3*(exp(q*Eg/(k*n)*((1/T)-(1/Ta))))
Voc=(log(Isc)-log(Ion1))*(n*Vth1*Nsc)
Voc2=vocstc+Kv*dT+(1.1811e-3*(G-Gn))+(-1.8544e-6*(G-Gn)^2)
Io=Isc/(exp(Voc/(n*Vth1*Nsc)))
Ki= 0.00135;
Ippt1=(Ippt+Ki*dT)*G/Gn
no=(vocstc-Vppt)./(Vth*Ns*log(Iscn./(Iscn-Ippt)));
Vppto=Voc-(no*Vth1*Ns*log(Isc/(Isc-Ippt1)))%equation 26
Vppt4=Vppt+(-140e-3*dT)+(-9.6801e-5*(G-Gn))+(-2.73215e-6*(G-Gn)^2)
```

Appendix XI

Data Analysis Code for KC130GT at Various Temperatures Table 5.8)

```
clc
clear all
output_precision(8)
Iscn = 8.02;
vocstc = 21.9;
Ippt = 7.39;
Vppt = 17.6;
Pmax_e = Vppt*Ippt;
Kv = -0.0821;
Ki = 0.00318;
Nsc = 36;
T=298.15;
k=1.3806503*10^(-23);
q=1.6021764*10^(-19);
Vth=(k*T)/q;
Gn=1000;
Ta= 20
G=1000;
n=1.14;
Ion=Iscn/(exp(vocstc/(n*Vth*Nsc)));
Voc=(log(Iscn)-log(Ion))*(n*Vth*Nsc);
Ta=326.9;
dT=Ta-T;
Isc=(Iscn+Ki*dT)*G/Gn
Vth1=(k*Ta)/q;
Eg=1.12;
n=1.14;
Ion1=Ion*[Ta/T]^3*(exp(q*Eg/(k*n)*((1/T)-(1/Ta))));
Voc=(log(Isc)-log(Ion1))*(n*Vth1*Nsc)
Io=Isc/(exp(Voc/(n*Vth1*Nsc)));
Voc2=vocstc+Kv*dT+(1.1811e-3*(G-Gn))+(-1.8544e-6*(G-Gn)^2)
Ki= 0.0025;
Ippt1=(Ippt+Ki*dT)*G/Gn
no=(vocstc-Vppt)./(Vth*Nsc*log(Iscn./(Iscn-Ippt)));
Vppto=Voc-(no*Vth1*Nsc*log(Isc/(Isc-Ippt1)))
```

```
Vppt4=Vppt+(-140e-3*dT)+(-9.6801e-5*(G-Gn))+(-2.73215e-6*(G-Gn)^2)
Ion3=Isc/(exp(Voc/(n*Vth1*Nsc)));
Ta=25
G=1000;
n=1.34;
Ion=Iscn/(exp(vocstc/(n*Vth*Nsc)));
Voc=(log(Iscn)-log(Ion))*(n*Vth*Nsc);
Ta=331.9;
dT=Ta-T;
Isc=(Iscn+Ki*dT)*G/Gn
Vth1=(k*Ta)/q;
Eg=1.12;
n=1.14;
Ion1=Ion*[Ta/T]^3*(exp(q*Eg/(k*n)*((1/T)-(1/Ta))));
Voc=(log(Isc)-log(Ion1))*(n*Vth1*Nsc)
Io=Isc/(exp(Voc/(n*Vth1*Nsc)));
Voc2=vocstc+Kv*dT+(1.1811e-3*(G-Gn))+(-1.8544e-6*(G-Gn)^2)
Ki= 0.0025;
Ippt1=(Ippt+Ki*dT)*G/Gn
no=(vocstc-Vppt)./(Vth*Nsc*log(Iscn./(Iscn-Ippt)));
Vppto=Voc-(no*Vth1*Nsc*log(Isc/(Isc-Ippt1)))
Vppt4=Vppt+(-140e-3*dT)+(-9.6801e-5*(G-Gn))+(-2.73215e-6*(G-Gn)^2)%
    Zaimi et al 2019
Ion3=Isc/(exp(Voc/(n*Vth1*Nsc)));
Ta= 30
G=1000;
n=1.14;
Ion=Iscn/(exp(vocstc/(n*Vth*Nsc)));
Voc=(log(Iscn)-log(Ion))*(n*Vth*Nsc);
Ta=336.9;
dT=Ta-T;
Isc=(Iscn+Ki*dT)*G/Gn
Vth1=(k*Ta)/q;
Eg=1.12;
n=1.14;
Ion1=Ion*[Ta/T]^3*(exp(q*Eg/(k*n)*((1/T)-(1/Ta))));
Voc=(log(Isc)-log(Ion1))*(n*Vth1*Nsc)
Io=Isc/(exp(Voc/(n*Vth1*Nsc)));
Voc2=vocstc+Kv*dT+(1.1811e-3*(G-Gn))+(-1.8544e-6*(G-Gn)^2)
Ki= 0.0025;
Ippt1=(Ippt+Ki*dT)*G/Gn
no=(vocstc-Vppt)./(Vth*Nsc*log(Iscn./(Iscn-Ippt)));
Vppto=Voc-(no*Vth1*Nsc*log(Isc/(Isc-Ippt1)))
Vppt4=Vppt+(-140e-3*dT)+(-9.6801e-5*(G-Gn))+(-2.73215e-6*(G-Gn)^2)
Ion3=Isc/(exp(Voc/(n*Vth1*Nsc)));
Ta=35
G=1000;
n=1.34;
Ion=Iscn/(exp(vocstc/(n*Vth*Nsc)));
Voc=(log(Iscn)-log(Ion))*(n*Vth*Nsc);
```

```
Ta=341.9;
dT=Ta-T;
Isc=(Iscn+Ki*dT)*G/Gn
Vth1=(k*Ta)/q;
Eg=1.12;
n=1.34;
Ion1=Ion*[Ta/T]^3*(exp(q*Eg/(k*n)*((1/T)-(1/Ta))));
Voc=(log(Isc)-log(Ion1))*(n*Vth1*Nsc)
Io=Isc/(exp(Voc/(n*Vth1*Nsc)));
Voc2=vocstc+Kv*dT+(1.1811e-3*(G-Gn))+(-1.8544e-6*(G-Gn)^2)
Ki= 0.0025;
Ippt1=(Ippt+Ki*dT)*G/Gn
no=(vocstc-Vppt)./(Vth*Nsc*log(Iscn./(Iscn-Ippt)));
Vppto=Voc-(no*Vth1*Nsc*log(Isc/(Isc-Ippt1)))
Vppt4=Vppt+(-140e-3*dT)+(-9.6801e-5*(G-Gn))+(-2.73215e-6*(G-Gn)^2)
Ion3=Isc/(exp(Voc/(n*Vth1*Nsc)));
Ta=40
G=1000;
n=1.34;
Ion=Iscn/(exp(vocstc/(n*Vth*Nsc)));
Voc=(log(Iscn)-log(Ion))*(n*Vth*Nsc);
Ta=346.9;
dT=Ta-T;
Isc=(Iscn+Ki*dT)*G/Gn
Vth1=(k*Ta)/q;
Eg=1.12;
n=1.34;
Ion1=Ion*[Ta/T]^3*(exp(q*Eg/(k*n)*((1/T)-(1/Ta))));
Voc=(log(Isc)-log(Ion1))*(n*Vth1*Nsc)
Io=Isc/(exp(Voc/(n*Vth1*Nsc)));
Voc2=vocstc+Kv*dT+(1.1811e-3*(G-Gn))+(-1.8544e-6*(G-Gn)^2)
Ki= 0.0025;
Ippt1=(Ippt+Ki*dT)*G/Gn
no=(vocstc-Vppt)./(Vth*Nsc*log(Iscn./(Iscn-Ippt)));
Vppto=Voc-(no*Vth1*Nsc*log(Isc/(Isc-Ippt1)))
Vppt4=Vppt+(-140e-3*dT)+(-9.6801e-5*(G-Gn))+(-2.73215e-6*(G-Gn)^2)
Ion3=Isc/(exp(Voc/(n*Vth1*Nsc)));
Ta=45
G=1000;
n=1.34;
Ion=Iscn/(exp(vocstc/(n*Vth*Nsc)));
Voc=(log(Iscn)-log(Ion))*(n*Vth*Nsc);
Ta=351.9;
dT=Ta-T;
Isc=(Iscn+Ki*dT)*G/Gn
Vth1=(k*Ta)/q;
Eg=1.12;
n=1.34;
Ion1=Ion*[Ta/T]^3*(exp(q*Eg/(k*n)*((1/T)-(1/Ta))));
Voc=(log(Isc)-log(Ion1))*(n*Vth1*Nsc)
```

```
Io=Isc/(exp(Voc/(n*Vth1*Nsc)));
Voc2=vocstc+Kv*dT+(1.1811e-3*(G-Gn))+(-1.8544e-6*(G-Gn)^2)
Ki= 0.0025;
Ippt1=(Ippt+Ki*dT)*G/Gn
no=(vocstc-Vppt)./(Vth*Nsc*log(Iscn./(Iscn-Ippt)));
Vppto=Voc-(no*Vth1*Nsc*log(Isc/(Isc-Ippt1)))
Vppt4=Vppt+(-140e-3*dT)+(-9.6801e-5*(G-Gn))+(-2.73215e-6*(G-Gn)^2)
Ion3=Isc/(exp(Voc/(n*Vth1*Nsc)));
Ta=50
G=1000;
n=1.34;
Ion=Iscn/(exp(vocstc/(n*Vth*Nsc)));
Voc=(log(Iscn)-log(Ion))*(n*Vth*Nsc);
Ta=356.9;
dT=Ta-T;
Isc=(Iscn+Ki*dT)*G/Gn
Vth1=(k*Ta)/q;
Eg=1.12;
n=1.34;
Ion1=Ion*[Ta/T]^3*(exp(q*Eg/(k*n)*((1/T)-(1/Ta))));
Voc=(log(Isc)-log(Ion1))*(n*Vth1*Nsc)
Io=Isc/(exp(Voc/(n*Vth1*Nsc)));
Voc2=vocstc+Kv*dT+(1.1811e-3*(G-Gn))+(-1.8544e-6*(G-Gn)^2)
Ki= 0.0025;
Ippt1=(Ippt+Ki*dT)*G/Gn
no=(vocstc-Vppt)./(Vth*Nsc*log(Iscn./(Iscn-Ippt)));
Vppto=Voc-(no*Vth1*Nsc*log(Isc/(Isc-Ippt1)))
Vppt4=Vppt+(-140e-3*dT)+(-9.6801e-5*(G-Gn))+(-2.73215e-6*(G-Gn)^2)
Ion3=Isc/(exp(Voc/(n*Vth1*Nsc)));
```

Appendix XII

I-V Curve Code for KC130GT at Various Irradiances (Figure 5.17)

```
clc
clear all
output_precision(8)
sa= 1000 %Irradiance=1000W/m2, Ta=20^oC TNOCT=^oC, Tcell=320.15K
Iscn= 8.09;
Ippt= 7.4197;
Vppt= 15.7475;
vocstc= 20.2681;
Pmax_e = Vppt*Ippt;
Nsc = 36;
T=320.15;
k=1.3806503*10^(-23);
q=1.6021764*10^(-19);
Vth=(k*T)/q;
Rsrinc=0.001;
to1=0.001;
n_top=100;
nimax=2;
Rsr_max=(vocstc-Vppt)./Ippt;
Rshr_min=Vppt/(Iscn-Ippt)-Rsr_max;
Rshr=Rshr_min;
perror=Inf;
ni=0;
Rsr=0.156;
A=1.34;
while (perror¿to1)&&(Rshr¿0)&&(ni<nimax)
Iph=(Rsr+Rshr)/Rshr*Iscn;
ni=ni+1 ;
Isc=Iscn;
Voc=vocstc;
Io=Isc./exp(Voc./(n*Nsc*Vth));
Rsr=Rsr+Rsrinc;
Rshr=(Vppt+Ippt*Rsr)./(Iph-Ippt-(Io*(exp((Vppt+Ippt*Rsr)./(n*Nsc*Vth
    ))-1)));
clear V
```

```
clear I
V=0:vocstc/n_top:23;
I=zeros(1,size(V,2));
for w=1: size(V,2)
x(w)=Iph-Io*(exp((V(w)+I(w)*Rsr)/Vth/Nsc/n)-1)-(V(w)+I(w)*Rsr)/Rshr-I(w);
while (abs(x(w))¿0.001)
x(w)=Iph-Io*(exp((V(w)+I(w)*Rsr)/Vth/Nsc/n)-1)-(V(w)+I(w)*Rsr)/Rshr-I(w);
xlin(w)=-Io*Rsr/Vth/Nsc/n*exp((V(w)+I(w)*Rsr)./Vth/Nsc/n)-Rsr/Rshr-1;
I_(w)=I(w)-x(w)/xlin(w);
I(w)=I_(w);
end
end
P = (Iph-Io*(exp((V+I.*Rsr)/Vth/Nsc/n)-1)-(V+I.*Rsr)/Rshr).*V;
Pmax_m = max(P);
perror = (Pmax_m-Pmax_e);
end
figure(12)
box
hold on
axis([0 25 0 10]);
plot(V,I,'LineWidth',2,"k")
box
sa= 800 %Irradiance=1000W/m2, Ta=20^oC TNOCT=^oC, Tcell=320.15K
Iscn= 6.472;
Ippt= 5.9358;
Vppt= 15.4505;
vocstc= 19.9712;
Pmax_e = Vppt*Ippt;
Nsc = 36;
T=320.15;
k=1.3806503*10^(-23);
q=1.6021764*10^(-19);
Vth=(k*T)/q;
Rsrinc=0.001;
to1=0.001;
n_top=100;
nimax=2;
Rsr_max=(vocstc-Vppt)./Ippt;
Rshr_min=Vppt/(Iscn-Ippt)-Rsr_max;
Rshr=Rshr_min;
perror=Inf;
ni=0;
Rsr=0.20;
A=1.32;
while (perror¿to1)&&(Rshr¿0)&&(ni<nimax)
Iph=(Rsr+Rshr)/Rshr*Iscn;
ni=ni+1 ;
```

```
Isc=Iscn;
Voc=vocstc;
Io=Isc./exp(Voc./(n*Nsc*Vth));%method 2
Rsr=Rsr+Rsrinc;
Rshr=(Vppt+Ippt*Rsr)./(Iph-Ippt-(Io*(exp((Vppt+Ippt*Rsr)./(n*Nsc*Vth))-1))); %equation 27
clear V
clear I
V=0:vocstc/n_top:23;
I=zeros(1,size(V,2));
for w=1: size(V,2)
x(w)=Iph-Io*(exp((V(w)+I(w)*Rsr)/Vth/Nsc/n)-1)-(V(w)+I(w)*Rsr)/Rshr-I(w);
while (abs(x(w))¿0.001)
x(w)=Iph-Io*(exp((V(w)+I(w)*Rsr)/Vth/Nsc/n)-1)-(V(w)+I(w)*Rsr)/Rshr-I(w);
xlin(w)=-Io*Rsr/Vth/Nsc/n*exp((V(w)+I(w)*Rsr)./Vth/Nsc/n)-Rsr/Rshr-1;
I_(w)=I(w)-x(w)/xlin(w);
I(w)=I_(w);
end
end
P = (Iph-Io*(exp((V+I.*Rsr)/Vth/Nsc/n)-1)-(V+I.*Rsr)/Rshr).*V;
Pmax_m = max(P);
perror = (Pmax_m-Pmax_e);
end
figure(12)
box
hold on
axis([0 25 0 10]);
plot(V,I,'LineWidth',2,"r")
box
sa= 600 %Irradiance=1000W/m2, Ta=20^oC TNOCT=^oC, Tcell=320.15K
Iscn= 4.854;
Ippt= 4.4518;
Vppt= 15.0677;
vocstc= 19.5883;
Pmax_e = Vppt*Ippt;
Nsc = 36;
T=320.15;
k=1.3806503*10^(-23);
q=1.6021764*10^(-19);
Vth=(k*T)/q;
Rsrinc=0.001;
tol=0.001;
n_top=100;
nimax=2;
Rsr_max=(vocstc-Vppt)./Ippt;
Rshr_min=Vppt/(Iscn-Ippt)-Rsr_max;
Rshr=Rshr_min;
```

```
perror=Inf;
ni=0;
Rsr=0.3;
A=1.29;
while (perror¿tol)&&(Rshr¿0)&&(ni<nimax)
Iph=(Rsr+Rshr)/Rshr*Iscn;
ni=ni+1 ;
Isc=Iscn;
Voc=vocstc;
Io=Isc./exp(Voc./(n*Nsc*Vth));%method 2
Rsr=Rsr+Rsrinc;
Rshr=(Vppt+Ippt*Rsr)./(Iph-Ippt-(Io*(exp((Vppt+Ippt*Rsr)./(n*Nsc*Vth))-1))); %equation 27
clear V
clear I
V=0:vocstc/n_top:23;
I=zeros(1,size(V,2));
for w=1: size(V,2)
x(w)=Iph-Io*(exp((V(w)+I(w)*Rsr)/Vth/Nsc/n)-1)-(V(w)+I(w)*Rsr)/Rshr-I(w);
while (abs(x(w))¿0.001)
x(w)=Iph-Io*(exp((V(w)+I(w)*Rsr)/Vth/Nsc/n)-1)-(V(w)+I(w)*Rsr)/Rshr-I(w);
xlin(w)=-Io*Rsr/Vth/Nsc/n*exp((V(w)+I(w)*Rsr)./Vth/Nsc/n)-Rsr/Rshr-1;
I_(w)=I(w)-x(w)/xlin(w);
I(w)=I_(w);
end
end
P = (Iph-Io*(exp((V+I.*Rsr)/Vth/Nsc/n)-1)-(V+I.*Rsr)/Rshr).*V;
Pmax_m = max(P);
perror = (Pmax_m-Pmax_e);
end
figure(12)
box
hold on
axis([0 25 0 10]);
plot(V,I,'LineWidth',2,"b") %%
box
sa= 400 %Irradiance=1000W/m2, Ta=20^oC TNOCT=^oC, Tcell=320.15K
Iscn=3.236;
Ippt=2.968;
Vppt=14.528;
vocstc=19.0487;
Pmax_e = Vppt*Ippt;
Nsc = 36;
T=320.15;
k=1.3806503*10^(-23);
q=1.6021764*10^(-19);
Vth=(k*T)/q;
```

```
Rsrinc=0.001;
tol=0.001;
n_top=100;
nimax=2;
Rsr_max=(vocstc-Vppt)./Ippt;
Rshr_min=Vppt/(Iscn-Ippt)-Rsr_max;
Rshr=Rshr_min;
perror=Inf;
ni=0;
Rsr=0.36;
A=1.26;
while (perror¿tol)&&(Rshr¿0)&&(ni<nimax)
Iph=(Rsr+Rshr)/Rshr*Iscn;
ni=ni+1 ;
Isc=Iscn;
Voc=vocstc;
Io=Isc./exp(Voc./(n*Nsc*Vth));%method 2
Rsr=Rsr+Rsrinc;
Rshr=(Vppt+Ippt*Rsr)./(Iph-Ippt-(Io*(exp((Vppt+Ippt*Rsr)./(n*Nsc*Vth))-1))); %equation 27
clear V
clear I
V=0:vocstc/n_top:34;
I=zeros(1,size(V,2));
for w=1: size(V,2)
x(w)=Iph-Io*(exp((V(w)+I(w)*Rsr)/Vth/Nsc/n)-1)-(V(w)+I(w)*Rsr)/Rshr-I(w);
while (abs(x(w))¿0.001)
x(w)=Iph-Io*(exp((V(w)+I(w)*Rsr)/Vth/Nsc/n)-1)-(V(w)+I(w)*Rsr)/Rshr-I(w);
xlin(w)=-Io*Rsr/Vth/Nsc/n*exp((V(w)+I(w)*Rsr)./Vth/Nsc/n)-Rsr/Rshr-1;
I_(w)=I(w)-x(w)/xlin(w);
I(w)=I_(w);
end
end
P = (Iph-Io*(exp((V+I.*Rsr)/Vth/Nsc/n)-1)-(V+I.*Rsr)/Rshr).*V;
Pmax_m = max(P);
perror = (Pmax_m-Pmax_e);
end
figure(12)
box
hold on
axis([0 25  0 10]);
plot(V,I,'LineWidth',2,"g")
box
sa= 200 %Irradiance=1000W/m2, Ta=20^oC TNOCT=^oC, Tcell=320.15K
Iscn=1.618;
Ippt=1.4839;
Vppt=13.606;
```

```
vocstc=18.126;
Pmax_e = Vppt*Ippt;
Nsc = 36;
T=320.15;
k=1.3806503*10^(-23);
q=1.6021764*10^(-19);
Vth=(k*T)/q;
Rsrinc=0.001;
tol=0.001;
n_top=100;
nimax=2;
Rsr_max=(vocstc-Vppt)./Ippt;
Rshr_min=Vppt/(Iscn-Ippt)-Rsr_max;
Rshr=Rshr_min;
perror=Inf;
ni=0;
Rsr=1.15;
A=1.1;
while (perror¿tol)&&(Rshr¿0)&&(ni<nimax)
Iph=(Rsr+Rshr)/Rshr*Iscn;
ni=ni+1 ;
Isc=Iscn;
Voc=vocstc;
Io=Isc./exp(Voc./(n*Nsc*Vth));%method 2
Rsr=Rsr+Rsrinc;
Rshr=(Vppt+Ippt*Rsr)./(Iph-Ippt-(Io*(exp((Vppt+Ippt*Rsr)./(n*Nsc*Vth))-1))); %equation 27
clear V
clear I
V=0:vocstc/n_top:34;
I=zeros(1,size(V,2));
for w=1: size(V,2)
x(w)=Iph-Io*(exp((V(w)+I(w)*Rsr)/Vth/Nsc/n)-1)-(V(w)+I(w)*Rsr)/Rshr-I(w);
while (abs(x(w))¿0.001)
x(w)=Iph-Io*(exp((V(w)+I(w)*Rsr)/Vth/Nsc/n)-1)-(V(w)+I(w)*Rsr)/Rshr-I(w);
xlin(w)=-Io*Rsr/Vth/Nsc/n*exp((V(w)+I(w)*Rsr)./Vth/Nsc/n)-Rsr/Rshr-1;
I_(w)=I(w)-x(w)/xlin(w);
I(w)=I_(w);
end
end
P = (Iph-Io*(exp((V+I.*Rsr)/Vth/Nsc/n)-1)-(V+I.*Rsr)/Rshr).*V;
Pmax_m = max(P);
perror = (Pmax_m-Pmax_e);
end
figure(12)
box
hold on
```

```
axis([0 25  0 10]);
plot(V,I,'LineWidth',2,"c") %%
box
sa= 200; %Irradiance=1000W/m2, Ta=20^oC TNOCT=^oC, Tcell=320.15K
Iscn=1.618;
Ippt=1.4839;
Vppt=13.606;
vocstc=18.126;
Pmax_e = Vppt*Ippt;
Nsc = 36;
T=320.15;
k=1.3806503*10^(-23);
q=1.6021764*10^(-19);
Vth=(k*T)/q;
Rsrinc=0.001;
tol=0.001;
n_top=100;
nimax=2;
Rsr_max=(vocstc-Vppt)./Ippt;
Rshr_min=Vppt/(Iscn-Ippt)-Rsr_max;
Rshr=Rshr_min;
perror=Inf;
ni=0;
Rsr=1.15;
A=1.1;
c={'w','w', 'w', 'w', 'w'};
for i=[1 2 3 4 5];
while (perror¿tol)&&(Rshr¿0)&&(ni<nimax)
Iph=(Rsr+Rshr)/Rshr*Iscn;
ni=ni+1 ;
Isc=Iscn;
Voc=vocstc;
Io=Ippt./(exp(Voc./(n*Nsc*Vth))-exp(Vppt./(n*Nsc*Vth))); %Method 4
Rsr=Rsr+Rsrinc;
Rshr=(Vppt+Ippt*Rsr)./(Iph-Ippt-(Io*(exp((Vppt+Ippt*Rsr)./(n*Nsc*Vth
    ))-1))); %equation 27
clear V
clear I
V=0:vocstc/n_top:23;
I=zeros(1,size(V,2));
for w=1: size(V,2)
x(w)=Iph-Io*(exp((V(w)+I(w)*Rsr)/Vth/Nsc/n)-1)-(V(w)+I(w)*Rsr)/Rshr-
    I(w);
while (abs(x(w))¿0.001)
x(w)=Iph-Io*(exp((V(w)+I(w)*Rsr)/Vth/Nsc/n)-1)-(V(w)+I(w)*Rsr)/Rshr-
    I(w);
xlin(w)=-Io*Rsr/Vth/Nsc/n*exp((V(w)+I(w)*Rsr)./Vth/Nsc/n)-Rsr/Rshr-1
    ;
I_(w)=I(w)-x(w)/xlin(w);
I(w)=I_(w);
```

```
end
end
P = (Iph-Io*(exp((V+I.*Rsr)/Vth/Nsc/n)-1)-(V+I.*Rsr)/Rshr).*V;
Pmax_m = max(P);
perror = (Pmax_m-Pmax_e);
end
figure(12)
box
hold on
set(gca, "linewidth", 1.5)
set(gca, "fontsize", 14)
xlabel('Voltage [V]',"fontsize", 20);
ylabel('Current [A]',"fontsize", 20);
axis([0 25  0 10]);
plot(V,I,'LineWidth',2,"c") %%
hleg = legend('Sa=1000W/m^2', 'Sa=800W/m^2','Sa=600W/m^2','Sa=400W/m
    ^2','Sa=200W/m^2', "location", "northeast");
set (hleg, "fontsize", 15);
legend boxoff
box
end
figure (12)
plot([0 15.748 20.268],[8.090 7.420 0],'o','LineWidth',2,'
    MarkeRsrize',6,'Color','k')
box
figure (12)
plot([0 15.451 19.971],[6.472 5.936 0 ],'o','LineWidth',2,'
    MarkeRsrize',5,'Color','r')
box
figure (12)
plot([0 15.068 19.588],[4.8540 4.452 0],'o','LineWidth',2,'
    MarkeRsrize',5,'Color','b')
box
figure (12)
plot([0 14.528 19.049],[3.2360 2.968  0],'o','LineWidth',2,'
    MarkeRsrize',5,'Color','g')
box
figure (12)
plot([0 13.606 18.126],[1.618 1.484 0],'o','LineWidth',2,'
    MarkeRsrize',5,'Color','c')
box
```

Appendix XIII

P-V Curve Code for KC130GT at Various Irradiances (Figure 5.18)

```
clc
clear all
output_precision(8)
sa= 1000 %Irradiance=1000W/m2, Ta=20^oC TNOCT=^oC, Tcell=320.15K
Iscn= 8.09;
Ippt= 7.4197;
Vppt= 15.7475;
vocstc= 20.2681;
Pmax_e = Vppt*Ippt;
Nsc = 36;
T=320.15;
k=1.3806503*10^(-23);
q=1.6021764*10^(-19);
Vth=(k*T)/q;
Rsrinc=0.001;
tol=0.001;
n_top=100;
nimax=2;
Rsr_max=(vocstc-Vppt)./Ippt;
Rshr_min=Vppt/(Iscn-Ippt)-Rsr_max;
Rshr=Rshr_min;
perror=Inf;
ni=0;
Rsr=0.156;
A=1.34;
while (perror¿tol)&&(Rshr¿0)&&(ni<nimax)
Iph=(Rsr+Rshr)/Rshr*Iscn;
ni=ni+1 ;
Isc=Iscn;
Voc=vocstc;
Io=Isc./exp(Voc./(n*Nsc*Vth));
Rsr=Rsr+Rsrinc;
Rshr=(Vppt+Ippt*Rsr)./(Iph-Ippt-(Io*(exp((Vppt+Ippt*Rsr)./(n*Nsc*Vth
    ))-1)));
clear V
```

```
clear I
V=0:vocstc/n_top:23;
I=zeros(1,size(V,2));
for w=1: size(V,2)
x(w)=Iph-Io*(exp((V(w)+I(w)*Rsr)/Vth/Nsc/n)-1)-(V(w)+I(w)*Rsr)/Rshr-I(w);
while (abs(x(w))¿0.001)
x(w)=Iph-Io*(exp((V(w)+I(w)*Rsr)/Vth/Nsc/n)-1)-(V(w)+I(w)*Rsr)/Rshr-I(w);
xlin(w)=-Io*Rsr/Vth/Nsc/n*exp((V(w)+I(w)*Rsr)./Vth/Nsc/n)-Rsr/Rshr-1;
I_(w)=I(w)-x(w)/xlin(w);
I(w)=I_(w);
end
end
P = (Iph-Io*(exp((V+I.*Rsr)/Vth/Nsc/n)-1)-(V+I.*Rsr)/Rshr).*V;
Pmax_m = max(P);
perror = (Pmax_m-Pmax_e);
end
figure(12)
box
hold on
axis([0 23 0 135]);
plot(V,P,'LineWidth',2,"k")
box
sa= 800 %Irradiance=1000W/m2, Ta=20^oC TNOCT=^oC, Tcell=320.15K
Iscn= 6.472;
Ippt= 5.9358;
Vppt= 15.4505;
vocstc= 19.9712;
Pmax_e = Vppt*Ippt;
Nsc = 36;
T=320.15;
k=1.3806503*10^(-23);
q=1.6021764*10^(-19);
Vth=(k*T)/q;
Rsrinc=0.001;
to1=0.001;
n_top=100;
nimax=2;
Rsr_max=(vocstc-Vppt)./Ippt;
Rshr_min=Vppt/(Iscn-Ippt)-Rsr_max;
Rshr=Rshr_min;
perror=Inf;
ni=0;
Rsr=0.20;
A=1.32;
while (perror¿to1)&&(Rshr¿0)&&(ni<nimax)
Iph=(Rsr+Rshr)/Rshr*Iscn;
ni=ni+1 ;
```

```
Isc=Iscn;
Voc=vocstc;
Io=Isc./exp(Voc./(n*Nsc*Vth));%method 2
Rsr=Rsr+Rsrinc;
Rshr=(Vppt+Ippt*Rsr)./(Iph-Ippt-(Io*(exp((Vppt+Ippt*Rsr)./(n*Nsc*Vth))-1)));
clear V
clear I
V=0:vocstc/n_top:23;
I=zeros(1,size(V,2));
for w=1: size(V,2)
x(w)=Iph-Io*(exp((V(w)+I(w)*Rsr)/Vth/Nsc/n)-1)-(V(w)+I(w)*Rsr)/Rshr-I(w);
while (abs(x(w))¿0.001)
x(w)=Iph-Io*(exp((V(w)+I(w)*Rsr)/Vth/Nsc/n)-1)-(V(w)+I(w)*Rsr)/Rshr-I(w);
xlin(w)=-Io*Rsr/Vth/Nsc/n*exp((V(w)+I(w)*Rsr)./Vth/Nsc/n)-Rsr/Rshr-1;
I_(w)=I(w)-x(w)/xlin(w);
I(w)=I_(w);
end
end
P = (Iph-Io*(exp((V+I.*Rsr)/Vth/Nsc/n)-1)-(V+I.*Rsr)/Rshr).*V;
Pmax_m = max(P);
perror = (Pmax_m-Pmax_e);
end
figure(12)
box
hold on
axis([0 23 0 135]);
plot(V,P,'LineWidth',2,"r")
box
sa= 600 %Irradiance=1000W/m2, Ta=20^oC TNOCT=^oC, Tcell=320.15K
Iscn= 4.854;
Ippt= 4.4518;
Vppt= 15.0677;
vocstc= 19.5883;
Pmax_e = Vppt*Ippt;
Ns = 36;
T=320.15;
k=1.3806503*10^(-23);
q=1.6021764*10^(-19);
Vth=(k*T)/q;
Rsrinc=0.001;
to1=0.001;
n_top=100;
nimax=2;
Rsr_max=(vocstc-Vppt)./Ippt;
Rshr_min=Vppt/(Iscn-Ippt)-Rsr_max;
Rshr=Rshr_min;
```

```
perror=Inf;
ni=0;
Rsr=0.3;
A=1.29;
while (perror¿tol)&&(Rshr¿0)&&(ni<nimax)
Iph=(Rsr+Rshr)/Rshr*Iscn;
ni=ni+1 ;
Isc=Iscn;
Voc=vocstc;
Io=Isc./exp(Voc./(n*Nsc*Vth));%method 2
Rsr=Rsr+Rsrinc;
Rshr=(Vppt+Ippt*Rsr)./(Iph-Ippt-(Io*(exp((Vppt+Ippt*Rsr)./(n*Nsc*Vth))-1))); %equation 27
clear V
clear I
V=0:vocstc/n_top:23;
I=zeros(1,size(V,2));
for w=1: size(V,2)
x(w)=Iph-Io*(exp((V(w)+I(w)*Rsr)/Vth/Nsc/n)-1)-(V(w)+I(w)*Rsr)/Rshr-I(w);
while (abs(x(w))¿0.001)
x(w)=Iph-Io*(exp((V(w)+I(w)*Rsr)/Vth/Nsc/n)-1)-(V(w)+I(w)*Rsr)/Rshr-I(w);
xlin(w)=-Io*Rsr/Vth/Nsc/n*exp((V(w)+I(w)*Rsr)./Vth/Nsc/n)-Rsr/Rshr-1;
I_(w)=I(w)-x(w)/xlin(w);
I(w)=I_(w);
end
end
P = (Iph-Io*(exp((V+I.*Rsr)/Vth/Nsc/n)-1)-(V+I.*Rsr)/Rshr).*V;
Pmax_m = max(P);
perror = (Pmax_m-Pmax_e);
end
figure(12)
box
hold on
axis([0 23  0 135]);
plot(V,P,'LineWidth',2,"b") %%
box
sa= 400 %Irradiance=1000W/m2, Ta=20^oC TNOCT=^oC, Tcell=320.15K
Iscn=3.236;
Ippt=2.968;
Vppt=14.528;
vocstc=19.0487;
Pmax_e = Vppt*Ippt;
Ns = 36;
T=320.15;
k=1.3806503*10^(-23);
q=1.6021764*10^(-19);
Vth=(k*T)/q;
```

```
Rsrinc=0.001;
tol=0.001;
n_top=100;
nimax=2;
Rsr_max=(vocstc-Vppt)./Ippt;
Rshr_min=Vppt/(Iscn-Ippt)-Rsr_max;
Rshr=Rshr_min;
perror=Inf;
ni=0;
Rsr=0.36;
A=1.26;
while (perror¿tol)&&(Rshr¿0)&&(ni<nimax)
Iph=(Rsr+Rshr)/Rshr*Iscn;
ni=ni+1 ;
Isc=Iscn;
Voc=vocstc;
Io=Isc./exp(Voc./(n*Nsc*Vth));%method 2
Rsr=Rsr+Rsrinc;
Rshr=(Vppt+Ippt*Rsr)./(Iph-Ippt-(Io*(exp((Vppt+Ippt*Rsr)./(n*Nsc*Vth
    ))-1)));
clear V
clear I
V=0:vocstc/n_top:23;
I=zeros(1,size(V,2));
for w=1: size(V,2)
x(w)=Iph-Io*(exp((V(w)+I(w)*Rsr)/Vth/Nsc/n)-1)-(V(w)+I(w)*Rsr)/Rshr-
    I(w);
while (abs(x(w))¿0.001)
x(w)=Iph-Io*(exp((V(w)+I(w)*Rsr)/Vth/Nsc/n)-1)-(V(w)+I(w)*Rsr)/Rshr-
    I(w);
xlin(w)=-Io*Rsr/Vth/Nsc/n*exp((V(w)+I(w)*Rsr)./Vth/Nsc/n)-Rsr/Rshr-1
    ;
I_(w)=I(w)-x(w)/xlin(w);
I(w)=I_(w);
end
end
P = (Iph-Io*(exp((V+I.*Rsr)/Vth/Nsc/n)-1)-(V+I.*Rsr)/Rshr).*V;
Pmax_m = max(P);
perror = (Pmax_m-Pmax_e);
end
figure(12)
box
hold on
axis([0 23 0 135]);
plot(V,P,'LineWidth',2,"g")
box
sa= 200 %Irradiance=1000W/m2, Ta=20^oC TNOCT=^oC, Tcell=320.15K
Iscn=1.618;
Ippt=1.4839;
Vppt=13.606;
```

```
vocstc=18.126;
Pmax_e = Vppt*Ippt;
Ns = 36;
T=320.15;
k=1.3806503*10^(-23);
q=1.6021764*10^(-19);
Vth=(k*T)/q;
Rsrinc=0.001;
tol=0.001;
n_top=100;
nimax=2;
Rsr_max=(vocstc-Vppt)./Ippt;
Rshr_min=Vppt/(Iscn-Ippt)-Rsr_max;
Rshr=Rshr_min;
perror=Inf;
ni=0;
Rsr=1.15;
A=1.1;
while (perror¿tol)&&(Rshr¿0)&&(ni<nimax)
Iph=(Rsr+Rshr)/Rshr*Iscn;
ni=ni+1  ;
Isc=Iscn;
Voc=vocstc;
Io=Isc./exp(Voc./(n*Nsc*Vth));%method 2
Rsr=Rsr+Rsrinc;
Rshr=(Vppt+Ippt*Rsr)./(Iph-Ippt-(Io*(exp((Vppt+Ippt*Rsr)./(n*Nsc*Vth))-1))); %equation 27
clear V
clear I
V=0:vocstc/n_top:34;
I=zeros(1,size(V,2));
for w=1: size(V,2)
x(w)=Iph-Io*(exp((V(w)+I(w)*Rsr)/Vth/Nsc/n)-1)-(V(w)+I(w)*Rsr)/Rshr-I(w);
while (abs(x(w))¿0.001)
x(w)=Iph-Io*(exp((V(w)+I(w)*Rsr)/Vth/Nsc/n)-1)-(V(w)+I(w)*Rsr)/Rshr-I(w);
xlin(w)=-Io*Rsr/Vth/Nsc/n*exp((V(w)+I(w)*Rsr)./Vth/Nsc/n)-Rsr/Rshr-1;
I_(w)=I(w)-x(w)/xlin(w);
I(w)=I_(w);
end
end
P = (Iph-Io*(exp((V+I.*Rsr)/Vth/Nsc/n)-1)-(V+I.*Rsr)/Rshr).*V;
Pmax_m = max(P);
perror = (Pmax_m-Pmax_e);
end
figure(12)
box
hold on
```

```
axis([0 23   0 135]);
plot(V,P, 'LineWidth',2,"c") %%
box
sa= 200; %Irradiance=1000W/m2, Ta=20^oC TNOCT=^oC, Tcell=320.15K
Iscn=1.618;
Ippt=1.4839;
Vppt=13.606;
vocstc=18.126;
Pmax_e = Vppt*Ippt;
Ns = 36;
T=320.15;
k=1.3806503*10^(-23);
q=1.6021764*10^(-19);
Vth=(k*T)/q;
Rsrinc=0.001;
tol=0.001;
n_top=100;
nimax=2;
Rsr_max=(vocstc-Vppt)./Ippt;
Rshr_min=Vppt/(Iscn-Ippt)-Rsr_max;
Rshr=Rshr_min;
perror=Inf;
ni=0;
Rsr=1.15;
A=1.1;
c={'w', 'w',  'w',  'w',  'w'};
for  i=[1 2 3 4 5];
while  (perror¿tol)&&(Rshr¿0)&&(ni<nimax)
Iph=(Rsr+Rshr)/Rshr*Iscn;
ni=ni+1  ;
Isc=Iscn;
Voc=vocstc;
Io=Ippt./(exp(Voc./(n*Nsc*Vth))-exp(Vppt./(n*Nsc*Vth))); %Method 4
Rsr=Rsr+Rsrinc;
Rshr=(Vppt+Ippt*Rsr)./(Iph-Ippt-(Io*(exp((Vppt+Ippt*Rsr)./(n*Nsc*Vth))-1))); %equation 27
clear  V
clear  I
V=0:vocstc/n_top:23;
I=zeros(1,size(V,2));
for  w=1:  size(V,2)
x(w)=Iph-Io*(exp((V(w)+I(w)*Rsr)/Vth/Nsc/n)-1)-(V(w)+I(w)*Rsr)/Rshr-I(w);
while  (abs(x(w))¿0.001)
x(w)=Iph-Io*(exp((V(w)+I(w)*Rsr)/Vth/Nsc/n)-1)-(V(w)+I(w)*Rsr)/Rshr-I(w);
xlin(w)=-Io*Rsr/Vth/Nsc/n*exp((V(w)+I(w)*Rsr)./Vth/Nsc/n)-Rsr/Rshr-1;
I_(w)=I(w)-x(w)/xlin(w);
I(w)=I_(w);
```

```
end
end
P = (Iph-Io*(exp((V+I.*Rsr)/Vth/Nsc/n)-1)-(V+I.*Rsr)/Rshr).*V;
Pmax_m = max(P);
perror = (Pmax_m-Pmax_e);
end
figure(12)
box
hold on
set(gca, "linewidth", 1.5)
set(gca, "fontsize", 14)
xlabel('Voltage [V]',"fontsize", 20);
ylabel('Power [W]',"fontsize", 20);
axis([0 23  0 135]);
plot(V,P,'LineWidth',2,"c") %%
hleg = legend('Sa=1000W/m^2', 'Sa=800W/m^2','Sa=600W/m^2','Sa=400W/m^2','Sa=200W/m^2', "location", "northwest");
set (hleg, "fontsize", 15);
legend boxoff
box
end
figure (12)
plot([0 15.748 20.268],[0 116.845 0 ],'o','LineWidth',2,'MarkeRsrize',6,'Color','k')
box
figure (12)
plot([0 15.451 19.971],[0 91.712   0 ],'o','LineWidth',2,'MarkeRsrize',6,'Color','r')
box
figure (12)
plot([0 15.068 19.588],[0 67.079 0 ],'o','LineWidth',2,'MarkeRsrize',6,'Color','b')
box
figure (12)
plot([0 14.528  19.049],[0 43.887 0 ],'o','LineWidth',2,'MarkeRsrize',6,'Color','g')
box
figure (12)
plot([0 13.606  18.126],[0  20.213 0 ],'o','LineWidth',2,'MarkeRsrize',6,'Color','c')
box
```

Appendix IX

I-V Curve Code for KC130GT at various temperatures (Figure 5.19)

```
clc
clear all
output_precision(8)
Ta=20 %@1000W/m2 20oC
Iscn =8.1114;
Ippt= 7.4288;
Vppt= 15.177;
vocstc =19.764;
Pmax_e = Vppt*Ippt;
Ns = 36;
T=326.9;
k=1.3806503*10^(-23);
q=1.6021764*10^(-19);
Vth=(k*T)/q;
Rsrinc=0.001;
to1=0.001;
n_top=100;
nimax=2;
Rsr_max=(vocstc-Vppt)./Ippt;
Rshr_min=Vppt/(Iscn-Ippt)-Rsr_max;
Rshr=Rshr_min;
perror=Inf;
ni=0;
Rsr=0.163;
A=1.33;
while (perror¿to1)&&(Rshr¿0)&&(ni<nimax)
Iph=(Rsr+Rshr)/Rshr*Iscn;
ni=ni+1 ;
Isc=Iscn;
Voc=vocstc;
Io=Isc./exp(Voc./(n*Nsc*Vth));
Rsr=Rsr+Rsrinc;
Rshr=(Vppt+Ippt*Rsr)./(Iph-Ippt-(Io*(exp((Vppt+Ippt*Rsr)./(n*Nsc*Vth
    ))-1)));
clear V
```

```
clear I
V=0:vocstc/n_top:23;
I=zeros(1,size(V,2));
for w=1: size(V,2)
x(w)=Iph-Io*(exp((V(w)+I(w)*Rsr)/Vth/Nsc/n)-1)-(V(w)+I(w)*Rsr)/Rshr-I(w);
while (abs(x(w))¿0.001)
x(w)=Iph-Io*(exp((V(w)+I(w)*Rsr)/Vth/Nsc/n)-1)-(V(w)+I(w)*Rsr)/Rshr-I(w);
xlin(w)=-Io*Rsr/Vth/Nsc/n*exp((V(w)+I(w)*Rsr)./Vth/Nsc/n)-Rsr/Rshr-1;
I_(w)=I(w)-x(w)/xlin(w);
I(w)=I_(w);
end
end
P = (Iph-Io*(exp((V+I.*Rsr)/Vth/Nsc/n)-1)-(V+I.*Rsr)/Rshr).*V;
Pmax_m = max(P);
perror = (Pmax_m-Pmax_e);
end
figure(12)
box
hold on
axis([0 25 0 10]);
plot(V,I,'LineWidth',2,"r") % %
box
Ta=25 % @1000W/m2 25oC
Iscn= 8.1273;
Ippt= 7.4356;
Vppt= 14.754;
vocstc= 19.389;
Pmax_e = Vppt*Ippt;
T=331.9;
Rsrinc=0.001;
tol=0.001;
n_top=100;
nimax=2;
Rsr_max=(vocstc-Vppt)./Ippt;
Rshr_min=Vppt/(Iscn-Ippt)-Rsr_max;
Rshr=Rshr_min;
perror=Inf;
ni=0;
Rsr=0.18;
A=1.3;
while (perror¿tol)&&(Rshr¿0)&&(ni<nimax)
Iph=(Rsr+Rshr)/Rshr*Iscn;
ni=ni+1 ;
Isc=Iscn;
Voc=vocstc;
Io=Isc./exp(Voc./(n*Nsc*Vth));
Rsr=Rsr+Rsrinc;
```

```
Rshr=(Vppt+Ippt*Rsr)./(Iph-Ippt-(Io*(exp((Vppt+Ippt*Rsr)./(n*Nsc*Vth))-1)));
clear V
clear I
V=0:vocstc/n_top:23;
I=zeros(1,size(V,2));
for w=1: size(V,2)
x(w)=Iph-Io*(exp((V(w)+I(w)*Rsr)/Vth/Nsc/n)-1)-(V(w)+I(w)*Rsr)/Rshr-I(w);
while (abs(x(w))¿0.001)
x(w)=Iph-Io*(exp((V(w)+I(w)*Rsr)/Vth/Nsc/n)-1)-(V(w)+I(w)*Rsr)/Rshr-I(w);
xlin(w)=-Io*Rsr/Vth/Nsc/n*exp((V(w)+I(w)*Rsr)./Vth/Nsc/n)-Rsr/Rshr-1;
I_(w)=I(w)-x(w)/xlin(w);
I(w)=I_(w);
end
end
P = (Iph-Io*(exp((V+I.*Rsr)/Vth/Nsc/n)-1)-(V+I.*Rsr)/Rshr).*V;
Pmax_m = max(P);
perror = (Pmax_m-Pmax_e);
end
figure(12)
hold on
axis([0 25 0 10]);
plot(V,I,'LineWidth',2,"k") % %
box
Ta =30 % @1000W/m2 30oC
Iscn=8.1432;
Ippt= 7.4423;
Vppt= 14.330;
vocstc=19.014;
Pmax_e = Vppt*Ippt;
T=336.9;
Rsrinc=0.001;
tol=0.001;
n_top=100;
nimax=2;
Rsr_max=(vocstc-Vppt)./Ippt;
Rshr_min=Vppt/(Iscn-Ippt)-Rsr_max;
Rshr=Rshr_min;
perror=Inf;
ni=0;
Rsr=0.201;
A=1.29;
while (perror¿tol)&&(Rshr¿0)&&(ni<nimax)
Iph=(Rsr+Rshr)/Rshr*Iscn;
ni=ni+1 ;
Isc=Iscn;
Voc=vocstc;
```

```
Io=Isc./exp(Voc./(n*Nsc*Vth));
Rsr=Rsr+Rsrinc;
Rshr=(Vppt+Ippt*Rsr)./(Iph-Ippt-(Io*(exp((Vppt+Ippt*Rsr)./(n*Nsc*Vth))-1)));
clear V
clear I
V=0:vocstc/n_top:23;
I=zeros(1,size(V,2));
for w=1: size(V,2)
x(w)=Iph-Io*(exp((V(w)+I(w)*Rsr)/Vth/Nsc/n)-1)-(V(w)+I(w)*Rsr)/Rshr-I(w);
while (abs(x(w))¿0.001)
x(w)=Iph-Io*(exp((V(w)+I(w)*Rsr)/Vth/Nsc/n)-1)-(V(w)+I(w)*Rsr)/Rshr-I(w);
xlin(w)=-Io*Rsr/Vth/Nsc/n*exp((V(w)+I(w)*Rsr)./Vth/Nsc/n)-Rsr/Rshr-1;
I_(w)=I(w)-x(w)/xlin(w);
I(w)=I_(w);
end
end
P = (Iph-Io*(exp((V+I.*Rsr)/Vth/Nsc/n)-1)-(V+I.*Rsr)/Rshr).*V;
Pmax_m = max(P);
perror = (Pmax_m-Pmax_e);
end
figure(12)
hold on
axis([0 25 0 10]);
plot(V,I,'LineWidth',2,"c") % %
box
Ta=35 % @1000W/m2 35oC
Iscn=8.1591;
Ippt=7.4491;
Vppt=13.905;
vocstc=18.638;
Pmax_e = Vppt*Ippt;
T=341.9;
Rsrinc=0.001;
to1=0.001;
n_top=100;
nimax=2;
Rsr_max=(vocstc-Vppt)./Ippt;
Rshr_min=Vppt/(Iscn-Ippt)-Rsr_max;
Rshr=Rshr_min;
perror=Inf;
ni=0;
Rsr=0.223;
A=1.27;
while (perror¿to1)&&(Rshr¿0)&&(ni<nimax)
Iph=(Rsr+Rshr)/Rshr*Iscn;
ni=ni+1 ;
```

```
Isc=Iscn;
Voc=vocstc;
Io=Isc./exp(Voc./(n*Nsc*Vth));
Rsr=Rsr+Rsrinc;
Rshr=(Vppt+Ippt*Rsr)./(Iph-Ippt-(Io*(exp((Vppt+Ippt*Rsr)./(n*Nsc*Vth))-1))); %equation 27
clear V
clear I
V=0:vocstc/n_top:23;
I=zeros(1,size(V,2));
for w=1: size(V,2)
x(w)=Iph-Io*(exp((V(w)+I(w)*Rsr)/Vth/Nsc/n)-1)-(V(w)+I(w)*Rsr)/Rshr-I(w);
while (abs(x(w))¿0.001)
x(w)=Iph-Io*(exp((V(w)+I(w)*Rsr)/Vth/Nsc/n)-1)-(V(w)+I(w)*Rsr)/Rshr-I(w);
xlin(w)=-Io*Rsr/Vth/Nsc/n*exp((V(w)+I(w)*Rsr)./Vth/Nsc/n)-Rsr/Rshr-1;
I_(w)=I(w)-x(w)/xlin(w);
I(w)=I_(w);
end
end
P = (Iph-Io*(exp((V+I.*Rsr)/Vth/Nsc/n)-1)-(V+I.*Rsr)/Rshr).*V;
Pmax_m = max(P);
perror = (Pmax_m-Pmax_e);
end
figure(12)
hold on
axis([0 25 0 10]);
plot(V,I,'LineWidth',2,"g")
box
Ta=40 %@1000W/m2 40oC
Iscn =8.1750;
Ippt= 7.4558;
Vppt= 13.480;
vocstc =18.261;
Pmax_e = Vppt*Ippt;
T=346.9;
Rsrinc=0.001;
tol=0.001;
n_top=100;
nimax=2;
Rsr_max=(vocstc-Vppt)./Ippt;
Rshr_min=Vppt/(Iscn-Ippt)-Rsr_max;
Rshr=Rshr_min;
perror=Inf;
ni=0;
Rsr=0.235;
A=1.22;
while (perror¿tol)&&(Rshr¿0)&&(ni<nimax)
```

```
Iph=(Rsr+Rshr)/Rshr*Iscn;
ni=ni+1  ;
Isc=Iscn;
Voc=vocstc;
Io=Isc./exp(Voc./(n*Nsc*Vth));
Rsr=Rsr+Rsrinc;
Rshr=(Vppt+Ippt*Rsr)./(Iph-Ippt-(Io*(exp((Vppt+Ippt*Rsr)./(n*Nsc*Vth
    ))-1))); %equation 27
clear V
clear I
V=0:vocstc/n_top:23;
I=zeros(1,size(V,2));
for w=1: size(V,2)
x(w)=Iph-Io*(exp((V(w)+I(w)*Rsr)/Vth/Nsc/n)-1)-(V(w)+I(w)*Rsr)/Rshr-
    I(w);
while (abs(x(w))¿0.001)
x(w)=Iph-Io*(exp((V(w)+I(w)*Rsr)/Vth/Nsc/n)-1)-(V(w)+I(w)*Rsr)/Rshr-
    I(w);
xlin(w)=-Io*Rsr/Vth/Nsc/n*exp((V(w)+I(w)*Rsr)./Vth/Nsc/n)-Rsr/Rshr-1
    ;
I_(w)=I(w)-x(w)/xlin(w);
I(w)=I_(w);
end
end
P = (Iph-Io*(exp((V+I.*Rsr)/Vth/Nsc/n)-1)-(V+I.*Rsr)/Rshr).*V;
Pmax_m = max(P);
perror = (Pmax_m-Pmax_e);
end
figure(12)
hold on
axis([0 25 0 10]);
plot(V,I,'LineWidth',2,"m")
box
Ta=45 %@1000W/m2 45oC
Iscn= 8.1909;
Ippt= 7.4626;
Vppt= 13.055;
vocstc= 17.883;
Pmax_e = Vppt*Ippt;
T=351.9;
Rsrinc=0.001;
tol=0.001;
n_top=100;
nimax=2;
Rsr_max=(vocstc-Vppt)./Ippt;
Rshr_min=Vppt/(Iscn-Ippt)-Rsr_max;
Rshr=Rshr_min;
perror=Inf;
ni=0;
Rsr=0.246;
```

```
A=1.21;
while (perror¿tol)&&(Rshr¿0)&&(ni<nimax)
Iph=(Rsr+Rshr)/Rshr*Iscn;
ni=ni+1  ;
Isc=Iscn;
Voc=vocstc;
Io=Isc./exp(Voc./(n*Nsc*Vth));
Rsr=Rsr+Rsrinc;
Rshr=(Vppt+Ippt*Rsr)./(Iph-Ippt-(Io*(exp((Vppt+Ippt*Rsr)./(n*Nsc*Vth))-1))); %equation 27
clear V
clear I
V=0:vocstc/n_top:23;
I=zeros(1,size(V,2));
for w=1: size(V,2)
x(w)=Iph-Io*(exp((V(w)+I(w)*Rsr)/Vth/Nsc/n)-1)-(V(w)+I(w)*Rsr)/Rshr-I(w);
while (abs(x(w))¿0.001)
x(w)=Iph-Io*(exp((V(w)+I(w)*Rsr)/Vth/Nsc/n)-1)-(V(w)+I(w)*Rsr)/Rshr-I(w);
xlin(w)=-Io*Rsr/Vth/Nsc/n*exp((V(w)+I(w)*Rsr)./Vth/Nsc/n)-Rsr/Rshr-1;
I_(w)=I(w)-x(w)/xlin(w);
I(w)=I_(w);
end
end
P = (Iph-Io*(exp((V+I.*Rsr)/Vth/Nsc/n)-1)-(V+I.*Rsr)/Rshr).*V;
Pmax_m = max(P);
perror = (Pmax_m-Pmax_e);
end
figure(12)
hold on
axis([0 25 0 10]);
plot(V,I,'LineWidth',2,"--k") %%
box
Ta=50 %@1000W/m2 50oC
Iscn= 8.2068;
Ippt= 7.4693;
Vppt= 12.629;
vocstc= 17.504;
Pmax_e = Vppt*Ippt;
T=356.9;
Rsrinc=0.001;
tol=0.001;
n_top=100;
nimax=2;
Rsr_max=(vocstc-Vppt)./Ippt;
Rshr_min=Vppt/(Iscn-Ippt)-Rsr_max;
Rshr=Rshr_min;
perror=Inf;
```

```
ni=0;
Rsr=0.277;
A=1.18;
c={'w', 'w', 'w', 'w', 'w', 'w', 'w'};
for i=[1 2 3 4 5 6 7];
while (perror¿tol)&&(Rshr¿0)&&(ni<nimax)
Iph=(Rsr+Rshr)/Rshr*Iscn;
ni=ni+1 ;
Isc=Iscn;
Voc=vocstc;
Io=Ippt./(exp(Voc./(n*Nsc*Vth))-exp(Vppt./(n*Nsc*Vth)));
Rsr=Rsr+Rsrinc;
Rshr=(Vppt+Ippt*Rsr)./(Iph-Ippt-(Io*(exp((Vppt+Ippt*Rsr)./(n*Nsc*Vth))-1)));
clear V
clear I
V=0:vocstc/n_top:23;
I=zeros(1,size(V,2));
for w=1: size(V,2)
x(w)=Iph-Io*(exp((V(w)+I(w)*Rsr)/Vth/Nsc/n)-1)-(V(w)+I(w)*Rsr)/Rshr-I(w);
while (abs(x(w))¿0.001)
x(w)=Iph-Io*(exp((V(w)+I(w)*Rsr)/Vth/Nsc/n)-1)-(V(w)+I(w)*Rsr)/Rshr-I(w);
xlin(w)=-Io*Rsr/Vth/Nsc/n*exp((V(w)+I(w)*Rsr)./Vth/Nsc/n)-Rsr/Rshr-1;
I_(w)=I(w)-x(w)/xlin(w);
I(w)=I_(w);
end
end
P = (Iph-Io*(exp((V+I.*Rsr)/Vth/Nsc/n)-1)-(V+I.*Rsr)/Rshr).*V;
Pmax_m = max(P);
perror = (Pmax_m-Pmax_e);
end
figure(12)
box
hold on
set(gca, "linewidth", 1.5)
set(gca, "fontsize", 14)
xlabel('Voltage [V]',"fontsize", 20);
ylabel('Current [A]',"fontsize", 20);
axis([0 25 0 10]);
plot(V,I,'LineWidth',2,"b") %%
hleg = legend('Ta=20^oC', 'Ta=25^oC','Ta=30^oC','Ta=35^oC','Ta=40^oC', 'Ta=45^oC','Ta=50^oC',"location", "northeast");
set (hleg, "fontsize", 15);
legend boxoff
box
end
figure (12)
```

```
plot([0 15.177  19.764],[8.1114 7.4288 0 ],'o','LineWidth',2,'
    MarkeRsrize',5,'Color','r')
box
figure (12)
plot([0 14.754  19.389],[8.1273 7.4356 0 ],'o','LineWidth',2,'
    MarkeRsrize',5,'Color','k')
box
figure (12)
plot([0 14.330  19.014],[8.1432 7.4423 0 ],'o','LineWidth',2,'
    MarkeRsrize',5,'Color','c')
box
figure (12)
plot([0 13.905  18.638],[8.1591 7.4491 0 ],'o','LineWidth',2,'
    MarkeRsrize',5,'Color','g')
box
figure (12)
plot([0 13.480  18.261],[8.1750 7.4558 0 ],'o','LineWidth',2,'
    MarkeRsrize',5,'Color','m')
box
figure (12)
plot([0 13.055  17.883],[8.1909 7.4626 0 ],'o','LineWidth',2,'
    MarkeRsrize',5,'Color','k')
box
figure (12)
box
plot([0 12.629  17.504],[8.2068 7.4693 0 ],'o','LineWidth',2,'
    MarkeRsrize',5,'Color','b')
box
```

Appendix XV

P-V Curve Code for KC130GT at various temperatures (Figure 5.20)

```
clc
clear all
output_precision(8)
Ta=20 %@1000W/m2 20oC
Iscn =8.1114;
Ippt= 7.4288;
Vppt= 15.177;
vocstc =19.764;
Pmax_e = Vppt*Ippt;
Nsc = 36;
T=326.9;
k=1.3806503*10^(-23);
q=1.6021764*10^(-19);
Vth=(k*T)/q;
Rsrinc=0.001;
tol=0.001;
n_top=100;
nimax=2;
Rsr_max=(vocstc-Vppt)./Ippt;
Rshr_min=Vppt/(Iscn-Ippt)-Rsr_max;
Rshr=Rshr_min;
perror=Inf;
ni=0;
Rsr=0.163;
A=1.33;
while (perror¿tol)&&(Rshr¿0)&&(ni<nimax)
Iph=(Rsr+Rshr)/Rshr*Iscn;
ni=ni+1 ;
Isc=Iscn;
Voc=vocstc;
Io=Isc./exp(Voc./(n*Nsc*Vth));
Rsr=Rsr+Rsrinc;
Rshr=(Vppt+Ippt*Rsr)./(Iph-Ippt-(Io*(exp((Vppt+Ippt*Rsr)./(n*Nsc*Vth))-1)));
clear V
```

```
clear I
V=0:vocstc/n_top:23;
I=zeros(1,size(V,2));
for w=1: size(V,2)
x(w)=Iph-Io*(exp((V(w)+I(w)*Rsr)/Vth/Nsc/n)-1)-(V(w)+I(w)*Rsr)/Rshr-I(w);
while (abs(x(w))¿0.001)
x(w)=Iph-Io*(exp((V(w)+I(w)*Rsr)/Vth/Nsc/n)-1)-(V(w)+I(w)*Rsr)/Rshr-I(w);
xlin(w)=-Io*Rsr/Vth/Nsc/n*exp((V(w)+I(w)*Rsr)./Vth/Nsc/n)-Rsr/Rshr-1;
I_(w)=I(w)-x(w)/xlin(w);
I(w)=I_(w);
end
end
P = (Iph-Io*(exp((V+I.*Rsr)/Vth/Nsc/n)-1)-(V+I.*Rsr)/Rshr).*V;
Pmax_m = max(P);
perror = (Pmax_m-Pmax_e);
end
figure(12)
box
hold on
axis([0 23 0 135]);
plot(V,P,'LineWidth',2,"r") % %
box
Ta=25 % @1000W/m2 25oC
Iscn= 8.1273;
Ippt= 7.4356;
Vppt= 14.754;
vocstc= 19.389;
Pmax_e = Vppt*Ippt;
T=331.9;
Rsrinc=0.001;
tol=0.001;
n_top=100;
nimax=2;
Rsr_max=(vocstc-Vppt)./Ippt;
Rshr_min=Vppt/(Iscn-Ippt)-Rsr_max;
Rshr=Rshr_min;
perror=Inf;
ni=0;
Rsr=0.18;
A=1.3;
while (perror¿tol)&&(Rshr¿0)&&(ni<nimax)
Iph=(Rsr+Rshr)/Rshr*Iscn;
ni=ni+1 ;
Isc=Iscn;
Voc=vocstc;
Io=Isc./exp(Voc./(n*Nsc*Vth));
Rsr=Rsr+Rsrinc;
```

```
Rshr=(Vppt+Ippt*Rsr)./(Iph-Ippt-(Io*(exp((Vppt+Ippt*Rsr)./(n*Nsc*Vth))-1)));
clear V
clear I
V=0:vocstc/n_top:23;
I=zeros(1,size(V,2));
for w=1: size(V,2)
x(w)=Iph-Io*(exp((V(w)+I(w)*Rsr)/Vth/Nsc/n)-1)-(V(w)+I(w)*Rsr)/Rshr-I(w);
while (abs(x(w))¿0.001)
x(w)=Iph-Io*(exp((V(w)+I(w)*Rsr)/Vth/Nsc/n)-1)-(V(w)+I(w)*Rsr)/Rshr-I(w);
xlin(w)=-Io*Rsr/Vth/Nsc/n*exp((V(w)+I(w)*Rsr)./Vth/Nsc/n)-Rsr/Rshr-1;
I_(w)=I(w)-x(w)/xlin(w);
I(w)=I_(w);
end
end
P = (Iph-Io*(exp((V+I.*Rsr)/Vth/Nsc/n)-1)-(V+I.*Rsr)/Rshr).*V;
Pmax_m = max(P);
perror = (Pmax_m-Pmax_e);
end
figure(12)
hold on
axis([0 23 0 135]);
plot(V,P,'LineWidth',2,"k") % %
box
Ta =30 % @1000W/m2 30oC
Iscn=8.1432;
Ippt= 7.4423;
Vppt= 14.330;
vocstc=19.014;
Pmax_e = Vppt*Ippt;
T=336.9;
Rsrinc=0.001;
tol=0.001;
n_top=100;
nimax=2;
Rsr_max=(vocstc-Vppt)./Ippt;
Rshr_min=Vppt/(Iscn-Ippt)-Rsr_max;
Rshr=Rshr_min;
perror=Inf;
ni=0;
Rsr=0.201;
A=1.29;
while (perror¿tol)&&(Rshr¿0)&&(ni<nimax)
Iph=(Rsr+Rshr)/Rshr*Iscn;
ni=ni+1 ;
Isc=Iscn;
Voc=vocstc;
```

```
Io=Isc./exp(Voc./(n*Nsc*Vth));
Rsr=Rsr+Rsrinc;
Rshr=(Vppt+Ippt*Rsr)./(Iph-Ippt-(Io*(exp((Vppt+Ippt*Rsr)./(n*Nsc*Vth))-1)));
clear V
clear I
V=0:vocstc/n_top:23;
I=zeros(1,size(V,2));
for w=1: size(V,2)
x(w)=Iph-Io*(exp((V(w)+I(w)*Rsr)/Vth/Nsc/n)-1)-(V(w)+I(w)*Rsr)/Rshr-I(w);
while (abs(x(w))¿0.001)
x(w)=Iph-Io*(exp((V(w)+I(w)*Rsr)/Vth/Nsc/n)-1)-(V(w)+I(w)*Rsr)/Rshr-I(w);
xlin(w)=-Io*Rsr/Vth/Nsc/n*exp((V(w)+I(w)*Rsr)./Vth/Nsc/n)-Rsr/Rshr-1;
I_(w)=I(w)-x(w)/xlin(w);
I(w)=I_(w);
end
end
P = (Iph-Io*(exp((V+I.*Rsr)/Vth/Nsc/n)-1)-(V+I.*Rsr)/Rshr).*V;
Pmax_m = max(P);
perror = (Pmax_m-Pmax_e);
end
figure(12)
hold on
axis([0 23 0 135]);
plot(V,P,'LineWidth',2,"c") % %
box
Ta=35 % @1000W/m2 35oC
Iscn=8.1591;
Ippt=7.4491;
Vppt=13.905;
vocstc=18.638;
Pmax_e = Vppt*Ippt;
T=341.9;
Rsrinc=0.001;
to1=0.001;
n_top=100;
nimax=2;
Rsr_max=(vocstc-Vppt)./Ippt;
Rshr_min=Vppt/(Iscn-Ippt)-Rsr_max;
Rshr=Rshr_min;
perror=Inf;
ni=0;
Rsr=0.223;
A=1.27;
while (perror¿to1)&&(Rshr¿0)&&(ni<nimax)
Iph=(Rsr+Rshr)/Rshr*Iscn;
ni=ni+1 ;
```

```
Isc=Iscn;
Voc=vocstc;
Io=Isc./exp(Voc./(n*Nsc*Vth));
Rsr=Rsr+Rsrinc;
Rshr=(Vppt+Ippt*Rsr)./(Iph-Ippt-(Io*(exp((Vppt+Ippt*Rsr)./(n*Nsc*Vth))-1)));
clear V
clear I
V=0:vocstc/n_top:23;
I=zeros(1,size(V,2));
for w=1: size(V,2)
x(w)=Iph-Io*(exp((V(w)+I(w)*Rsr)/Vth/Nsc/n)-1)-(V(w)+I(w)*Rsr)/Rshr-I(w);
while (abs(x(w))¿0.001)
x(w)=Iph-Io*(exp((V(w)+I(w)*Rsr)/Vth/Nsc/n)-1)-(V(w)+I(w)*Rsr)/Rshr-I(w);
xlin(w)=-Io*Rsr/Vth/Nsc/n*exp((V(w)+I(w)*Rsr)./Vth/Nsc/n)-Rsr/Rshr-1;
I_(w)=I(w)-x(w)/xlin(w);
I(w)=I_(w);
end
end
P = (Iph-Io*(exp((V+I.*Rsr)/Vth/Nsc/n)-1)-(V+I.*Rsr)/Rshr).*V;
Pmax_m = max(P);
perror = (Pmax_m-Pmax_e);
end
figure(12)
hold on
axis([0 23 0 135]);
plot(V,P,'LineWidth',2,"g")
box
Ta=40 %@1000W/m2 40oC
Iscn =8.1750;
Ippt= 7.4558;
Vppt= 13.480;
vocstc =18.261;
Pmax_e = Vppt*Ippt;
T=346.9;
Rsrinc=0.001;
tol=0.001;
n_top=100;
nimax=2;
Rsr_max=(vocstc-Vppt)./Ippt;
Rshr_min=Vppt/(Iscn-Ippt)-Rsr_max;
Rshr=Rshr_min;
perror=Inf;
ni=0;
Rsr=0.235;
A=1.22;
while (perror¿tol)&&(Rshr¿0)&&(ni<nimax)
```

```
Iph=(Rsr+Rshr)/Rshr*Iscn;
ni=ni+1 ;
Isc=Iscn;
Voc=vocstc;
Io=Isc./exp(Voc./(n*Nsc*Vth));
Rsr=Rsr+Rsrinc;
Rshr=(Vppt+Ippt*Rsr)./(Iph-Ippt-(Io*(exp((Vppt+Ippt*Rsr)./(n*Nsc*Vth))-1))); %equation 27
clear V
clear I
V=0:vocstc/n_top:23;
I=zeros(1,size(V,2));
for w=1: size(V,2)
x(w)=Iph-Io*(exp((V(w)+I(w)*Rsr)/Vth/Nsc/n)-1)-(V(w)+I(w)*Rsr)/Rshr-I(w);
while (abs(x(w))¿0.001)
x(w)=Iph-Io*(exp((V(w)+I(w)*Rsr)/Vth/Nsc/n)-1)-(V(w)+I(w)*Rsr)/Rshr-I(w);
xlin(w)=-Io*Rsr/Vth/Nsc/n*exp((V(w)+I(w)*Rsr)./Vth/Nsc/n)-Rsr/Rshr-1;
I_(w)=I(w)-x(w)/xlin(w);
I(w)=I_(w);
end
end
P = (Iph-Io*(exp((V+I.*Rsr)/Vth/Nsc/n)-1)-(V+I.*Rsr)/Rshr).*V;
Pmax_m = max(P);
perror = (Pmax_m-Pmax_e);
end
figure(12)
hold on
axis([0 23 0 135]);
plot(V,P,'LineWidth',2,"m")
box
Ta=45 %@1000W/m2 45oC
Iscn= 8.1909;
Ippt= 7.4626;
Vppt= 13.055;
vocstc= 17.883;
Pmax_e = Vppt*Ippt;
T=351.9;
Rsrinc=0.001;
tol=0.001;
n_top=100;
nimax=2;
Rsr_max=(vocstc-Vppt)./Ippt;
Rshr_min=Vppt/(Iscn-Ippt)-Rsr_max;
Rshr=Rshr_min;
perror=Inf;
ni=0;
Rsr=0.246;
```

```
A=1.21;
while (perror¿tol)&&(Rshr¿0)&&(ni<nimax)
Iph=(Rsr+Rshr)/Rshr*Iscn;
ni=ni+1 ;
Isc=Iscn;
Voc=vocstc;
Io=Isc./exp(Voc./(n*Nsc*Vth));
Rsr=Rsr+Rsrinc;
Rshr=(Vppt+Ippt*Rsr)./(Iph-Ippt-(Io*(exp((Vppt+Ippt*Rsr)./(n*Nsc*Vth))-1))); %equation 27
clear V
clear I
V=0:vocstc/n_top:23;
I=zeros(1,size(V,2));
for w=1: size(V,2)
x(w)=Iph-Io*(exp((V(w)+I(w)*Rsr)/Vth/Nsc/n)-1)-(V(w)+I(w)*Rsr)/Rshr-I(w);
while (abs(x(w))¿0.001)
x(w)=Iph-Io*(exp((V(w)+I(w)*Rsr)/Vth/Nsc/n)-1)-(V(w)+I(w)*Rsr)/Rshr-I(w);
xlin(w)=-Io*Rsr/Vth/Nsc/n*exp((V(w)+I(w)*Rsr)./Vth/Nsc/n)-Rsr/Rshr-1;
I_(w)=I(w)-x(w)/xlin(w);
I(w)=I_(w);
end
end
P = (Iph-Io*(exp((V+I.*Rsr)/Vth/Nsc/n)-1)-(V+I.*Rsr)/Rshr).*V;
Pmax_m = max(P);
perror = (Pmax_m-Pmax_e);
end
figure(12)
hold on
axis([0 23 0 135]);
plot(V,P,'LineWidth',2,"--k") %%
box
Ta=50 %@1000W/m2 50oC
Iscn= 8.2068;
Ippt= 7.4693;
Vppt= 12.629;
vocstc= 17.504;
Pmax_e = Vppt*Ippt;
T=356.9;
Rsrinc=0.001;
tol=0.001;
n_top=100;
nimax=2;
Rsr_max=(vocstc-Vppt)./Ippt;
Rshr_min=Vppt/(Iscn-Ippt)-Rsr_max;
Rshr=Rshr_min;
perror=Inf;
```

```
ni=0;
Rsr=0.277;
A=1.18;
c={'w', 'w', 'w', 'w', 'w', 'w', 'w'};
for i=[1 2 3 4 5 6 7];
while (perror¿tol)&&(Rshr¿0)&&(ni<nimax)
Iph=(Rsr+Rshr)/Rshr*Iscn;
ni=ni+1 ;
Isc=Iscn;
Voc=vocstc;
Io=Ippt./(exp(Voc./(n*Nsc*Vth))-exp(Vppt./(n*Nsc*Vth)));
Rsr=Rsr+Rsrinc;
Rshr=(Vppt+Ippt*Rsr)./(Iph-Ippt-(Io*(exp((Vppt+Ippt*Rsr)./(n*Nsc*Vth))-1)));
clear V
clear I
V=0:vocstc/n_top:23;
I=zeros(1,size(V,2));
for w=1: size(V,2)
x(w)=Iph-Io*(exp((V(w)+I(w)*Rsr)/Vth/Nsc/n)-1)-(V(w)+I(w)*Rsr)/Rshr-I(w);
while (abs(x(w))¿0.001)
x(w)=Iph-Io*(exp((V(w)+I(w)*Rsr)/Vth/Nsc/n)-1)-(V(w)+I(w)*Rsr)/Rshr-I(w);
xlin(w)=-Io*Rsr/Vth/Nsc/n*exp((V(w)+I(w)*Rsr)./Vth/Nsc/n)-Rsr/Rshr-1;
I_(w)=I(w)-x(w)/xlin(w);
I(w)=I_(w);
end
end
P = (Iph-Io*(exp((V+I.*Rsr)/Vth/Nsc/n)-1)-(V+I.*Rsr)/Rshr).*V;
Pmax_m = max(P);
perror = (Pmax_m-Pmax_e);
end
figure(12)
box
hold on
set(gca, "linewidth", 1.5)
set(gca, "fontsize", 14)
xlabel('Voltage [V]',"fontsize", 20);
ylabel('Power [W]',"fontsize", 20);
axis([0 23 0 135]);
plot(V,P,'LineWidth',2,"b") %%
hleg = legend('Ta=20^oC', 'Ta=25^oC','Ta=30^oC','Ta=35^oC','Ta=40^oC', 'Ta=45^oC','Ta=50^oC',"location", "northwest");
set (hleg, "fontsize", 15);
legend boxoff
box
end
figure (12)
```

```
plot([0 15.177  19.764],[0  112.746 0 ],'o','LineWidth',2,'
    MarkeRsrize',5,'Color','r')
box
figure (12)
plot([0 14.754  19.389],[0  109.701 0 ],'o','LineWidth',2,'
    MarkeRsrize',5,'Color','k')
box
figure (12)
plot([0 14.330  19.014],[0  106.646 0 ],'o','LineWidth',2,'
    MarkeRsrize',5,'Color','c')
box
figure (12)
plot([0 13.905  18.638],[0  103.581 0 ],'o','LineWidth',2,'
    MarkeRsrize',5,'Color','g')
box
figure (12)
plot([0 13.480  18.261],[0  100.507 0 ],'o','LineWidth',2,'
    MarkeRsrize',5,'Color','m')
box
figure (12)
plot([0 13.055  17.883],[0  97.423 0 ],'o','LineWidth',2,'
    MarkeRsrize',5,'Color','k')
box
figure (12)
box
plot([0 12.629  17.504],[0  94.329 0 ],'o','LineWidth',2,'
    MarkeRsrize',5,'Color','b')
box
```